International Transaction Journal of Engineering, Management, & Applied Sciences & Technologies

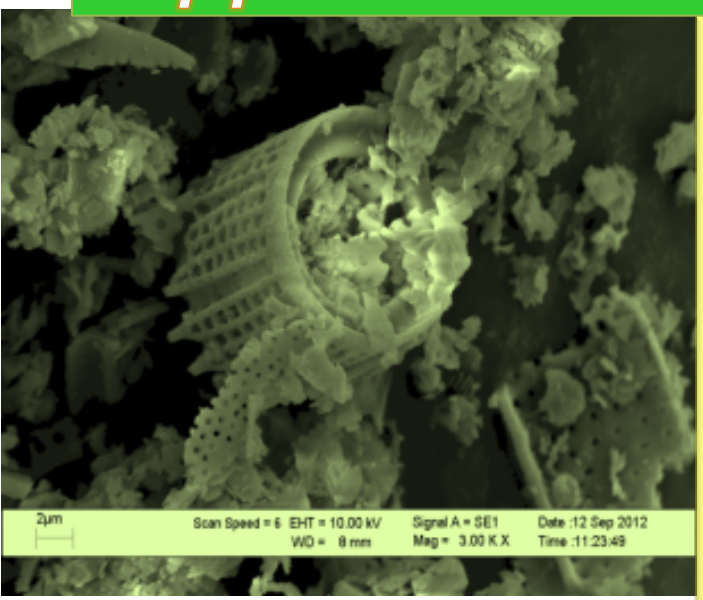

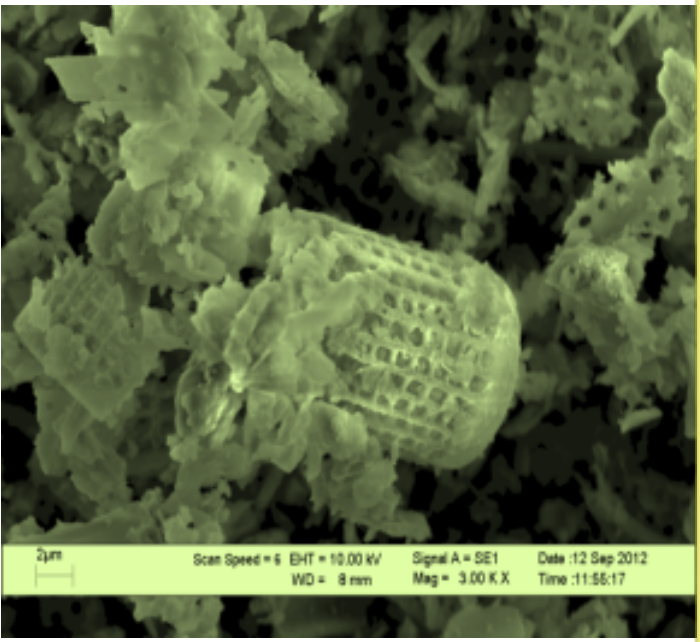

Volume 5 Issue 1 (January 2014)

ISSN 2228-9860
eISSN 1906-9642

http://TuEngr.com

In This Issue

Cover Photo is from published article ITJEMAST V5(1) of W. Pranee *et al*. (2014) "Effects of Calcination Treatment of Diatomite on Dimethyl Ether Synthesis from Methanol. Photos show scanning electron micrograph of diatomite with 1,000 magnification: Fresh DM (top) and DM500 (bottom).

TuEngr Group

International Transaction Journal of Engineering, Management, & Applied Sciences & Technologies

http://TuEngr.com

International Editorial Board

:: International Transaction Journal of Engineering, Management, & Applied Sciences & Technologies

Volume 5 Issue 1 (January, 2014) ISSN 2228-9860
http://TuEngr.com eISSN 1906-9642

FEATURE PEER-REVIEWED ARTICLES

Contact & Offices:

Associate Professor Dr. Ahmad Sanusi Hassan (Editor-in-Chief), School of Housing, Building and Planning, UNIVERSITI SAINS MALAYSIA, 11800 Minden, Penang, MALAYSIA. Tel: +60-4-653-2835 Fax: +60-4-657 6523, Sanusi@usm.my

Associate Professor Dr. Boonsap Witchayangkoon (Executive Editor), Faculty of Engineering, THAMMASAT UNIVERSITY, Klong-Luang, Pathumtani, 12120, THAILAND. Tel: +66-2-5643005 Ext 3101. Fax: +66-2-5643022 Editor@TuEngr.com

Postage Paid in Malaysia.

:: International Transaction Journal of Engineering, Management, & Applied Sciences & Technologies

http://TuEngr.com

Call-for-Papers:

ITJEMAST invites you to submit high quality papers for full peer-review and possible publication in areas pertaining to our scope including engineering, science, management and technology, especially interdisciplinary/cross-disciplinary/multidisciplinary subjects.

Next article continue on next page ➔

International Transaction Journal of Engineering, Management, & Applied Sciences & Technologies

http://TuEngr.com

Effects of Calcination Treatment of Diatomite on Dimethyl Ether Synthesis from Methanol

Watcharakorn Pranee [a], Pornsawan Assawasaengrat [b], Arthit Neramittagapong [a], and Sutasinee Neramittagapong [a*]

[a] *Department of Chemical Engineering, Faculty of Engineering, Khon Kaen University, Khon Kaen 40002, THAILAND*

[b] *Department of Chemical Engineering, Faculty of Engineering, King Mongkut's Institute of Technology Ladkrabang, Bangkok, 10520, THAILAND*

ARTICLEINFO

Article history:
Received 20 August 2013
Accepted 06 December 2013
Available online 09 December 2013

Keywords:
DME;
Renewable energy;
Methanol;
Acid catalyst.

ABSTRACT

The synthesis of dimethyl ether via methanol dehydration over diatomite catalysts was investigated. The reactions were carried out in a fixed bed reactor. The effects of calcinations of diatomite on its catalytic performance were studied. Diatomite calcined at 500°C (DM500) gave the higher BET surface than fresh diatomite (DM) due to the loss of ignition. The rate of reaction over DM500 catalyst was lower than fresh DM due to the loss of active sites on the catalyst surface. However, the decrease of basicity of DM500 surface showed the higher selectivity to DME than fresh DM. The DM500 catalyst exhibits better DME yield than fresh DM catalyst, although it can be used as a selective catalyst for DME synthesis from methanol.

1. Introduction

Dimethyl ether (DME) is one of the most promising energy resources because it has better environmental performance and its properties are similar to traditional fuels (West, *et al.*, 2009). Especially, it also has a high cetane number about 55-60 which is significantly alternated to the fossil fuel such as conventional diesel. In Thailand, it can be improved the properties of natural gas by blending it up to 20% into LPG.

*Corresponding author (S.Neramittagapong). Tel: +66-43-362240 E-mail: sutasineene@kku.ac.th © 2014. International Transaction Journal of Engineering, Management, & Applied Sciences & Technologies. Volume 5 No.1 ISSN 2228-9860 eISSN 1906-9642. Online available at http://tuengr.com/V05/0001.pdf .

DME can be synthesized via direct synthesis from syngas and methanol dehydration. There are many research focused on the methanol dehydration. There were various types of catalysts such as NaH-ZSM-5 (Vishwanathan, *et al.*, 2004), Au/ZnO/Lz-Y52 (Mpela, *et al.*, 2007), Al-modified Mordenite (Khandan, *et al.*, 2008), and SAPO-11 (Dai, *et al.*, 2011) which could be used for methanol dehydration. It has been reported that there were many parameters affected to DME yield from the methanol dehydration to DME such as the reaction temperature, the methanol flow rate, the catalyst calcination temperature and the acidity of catalysts. It has been concluded that the acid solid catalyst is the most active for catalyzing this reaction; however, the moderate acidity of the surface has been showed the higher yield of DME than the strong acidity catalyst. The zeolite has been selected to be the most active for this reaction. It consists of two main elements which are silica and alumina (Jia, *et al.*, 2008). Their disadvantages bring about unstable catalysts and unexpected products. In this study, the natural porous clay named diatomite has been used as the catalyst due to many acid sites over skeletal form of its surface. Furthermore, it mainly consists of silica and alumina which are similar to natural zeolite. In 2009, the researcher proposed the natural zeolite which was calcined in the temperature range of 500 to 600°C (San, *et al.*, 2009). From this investigation, it has been found that the increasing of its surface area depends on the calcination temperatures. Moreover, there are many types of zeolites, for example Zn/H-ZSM-5 (Yiwen, *et al.*, 2010), aluminophosphate and silico-aluminophosphate (Dai, *et al.*, 2011), and SAPO-34 (Pop and Theodorescu, 2000) which were calcined at the temperature range of 500 to 600°C.

The aim of this research is to study the way to use diatomite as a catalyst for DME synthesis from methanol. It has been focused on the effects of the calcination method and the reaction temperature to the DME yield.

2. Experimental

2.1 Catalysts Preparation

Diatomite was collected from the northern area of Chiangmai Province in Thailand. Diatomite was dried in the oven at 80°C for 24 h, and then it was ground with ball mill and sieved using a 180-mm screen. Afterwards, it was calcined in th oven under air atmosphere at 500°C. The calcined diatomite was labeled as DM500 and diatomite without calcination was called fresh DM.

2.2 Catalyst Characterization

Diatomite microstructure and crystal morphology analysis were determined by scanning electron microscope LEO 1455VP. Thermal gravimetric analysis (TGA) was set to analyze the weight loss of catalysts. Catalysts were placed in alumina cell and heated with the temperature-raising rate of 10°C/min starting from the room temperature to 100°C under nitrogen flow and then the temperature was held at 100°C for 10 minutes. After that, the temperature was increased from 100 to 700 °C with raising rate of 10°C/min under air flow. The signal of TGA was detected by TGA-50H SHIMADZU. X-ray fluorescence analysis (XRF) was used to determine the chemical composition and loss of ignition (LOI) of catalysts to methanol dehydration to dimethyl ether with the parameters to supply in the measurement as 50 kV and 60 mA with rhodium X-ray source to analyze of SRS 340. The catalyst was measured the Brunauer-Emmett-Teller (BET) specific surface area by Microelectronics ASAP2010 physical adsorption apparatus in the condition for N_2 adsorption at -196°C. The X-ray diffraction (XRD) patterns were investigated by Miniflex goniometer fitted with using Ni-filtered CuKα radiation and 2θ continuous-scanning mode and electrical parameters were operated at 30 kV and 15 mA. The acidity of catalysts were measured by the temperature-programmed desorption of ammonia (NH_3-TPD) conducted on BEL JAPAN model BELCAT-B with a thermal conductivity detector (TCD), in the prior experiment, 0.05 g of catalyst was tested under 5% NH_3 and the flow rate of carrier-gas helium at 30 ml/min from 100 to 950°C. And then the basicity of catalysts was measured by the temperature-programmed desorption of carbondioxide (CO_2-TPD) conducted on BEL JAPAN model BELCAT-B with a thermal conductivity detector (TCD), during adsorption and desorption, 0.05 g of catalyst was tested under CO_2 with the flow rate of carrier-gas helium at ml/min from 100 to 800°C.

2.3 Methanol Dehydration

During the methanol dehydration, 0.5 g of activated catalysts (fresh DM and DM500) was loaded into the fixed-bed quartz reactor while methanol was pumped through a syringe peristaltic pump at 0.5 ml/min. The gas condition of MeOH:N_2 was 1:4 (with N_2 flow of 60 ml/min at the atmospheric pressure). The feed was flowed through a peristalsis pump system and changed into the gas state before it was passed through the fixed-bed reactor system using nitrogen gas flow as a carrier gas shown in Figure 1. All products of methanol dehydration

*Corresponding author (S.Neramittagapong). Tel: +66-43-362240 E-mail: sutasineene@kku.ac.th

International Transaction Journal of Engineering, Management, & Applied Sciences & Technologies. Volume 5 No.1 ISSN 2228-9860 eISSN 1906-9642. Online available at http://tuengr.com/V05/0001.pdf .

were directly analyzed by on-line gas chromatography with FID and TCD detectors, whereas Porapak T and Molecular Sieve 13X (Shimadzu, GC-14B and Shimadzu, C-R4A) were equipped in these columns. The range of reaction temperature was set between the temperatures of 250°C to 350°C in order to catalyze the reaction.

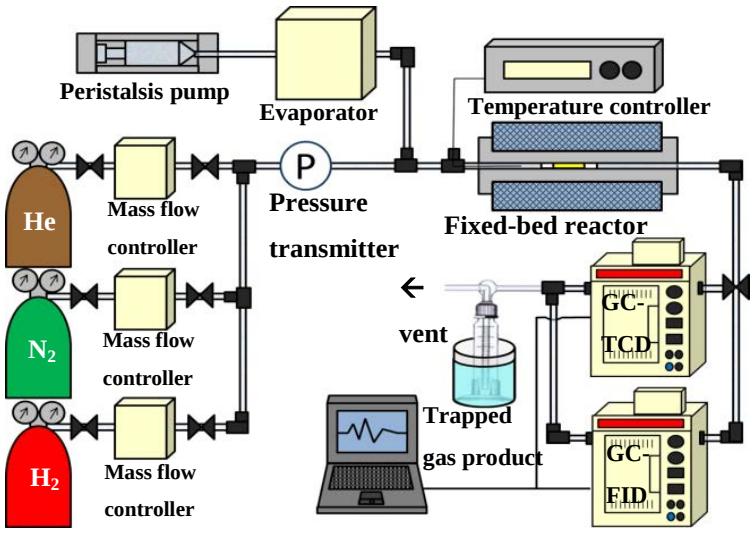

Figure 1: Schematic view of methanol dehydration to dimethyl ether set-up

3. Results and Discussion

Table 1: The physical properties of DM and DM500 catalysts

Catalyst	Composition (% wt)					Si/Al	S_{BET} (m^2/g)
	SiO_2	Al_2O_3	Fe_2O_3	Other	LOI		
Fresh DM	80	9.6	2.5	1.8	6.14	8.3	25
DM500	82	10	4.2	2.5	0.72	8.1	37

Denote: LOI is loss of ignition and S_{BET} is BET surface area

3.1 The effects of calcination treatment on the physical

The physical properties of catalysts are summarized in Table 1, the results of chemical composition of fresh DM and DM500 by XRF shown that the calcined temperature could not influence the chemical composition for metal compound and their surface areas, but it could only decrease the organic compounds (as LOI composition in XRF data) in their compositions. The fresh DM consisted of the organic compounds about 6.14% while the DM500 had only about 0.72%. The LOI from XRF data of DM500 was followed by TGA data in Figure 2, which there was no weight loss, while weight loss about 17% was present in fresh DM. The

BET surface area of fresh DM was increased from 25 to 37 m^2/g (about 50% of enhancement as compared with fresh DM) by calcined temperature treatment at 500°C. On the other hands, there was no effect on silica alumina ratio (8.1-8.3).

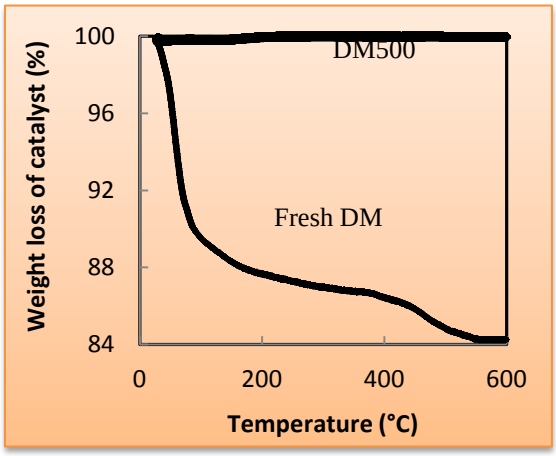

Figure 2: TGA data of fresh DM and DM500

According to the research data of San, et al., (San, et al., 2009) for characterizing composition and phases in Turkey diatomite, the XRD pattern is presented in all phases (quartz, albite, tridymite, orthoclase, microcline, aluminium silicate and magnesium silicate) which are similar to Chiangmai diatomite for this research. In amorphous phase of both catalysts; aluminium silicate, magnesium silicate and microcline are the main phases in this skeletal form. However, a significant crystalline phase is silica in the great majority of composition of quartz phase as shown in Figure 5. The phases of these catalysts were not changed in order to increase the calcinations temperature to 500°C.

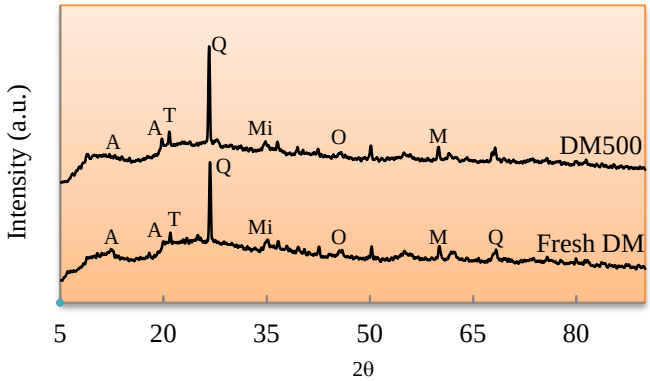

Figure 3: XRD patterns of fresh DM and DM500: A = Aluminium silicate, M = Magnesium silicate, Mi = Microline, O = Orthoclase, Q = Quartz and T = Tridymite

In the process of calcinations treatment at 500°C, there was no effect on morphology of

*Corresponding author (S.Neramittagapong). Tel: +66-43-362240 E-mail: sutasineene@kku.ac.th

International Transaction Journal of Engineering, Management, & Applied Sciences & Technologies. Volume 5 No.1 ISSN 2228-9860 eISSN 1906-9642. Online available at http://tuengr.com/V05/0001.pdf .

DM as shown in Figure 4 which illustrated the scanning electron micrographs of fresh DM and DM500. The shape of diatomite was not deformed at the temperature of 500°C since the main phase still had the open pores of skeletal-shaped diatomite. Furthermore, the hollow and porous structure of these catalysts was fully filled with the agglomerates of cracked structure and the unidentified particles, such as pre- and post-calcination treatments at this temperature. The morphology of both catalysts was similar to the data of (Chaisena and Rangsriwatananon, 2005) that there was no deformation in diatomite at the high-temperature calcination (1100°C, 5 h).

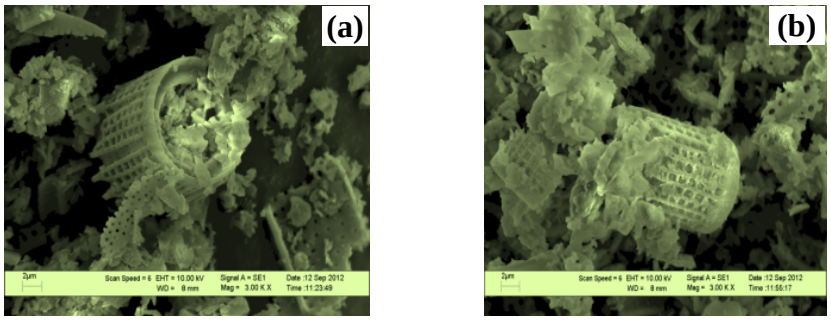

Figure 4: Scanning electron micrograph of diatomite with 1,000 magnification: (a) Fresh DM and (b) DM500

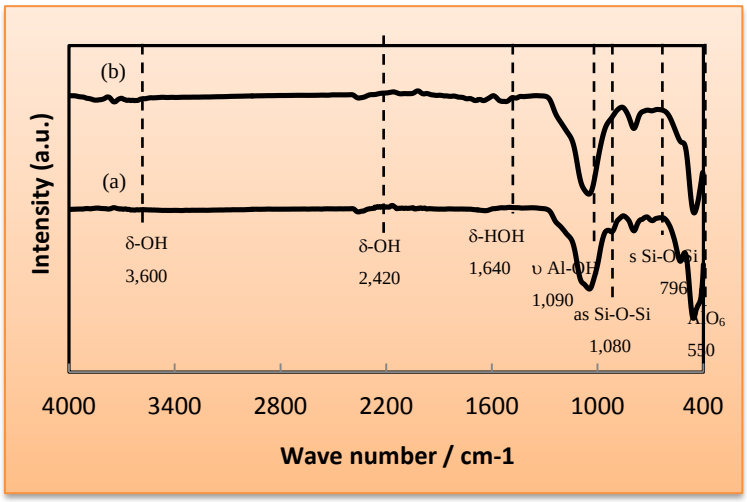

Figure 5: FT-IR spectra of Fresh DM and DM500: (a) Fresh DM and (b) DM500

By using this treatment, neither did the phases and the morphology of diatomite have any interaction, nor were the functional groups arranged in diatomite's structure influenced. Based on the FT-IR spectra from the identification of (Crisan, *et al*., 2006) there was the group of siloxane (Si-O-Si) at 1,080 cm^{-1} connected to the aluminium hydroxide group at 1,090 cm^{-1}, and silicon in the structure was bonded to hydroxyl group (-OH) to form the silinol group (S-OH) at 2,420 and 3,600 cm^{-1}. The observed FT-IR spectra of fresh DM and DM500 were illustrated in Figure 5.

3.2 The effects of calcination treatment on the activity of methanol dehydration to DME over diatomite catalysts

According to Table 1, the amounts of oxide compounds and LOI in fresh DM were changed by the cacination treatment at 500°C. However, this treatment had no effect on the silica-alumina ratio. For this stable ratio, there was no difference between the activity of fresh DM and that of DM500 as shown in Figure 6, suggesting that the activity was slightly influenced by calcination treatment at 500°C to methanol conversion rate via methanol dehydration to DME. On the contrary, the uncalcined diatomite exhibited DME showed lower selectivity than calcined diatomite at 500°C as seen from Figure 7.

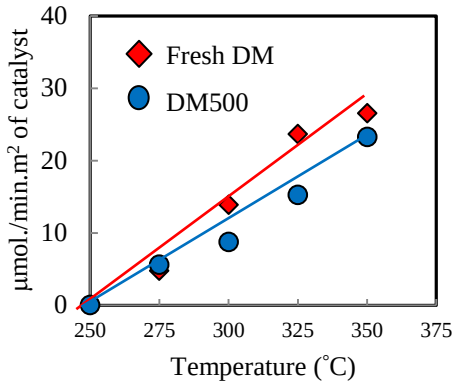

Figure 6: The effects of calcination treatment of diatomite on methanol conversion rate via methanol dehydration over fresh DM and DM500 catalysts at the reaction temperature from 250 to 350°C

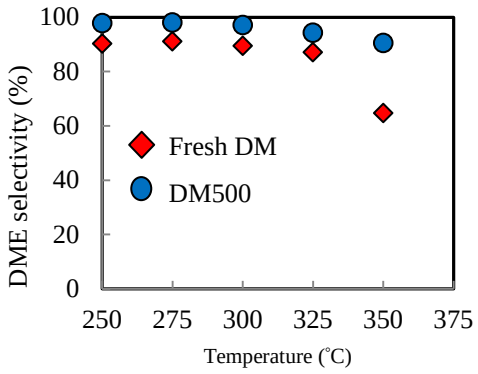

Figure 7: The effects of calcination treatment of diatomite on dimethyl ether selectivity via methanol dehydration over fresh DM and DM500 catalysts at the reaction temperature from 250 to 350°C

DME was selected to be the main product for both of catalysts whereas, for fresh DM, there were directly-gained DME and rapidly-increasable unexpected product as seen in Figure 8 (such as formaldehyde via methanol dehydrogenation) and depended on the reaction

*Corresponding author (S.Neramittagapong). Tel: +66-43-362240 E-mail: sutasineene@kku.ac.th

International Transaction Journal of Engineering, Management, & Applied Sciences & Technologies. Volume 5 No.1 ISSN 2228-9860 eISSN 1906-9642. Online available at http://tuengr.com/V05/0001.pdf .

temperature (250 to 350°C). The calcination treatment of catalyst at 500°C could not increase the by-product distribution because the DME selectivity, as it is seen in Figure 7, was kept to its 90% trend-line along the reaction temperature of 250 to 350°C. For catalytic characterizations – such as XRD, SEM and FT-IR, it could suggest that the methanol conversion rate and the selectivity of DME were independent from these characterizations. On the other hand, the increased surface area of diatomite after calcinations at 500°C had the influence in decreasing the acid sites per area of diatomite to lower than that of uncalcined diatomite as shown in Table 2, which was also confirmed with the decreased methanol conversion rate of DM500. By considering the acidity from Table 2 by NH_3-TPD method, it showed that DM500 had the greater number of acid sites per area than fresh DM. Hence, DME selectivity of DM500 less decreased than that of fresh DM. Nonetheless, the CO_2-TPD data in Table 3 could significantly support the unexpected products especially form methanol dehydration. The higher amount of basic sites per area of fresh DM than that of DM500 revealed that fresh DM should enhance the competitive reaction with increasing the reaction temperature.

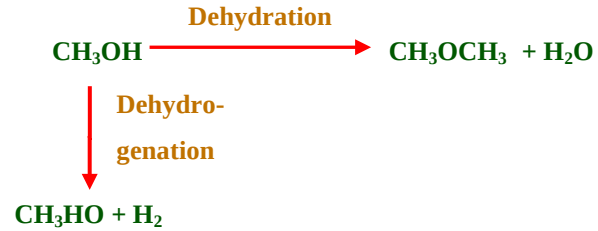

Figure 8: Methanol dehydration to dimethyl ether and methanol dehydrogenation to formaldehyde reaction pathway

Table 2: The amount of acid sites of catalysts from NH_3-TPD method

Catalysts	Weak acid at 190°C (µmol/m^2)	Strong acid at 630°C (µmol/m^2)	Total acidity (µmol/m^2)
Fresh DM	3.560	40.320	43.880
DM 500	3.162	29.351	32.514

Table 3: The amount of basic sites of catalysts from CO_2-TPD method

Catalysts	Weak base at 160°C (µmol/m^2)	Strong base at 630°C (µmol/m^2)	Total basicity (µmol/m^2)
Fresh DM	13.560	128.560	142.120
DM 500	8.297	77.243	85.541

From the calcination treatment result, it could suggest that DM500 was a more suitable catalyst than fresh DM to synthesize DME via methanol dehydration, though it still have lower methanol conversion rate than fresh DM.

4. Conclusion

It can be concluded that the calcination treatment had no effect on characterizations such as the ratio of silica and alumina, phases, morphology and functional groups in both diatomite catalysts. The calcination treatment at 500°C could decrease the LOI to lower than 1%, resulting in increasing of BET surface with no weight loss of diatomite.

In the catalytic activity study, the calcination at 500°C of diatomite had effects on higher acid sites per area, lower basic sites per area, and lower organic compound in its structure than fresh DM. DM500 exhibited high DME selectivity – over 90% – at the reaction temperature from 250 to 300°C while fresh DM had DME selectivity below 90% with many directly contributed products depending on the reaction temperature. Furthermore, it can be concluded that calcination treatment at 500°C also plays one important role in the effect of diatomite catalysts on synthesized dimethyl ether via methanol dehydration.

5. Acknowledgements

This work was supported by the Higher Education Research Promotion and National Research University Project of Thailand, Office of the Higher Education Commission.

6. References

Chaisena, A., and K. Rangsriwatananon. (2005). Synthesis of sodium zeolites from natural and modified diatomite. Mat. Lett., 59, 1474-1479.

Crisan, M., M. Raileanu, S. Preda, M. Zaharescu, A. M. Valean, E.J. Popovici, V. S. Teodorescu, and V. Matejec, J. Mrazek, (2006). Manganese doped sol-gel materials with catalytic properties. Journal Optoelectronics and advanced materials, 8, 2, 815-819.

Dai, W., W. Kong, G. Wu, N. Li, and N. Guan. (2011). Catalytic dehydration of methanol to dimethyl ether over aliminophosphate and silico-aluminophosphate molecular sieves. Cat. Com., 12, 535-538.

Jia Y., W. Ham, G. Xiong, and W. Yang. (2008). A method for diatomite zeolitization through steam-assisted crystallization with in-situ seeding. Mat. Lett., 62, 2400-2403.

Khandan, N., M. Kazemeini, and M. Aghaziarati. (2008). Determining an optimum catalyst for liquid-phase dehydration of methanol to dimethyl ether. Appl. Cat. A., 349, 6-12.

Kumar, V. S., A. H. Padmasri, C. V. V. Satyanarayana, I. A. Kumar Reddy, B. D. Raju, and K. S.

*Corresponding author (S.Neramittagapong). Tel: +66-43-362240 E-mail: sutasineene@kku.ac.th

Rama Rao. (2006). Nature and mode of addition of phosphate precursor in the synthesis of aluminium phosphate and its influence on methanol dehydration to dimethyl ether. Cat. Com., 7, 745-751.

Mpela, A., D. Hildebrandt, D. Glasser, M. S. Scurrell, and G. J. Hutchings. (2007). Low-pressure Methanol/Dimethyether Synthesis from Syngas on Gold-based Catalysts. Gold Bulletin., 40, 3, 219-224.

Pop, G. and C. Theodorescu. (2000). SAPO-34 Catalyst For Dimethylether Production. Surf. Sci. and Catal., 287-292.

San, O., R. Goren, and C. Ozgur. (2009). Purification of diatomite powder by acid leaching for use in fabrication of porous ceramics. Int. J. Miner. Process., 93, 6-10.

West, R. M., D. J. Braden and J. A. Dumesic. (2009). Dehydration of butane over solid acid catalysts in high water environments. J. Cat., 262, 134-143.

Yiwen, F., T. Ji, H. Xiaochang, S. Weibin, S. Yibing, and S. Changyong, Chin. (2010). Aromatization of Dimethyl Ether over Zn/H-ZSM-5 Catalyst. J. Catal., 31(2), 264-266.

Watcharakorn Pranee is a Ph.D. student in Chemical Engineering Department at Khon Kaen University. He received his B.Sc. from King Mongkut's Institute of Technology Ladkrabang in 2004. He earned his M.Eng. study from King Mongkut's Institute of Technology Ladkrabang in 2007. His current interests involve applications of catalysis to engineering.

Dr.Pornsawan Assawasaengrat earned her D.Eng. in Chemical Engineering from Chulalongkorn University in 2002. She holds a second class honors degree of bachelor in Chemical Engineering from Chulalongkorn University. She is currently Head of Chemical Engineering Department at King Mongkut's Institute of Technology Ladkrabang. She works in the area of chemical engineering, with emphasis on chemical reaction engineering and advanced materials. She focuses on the synthesis of adsorbents, adsorption, and separation.

Dr.Arthit Neramittagapong is an Assistant Professor in the Chemical Engineering Department at Khon Kaen University. He holds a B.Eng. in Chemical Engineering from Khon Kean University, M. Eng. in Chemical Engineering from Chulalongkorn University and D.Eng. in Environmental Chemistry and Engineering from Tokyo Institute of Technology. He has been working on the environmental catalysis, design of industrial catalysts, chemical reaction engineering, and hazardous waste treatment and pollution control.

Dr.Sutasinee Neramittagapong is an Assistant Professor in the Chemical Engineering Department at Khon Kaen University. She holds a B.Eng. in Chemical Engineering from Khon Kean University, M. Eng. in Chemical Engineering from Chulalongkorn University and D.Eng. in Environmental Chemistry and Engineering from Tokyo Institute of Technology. Her research works have been focused on the environmental catalysis, renewable energy, green productivity, synthesis of high value-added compounds from industrial or agriculture wastes, and hazardous waste treatment and pollution control.

Peer Review: This article has been internationally peer-reviewed and accepted for publication according to the guidelines in the journal's website. Note: Original version of this article was accepted and presented at the Third International-Thai Chemical Engineering and Applied Chemistry (TIChE) Conference, jointly organized by Department of Chemical Engineering, Faculty of Engineering, Khon Kaen University and Thai Institute of Chemical Engineering and Applied Chemistry, at Pullman Khon Kaen Raja Orchid Hotel, Khon Kaen, THAILAND, October 17-18, 2013.

International Transaction Journal of Engineering, Management, & Applied Sciences & Technologies

http://TuEngr.com

Effect of Blend Ratio on Cure Characteristics, Mechanical Properties, and Aging Resistance of Silica-filled ENR/SBR Blends

Chanin Ngudsuntear [a], Sunun Limtrakul [a], Terdthai Vatanatham [a], Adul Na Wichien [b] Garry L. Rempel [c], and Wanvimon Arayapranee [d*]

[a] *Department of Chemical Engineering, Kasetsart University, Bangkok, THAILAND*
[b] *Rubber Research Institute of Thailand, Ministry of Agriculture, Chatuchak, Bangkok, THAILAND*
[c] *Department of Chemical Engineering, University of Waterloo, Ontario, CANADA*
[d] *Department of Chemical and Material Engineering, Rangsit University, Phathum Thani, THAILAND*

ARTICLEINFO

Article history:
Received 20 August 2013
Accepted 06 December 2013
Available online 09 December 2013

Keywords:
Epoxidized natural rubber;
Tensile properties;
Oil resistance.

ABSTRACT

The effects of blend ratio on cure characteristics, tensile properties and the resistance to oil and thermal aging of epoxidized natural rubber (ENR) blended with styrene butadiene rubber (SBR) was investigated in the presence of silica selected as a reinforcing filler due to its unique characteristic to interact with ENR. The composition of ENR and SBR was varied from 0 to 100%. The results indicate that the Mooney viscosity and cure time, t_{c90} decreased with an increase of ENR in the blends. The silica-filled ENR exhibited higher tensile properties and high crosslink density compared to silica-filled SBR. The oil and thermal aging resistance of the ENR/SBR blend were increased with increasing ENR content.

1. Introduction

The blending of two or more polymers by physical or chemical means may improve a variety of physical and chemical properties of the constituent polymers (Jovanovic *et al.*, 2013). The blending of rubbers plays an important role in enhancing the physical properties of

*Corresponding author (W. Arayapranee). Tel: +66-2-997-2222 Ext.3330. E-mail address: wanvimon@rsu.ac.th

the final vulcanized product. The rubber blends are frequently used in the rubber industry to obtain the best combination of compound properties, processability, and cost. Natural rubber (NR) is a renewable and sustainable material, which has various good properties, such as high tensile strength, high elongation, and outstanding resilience, lending itself to be used in various applications. NR is an unsaturated polymer that consists of mainly of cis-1,4-polyisoprene. It nevertheless has some drawbacks such as poor oil resistance due to its nonpolar nature; high sensitivity to heat, oxygen, and ozone due to its reactive double bonds. A variety of synthetic counterparts are made to meet some specific requirements such as for high temperature applications or for oil-in contact products. To extend the use of NR, a variety of modification methods can be used to partly or completely alter the NR structure to enhance its properties to meet some specific requirements. The modification of NR via epoxidation reaction is probably the most common method used to prepare a product that has some improved properties than those of the unmodified one. Epoxidation of NR is the reaction of the carbon double bond with an active oxygen atom to yield a three membered ring structure containing oxygen. Reduction of the unsaturated unit or converting part of the carbon double bond of NR would improve its oil resistances and oxidative properties. Epoxidized natural rubber (ENR) containing 50% mole epoxidation (ENR50) has similar oil resistance to medium nitrile rubber and has properties which resemble those of synthetic rubbers, whereas the tensile properties are near those of NR because the ENR50 still has some remaining carbon double bonds but suffers from poor ozone resistance and heat aging properties (Chuayjuljit *et al*., 2006; Ismail *et al*., 2000). SBR, nonpolar synthetic rubber, describes families of synthetic rubbers derived from styrene and butadiene. It has good abrasion resistance and thermal aging properties (Goyanes *et al*., 2008). The ENR/SBR blend should be beneficial for improved thermal and oxidative stability.

The main aim of this work was to study the effect of blend ratio on cure characteristics, mechanical properties, and aging resistance of silica-filled ENR/SBR rubber blends over a range of blend ratios. The aging property studies are of interest for thermal aging at 100°C for 72 h and two types of oil, namely low polarity oil and high polarity oil at room temperature for 72 h.

2. Research Methodology

2.1 Materials

High ammonia natural rubber latex (dry rubber content, DRC = 60%) was purchased from Thai Hua Rubber PCL., Rayong, Thailand. The latex is composed almost entirely of cis-1,4-polyisoprene. 98% formic acid was produced by Merck. 50% hydrogen peroxide (commercial grade), Teric 16A16, Methanol, and Sodium carbonate were purchased from GSP products Co., LTD., Thailand. Styrene butadiene rubber (SBR-1502) rubber was produced by BST Elastomers co., Ltd., Rayong, Thailand. Zinc Oxide (white seal) was purchased from Thai lysaght Co., Ltd., Thailand. Silica (TOKUSIL 233) was produced by Tokuyama Asia Pacific Pte., Ltd., Singapore. Benzothiazy l-2-cyclohexylsulfenamide (CBS, Monflex) was produced by MONFLEX PTE., Ltd., Singapore. Polyethylene glycol (PEG-4000) was purchased from Imperial industrial chemicals Co., Ltd., Thailand. Tetramethyl thiumram disulfide (TMTD) was purchased from Vessel Chemical Co., Ltd., Thailand. Wingstay-L and sulphur were purchased from GSP products Co., LTD., Thailand.

2.2 Preparation of *in-situ* epoxidized natural rubber

The formulation of ENR is shown in Table 1 Initially, ENR was prepared from dilute natural rubber latex (60% to 20% DRC with distilled water), 10% Teric16A16, as nonionic surfactant, was added to a 1 liter three-necked flask reactor, in which a controlled speed stirrer was mounted. The latex was stirred for 1 h, before a given amount of formic acid and hydrogen peroxide were slowly dropped into the reactor respectively using a peristaltic pump for a controlled addition rate. The latex was continuous stirred at 300 rpm for 6 h. A water bath was used to maintain the temperature at 50ºC. After the reaction, the ENR latex was coagulated by ethanol and the coagulum was washed repeatedly and dried thoroughly. ^{1}H-NMR spectra were recorded on a Bruker 300 MHz spectrometer and the conversion was determined as mol % epoxide by calculation using equation (1)

$$\text{mol \% epoxide} = \frac{I_{2.7}}{I_{2.7}+I_{5.1}}\times 100\% \quad \frac{I_{2.7}}{I_{2.7}+I_{5.1}}\times 100\% \qquad (1),$$

where I is the intensity of the ^{1}H-NMR signals and the subscripts represent a value of the chemical shift.

*Corresponding author (W. Arayapranee). Tel: +66-2-997-2222 Ext.3330. E-mail address: wanvimon@rsu.ac.th Volume 5 No.1 ISSN 2228-9860 eISSN 1906-9642. Online available at http://tuengr.com/V05/0011.pdf .

Table 1: Formulation used for epoxidized natural rubber

Ingredients	
NR latex (20% DRC)	1.7 mole
Teric 16A16	2 phr*
98% Formic acid	0.39 mole
50% H_2O_2	1.3 mole

*phr = parts per hundred rubber

2.3 Compounding of ENR/SBR blends

ENR was prepared by the above method providing about 43% mole epoxidation. A ENR/SBR rubber blend compounded via conventional vulcanization (C.V.) using a two-roll mill with various chemicals, according to the formulations for rubber compounds is shown in Table 2 The SBR was masticated first on a two-roll mill by passing it through the rolls many times and then added ENR. After that, ZnO, stearic acid, and accelerator were added and mixed for 3 min. with a rolling bank and cut on each side. Then sulphur was added and mixed for 2 min. The mixing was completed by the addition of sulphur at 70°C for 3 min. Compounded rubbers were left overnight at room temperature. In advance of the processing, the optimum cure time (t_{c90}) was determined on the basis of the results of curing characteristics using a rheometer (TECH-PRO, Cuyahoga Falls, Ohio, USA) according to ISO-3414 for 30 min at 160°C. Each rubber compound was compression molded at 160°C and t_{c90} min using a hydraulic press.

Table 2: Formulations for rubber compound

Ingredients	phr
ENR	100-0
SBR	0-100
Zinc oxide	5
Stearic acid	2
Silica (TOKUSIL233)	40
PEG4000	3
Wingstay-L	2
CBS	1.6
TMTD	0.3
Sulphur	2.5

2.4 Tensile properties and aging properties

The tensile properties of blended vulcanizates were determined using a universal testing machine (Model 5565; Instron Corp., Canton, MA) with a crosshead speed of 500 mm/min

and a 500 N load cell. The specimens were dumbbell shaped. The test specimens were aged for 72 h with hot air at 100°C and oil resistance was determined in accordance with the method described by ASTM D471-06. The specimens to be tested were immersed in hydrocarbon oils at room temperature for 72hr. Oils used in this testing were, IRM 901 as low polarity oil and IRM 903 as high polarity oil. When the specified test time was reached, the test specimens were removed from the oil and wiped with tissue paper to remove the excess oil from the surface before properties testing.

2.5 Estimation of crosslink density

The estimation of crosslink density of rubber blends from the stress-stain data was used the relationship of $\sigma/(\lambda-\lambda^{-2})$ which respect to $1/\lambda$ according to equation (2), which is of the Mooney-Rivlin equation.

$$\frac{\sigma}{\lambda-\lambda^{-2}} = 2C_1 + \frac{2C_2}{\lambda} \tag{2}$$

where the constants C_1 and C_2 can be obtained. $2C_1$ represents the y-axis intercept of the curve whereas $2C_2$ represents the slope of the curve. From the plot, a linear trend is observed and the physically effective crosslink density (η_{PHY}) can thus be determined. Using the value of the y-axis intercept, the physically effective crosslink density is calculated by equation (3) with R, the gas constant (8.314 J.mole^{-1}K^{-1}) and T, the absolute temperature (273.15 K).

$$\eta_{PHY} = \frac{C_1}{RT} \tag{3}$$

2.6 Morphorogy of the blend

The morphology of the NR and ENR latex was examined using a JEM-1220 transmission electron micro-scope (TEM) with a magnification of 3,000 and 80 kV. A thorough understanding of blend morphology is important because the properties of polymer blends are strongly dependent upon it. A scanning electron microscopic (SEM) Model JEOL-5600LV; Tokyo, Japan was used to observe the tensile specimens fractured surface at a magnification of 3,000. The samples were mounted on aluminum stubs and sputter coated with a thin layer of gold to avoid electrostatic charging during examination.

*Corresponding author (W. Arayapranee). Tel: +66-2-997-2222 Ext.3330. E-mail address: wanvimon@rsu.ac.th

International Transaction Journal of Engineering, Management, & Applied Sciences & Technologies. Volume 5 No.1 ISSN 2228-9860 eISSN 1906-9642. Online available at http://tuengr.com/V05/0011.pdf .

3. Results and Discussion

The in situ epoxidation of the NR latex (Figure 1) using hydrogen peroxide and formic acid also yields epoxidized natural rubber (ENR). The characteristics of the ENR latex were analyzed based on proton nuclear magnetic resonance (^{1}H-NMR). The unsaturated methine protons of cis-1,4-isoprene units appeared at 1.68, 2.05, and 5.1 ppm, respectively. The characteristic peaks for olefinic and oxirane methine protons in the ^{1}H-NMR spectrums appear at 5.1 and 2.7 respectively. The results reveal that the increasing signals at 2.7, is a result of the increment of the epoxide group as shown in Figure 2. In Figure 3, the morphology of NR and the ENR latex were examined by transmission electron microscopy (TEM). The particles of NR and ENR are spherical and have a smooth surface and darker areas at the center represent the NR core regions, which contain the carbon double bonds stained with OsO_4, (Figure 3a) and the lighter color areas in Figure 3b show domains which indicate the region of lower carbon double bonds concentration. The observed proton NMR signals and TEM micrograph can be qualitatively used to confirm that the NR was epoxidized.

3.1 Processability and Cure characteristics

The result of the Mooney viscosity of ENR/SBR rubber blends is shown in Figure 4. With the increment of SBR, the value of the Mooney viscosity of ENR/SBR rubber blend increased with increasing SBR content due to the reduction of its bulkiness, which is attributed to the restriction of molecular chain movement. This resulted in an increase in the Mooney viscosity of the compound rubber blends. The optimum cure time is the time for the vulcanization reaction required to obtain optimum physical properties. It can be seen that each compound exhibits different cure characteristics, which is attributed to the fact that each type of rubber possesses difference properties, such as structure, polarity, and compatibility.

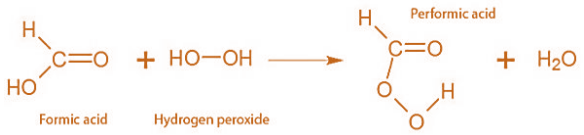

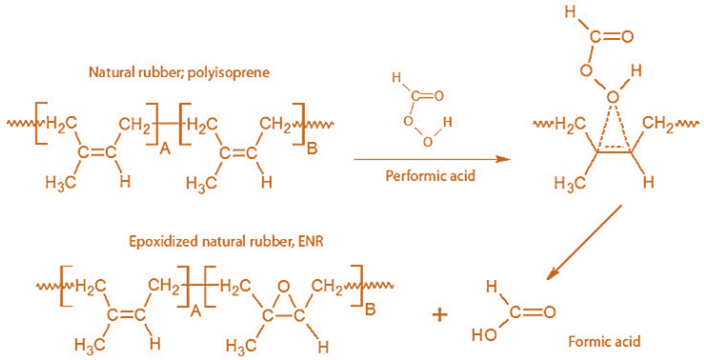

Figure 1: The *in-situ* epoxidation of NR employing hydrogen peroxide and formic acid.

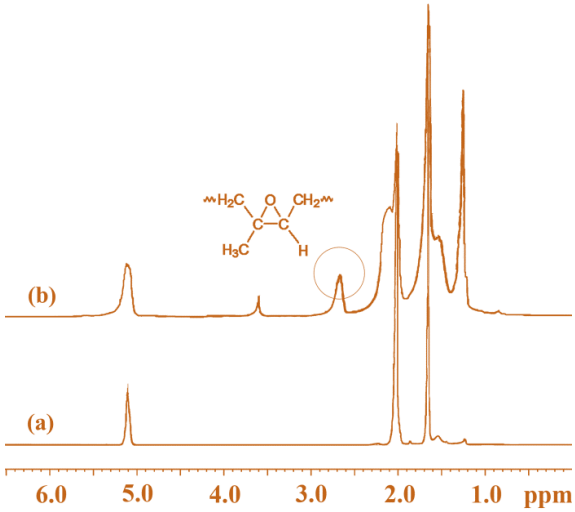

Figure 2: ^{1}H-NMR spectra for (a) NR, and (b) ENR containing 43% epoxide group.

Figure 5 shows the variation of optimum cure time of the SBR/ENR blend with blend ratio. It can be seen that t_{c90} decreases with increasing ENR composition in the blend. Owing to the activation of an adjacent double bond by the epoxide group (Sadequl et al., 1998), the optimum cure time for ENR is shorter than that of SBR. The reduction of t_{c90} with increasing ENR composition in the blend is more significant. This may be due to chain opening of the epoxy group on ENR (rubber-rubber interaction) which participated in the vulcanization reaction leading to a low cure time of the blends having high ENR content (Hakim *et al.*, 2009).

*Corresponding author (W. Arayapranee). Tel: +66-2-997-2222 Ext.3330. E-mail address: wanvimon@rsu.ac.th International Transaction Journal of Engineering, Management, & Applied Sciences & Technologies. Volume 5 No.1 ISSN 2228-9860 eISSN 1906-9642. Online available at http://tuengr.com/V05/0011.pdf .

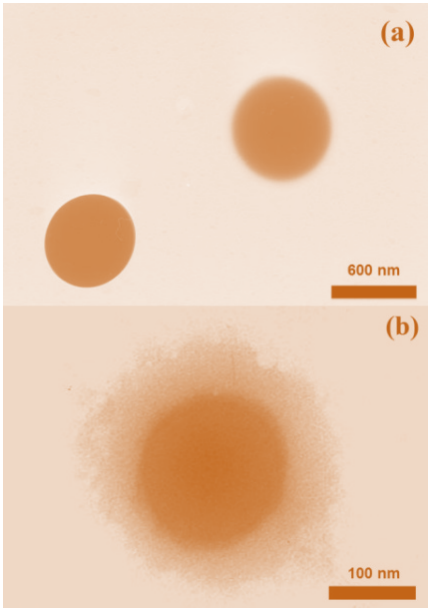

Figure 3: TEM micrograph at 80,000× (a) NR (b) ENR.

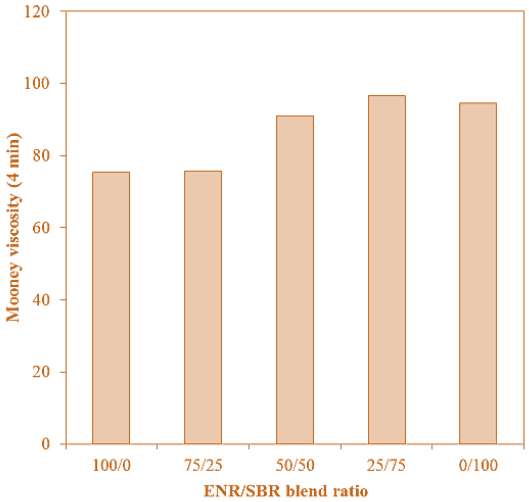

Figure 4: Mooney viscosity ENR/SBR blends.

3.2 Tensile properties and Crosslink density

The tensile instrument provided values of the tensile strength and tensile modulus. Figure 6 shows the tensile properties of vulcanizates of ENR/SBR blend. The tensile strength of high ENR blend ratio is higher than the low ENR blend ratio due to the remaining strain-induced crystallinity of ENR (Chuayjuljit *et al*., 2006). On the other hand, it can be seen that the silica filler distribution in rubber matrix is affected significantly by the difference in polarity between the ENR and SBR. This may be attributed to a higher filler-rubber interaction between the epoxide groups in ENR and the hydroxyls on the silica surface (Poh *et al*., 2002) which provided an improvement in the rubber-filler interaction (Manna *et al*., 1998) and led to a better distribution of filler in the rubber matrix; thus a higher tensile strength should be

observed in high ENR blend ratio when compared with that of high SBR blend ratio.

In Figure 6, it can be seen that the tensile modulus increased with increasing ENR content in the rubber blends. This is an indication of the rubber stiffness for high content of ENR due to the filler-rubber interactions. The data from stress-strain measurements for rubber films was used to construct plots of $\sigma/(\lambda-\lambda^{-2})$ against $1/\lambda$ to obtain the values of the elastic constants and estimation of crosslink density. The crosslink density is expressed in terms of moles of effective network chains per cubic centimeter of rubber as shown in Figure 7. It can be seen that the crosslink density increases as the ENR increase, resulting in high tensile strength.

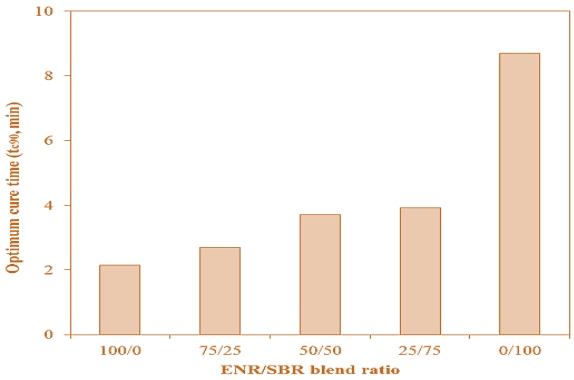

Figure 5: Optimum cure time of ENR/SBR blends.

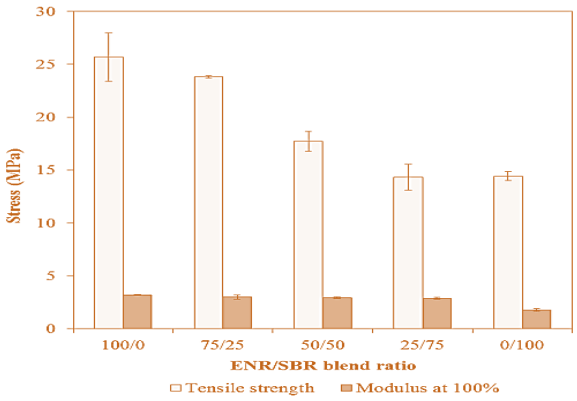

Figure 6: Tensile properties of ENR/SBR blends.

*Corresponding author (W. Arayapranee). Tel: +66-2-997-2222 Ext.3330. E-mail address: wanvimon@rsu.ac.th International Transaction Journal of Engineering, Management, & Applied Sciences & Technologies. Volume 5 No.1 ISSN 2228-9860 eISSN 1906-9642. Online available at http://tuengr.com/V05/0011.pdf .

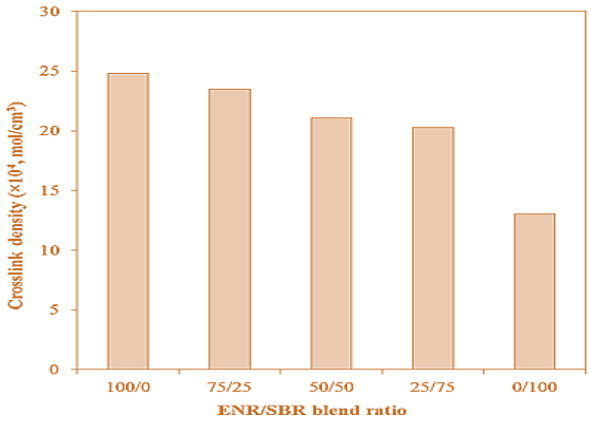

Figure 7: Crosslink density of ENR/SBR blends.

3.3 Thermal aging and oil resistance

The thermal aging and oil resistance results are presented as tensile properties. The thermal aging properties measurement at 100°C for 72 h is presented in Figure 8. It can be seen that the results of tensile strength are increased with increasing ENR; the lowest tensile strength was found for rich SBR and the highest tensile strength was found for rich ENR. This is due to the good filler-rubber and rubber-rubber interaction of ENR, whereas the tensile strength decreased compared with before aging. It can be seen that the lower of tensile strength after aging is due to thermal aging. Rubbers undergoing oxidation reactions resulted in chain scission or oxidative breakdown. For the case of oil resistance, it can be seen that tensile strength increased with increasing ENR because the small amount of unsaturated in ENR reduced the elasticity of the rubber chains leading to a rigid rubber material and better interaction of silica in the polar rubber matrix, which consequently resulted in less oil penetration into the rubber matrices. This also implies that the presence of polarity of the rubber plays a significant role in providing a good filler-rubber interaction which resisted the penetration of the oil into the gaps between the rubber chains.

Figure 9 shows the results of 100% Modulus of rubber vulcanizate, which indicates the stiffness of the material. It can be seen that the Modulus increased with increasing ENR due to chain scission or oxidative breakdown with oxygen while aging. This resulted in the generation of rubber macro-radicals, which formed rubber chains with some degree of branching. Thus the vulcanizates would become stiffer resulting in higher Modulus. In the case of oil immersion, the results show a similar trend of on oil immersion of tensile strength.

3.4 Morphology of blend

Morphology is a major factor of rubber blends, which determines the extent to which the blends are compatible. It is well known that the phase structure of the blend is influenced by several factors, including the surface characteristics, blend ratio, viscosity of each component and compounding process. The morphology of the rubber blend before aging tensile fracture surface at a magnification of 3000 is shown in Figure 10. After the polymer was stretched with high stress, it can be observed that the fracture had white fibrils on the surface, which is a typical feature in ductile failure. The ENR vulcanizate had a high amount of white fibrils and a rough surface, which is an indication of a higher tensile strength than observed for the SBR vulcanizates. This is due to high dispersion of silica in ENR matrix. In the case of SBR, the agglomeration of silica in the blend matrix occurred and smooth surface without white fibrils and many small pores indicated that the interaction between the silica and rubber was poor leading to the low values for the tensile properties. The morphology of the ENR/SBR blend with a 50/50 ratio is shown in Figure 10b; it can be seen that the small amount of white fibrils and many tiny holes are present. This implies that ENR/SBR blends are immiscible which may be due to the difference of polarity in each rubber component.

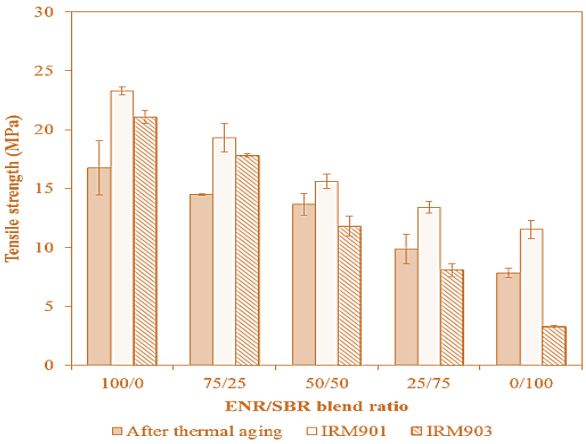

Figure 8: Tensile strength of ENR/SBR blends after aging.

*Corresponding author (W. Arayapranee). Tel: +66-2-997-2222 Ext.3330. E-mail address: wanvimon@rsu.ac.th International Transaction Journal of Engineering, Management, & Applied Sciences & Technologies. Volume 5 No.1 ISSN 2228-9860 eISSN 1906-9642. Online available at http://tuengr.com/V05/0011.pdf .

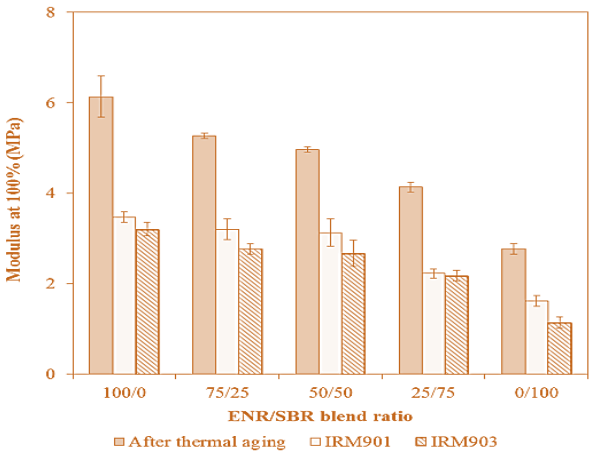

Figure 9: Modulus at 100% of ENR/SBR blends after aging.

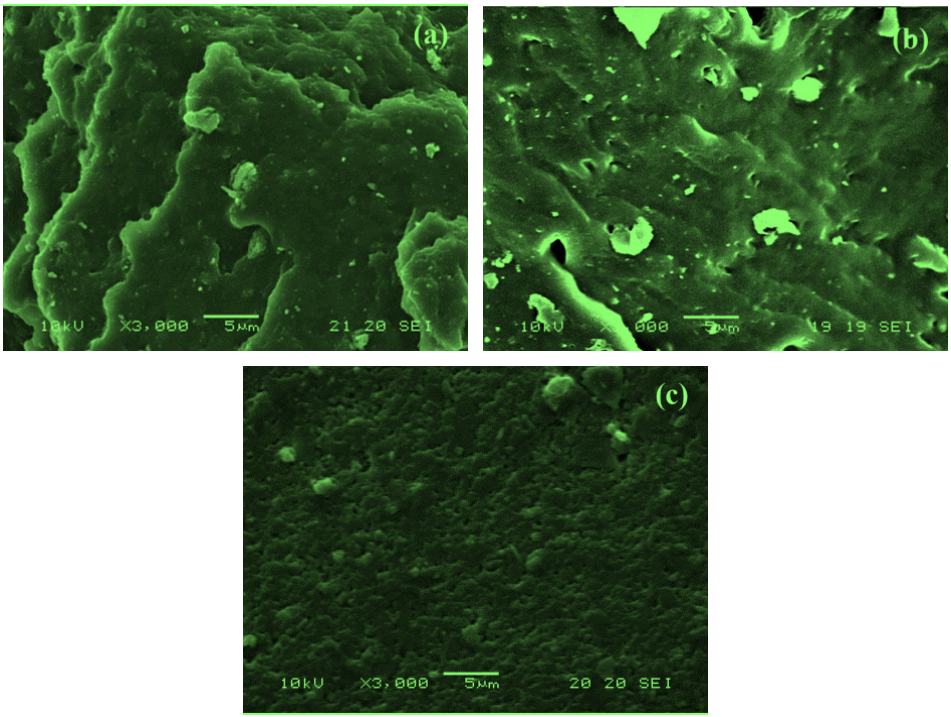

Figure 10: Crosslink density of ENR/SBR blends.

4. Conclusion

The effect of blend ratio on cure characteristics and physico-mechanical properties of silica-filled ENR/SBR blends were investigated. Mooney viscosity decreased with an increase in ENR content in the blends, whereas vulcanization was accelerated in the presence of ENR content in the blends. The tensile properties of the vulcanizate were increased with increasing ENR content in the rubber blends. In addition to the mechanical properties, attention was also given to the resistance to thermal aging and oil on the blends. Resistance to thermal aging and oil of the rubber blend was mainly governed by polar functional groups in the rubber matrix

as well as the silica. It is found that increasing ENR content in the silica-filled ENR/SBR blend led to an improvement in thermal aging and oil resistance, probably due to the improved silica dispersion in the rubber matrix.

5. Acknowledgements

We gratefully acknowledge the financial support of Thailand Research fund through the Royal Golden Jubilee Ph.D. Program (grant #PHD/0152/2554). We also thank the Rubber Research Institute of Thailand for assistance throughout the study.

6. References

Chuayjuljit, S., C. Yaowsang, N. Na-Ranong, and P. Potiyaraj. (2006). *Oil resistance and physical properties of in situ epoxidized natural Rubber from high ammonia concentrated latex. Journal of Applied Polymer Science,* 100(5), 3948–3955.

Goyanes, S., C.C. Lopez, G.H. Rubiolo, F. Quasso, and A.J. Marzocca. (2008). *Thermal properties in cured natural rubber/styrene butadiene rubber blends. European Polymer Journal*, 44(5), 1525-1534.

Hakim, R. N. and H. Ismail. (2009). *Comparison of the effects of organoclay loading on the curing and mechanical properties of organoclay-filled epoxidised natural rubber nanocomposites and organo-clay-filled, Journal of Applied Polymer Science*, 20(2), 37-59.

Hanafi Ismail and S. Suzaimah. (2000). *Styrene butadiene rubber/epoxidized natural rubber blends: dynamic properties, curing characteristics and swelling studies, Polymer Testing*, 19(8), 879–888.

Jovanovic, V., S. S. Jovanovic, J. B. Simendic, G. Markovic, and M. M. Cincovic. (2013). *Composites based on carbon black reinforced NBR/EPDM rubber blends. Composites Part B: Engineering,* 45(1), 333–340.

Manna, A. K., A. K. Bhattacharyya, P. P. De, D. K. Tripathy, S. K. De, and D. G. Peiffer. (1998) *Effect of silane coupling agent on the chemorheological behaviour of epoxidised natural rubber filled with precipitated silica. Polymer,* 39(26), 7113-7117.

Poh, B.T., H. Ismail, and K.S. Tan. (2002). *Effect of filler loading on tensile and tear properties of SMR L/ENR 25 and SMR L/SBR blends cured via a semi-efficient vulcanization system, Polymer Testing* 21(7), 801–806.

Sadequl, A. M., U. S. Ishiaku, H. Ismail and B. T. Poh. (1998).*The effect of accelerator /sulphur ratio on the scorch time of epoxidized natural rubber. European Polymer Journal*, 34(1), 51-57

*Corresponding author (W. Arayapranee). Tel: +66-2-997-2222 Ext.3330. E-mail address: wanvimon@rsu.ac.th

Chanin Ngudsuntear earned his bachelor degree in Chemical Engineering from Rangsit University in 2011. He has been studying for the Ph.D. Degree in the Department of Chemical Engineering at Kasetsart University, Thailand.

Dr.Sunun Limtrakul is an Associate Professor of Department of Chemical Engineering at Kasetsart University. She holds a B.Sc. in Industrial Chemistry from Chiengmai University, MS in Chemical Engineering from Chulalongkorn University and Ph.D. degrees in Chemical Engineering from Washington University. Dr. Sunun is interested in reaction engineering, modeling and simulation, transport phenomena, and polymer electrolyte membrane (PEM) fuel cell.

Dr. Terdthai Vatanatham earned his bachelor degree from Chulalongkorn University Thailand, Master degree in Structural Engineering from Pennsylvania State University Thailand and Ph.D. in Chemical Engineering from University of Akron. He is an Associate Professor at Kasetsart University, Thailand. He is interested in reaction engineering, equipment design, and PEM fuel cell.

Adul Na Wichien is a scientist, Professional Level, at Rubber Research Institute of Thailand (RRIT). He received his B.Eng. from Nakhon Sawan Rajabhat University. He focuses on applications and modified of natural rubber and its derivative and waste from agriculture.

Dr.Garry L Rempel is a Professor of Department of Chemical Engineering at University of Waterloo. He received his BSc and Ph.D. from University of British Columbia. He has authored or coauthored more than 300 publications and is the holder of 35 patents. He is interested in applied catalysis, green chemical engineering and advanced rubber technology

Dr.Wanvimon Arayapranee is an Associate Professor of Department of Chemical Engineering and Material Engineering at Rangsit University. She received her B.Sc. in Industrial Chemistry from Chiengmai Uniersity. She earned her Master's degree in Chemical Engineering from King Mongkut's University of Technology Thonburi and Ph.D. (Chemical Technology) from Chulalongkorn University. Dr.Wanvimon's current interests involve polymer engineering and modification of natural rubber.

Peer Review: This article has been internationally peer-reviewed and accepted for publication according to the guidelines in the journal's website. Note: Original version of this article was accepted and presented at the Third International-Thai Chemical Engineering and Applied Chemistry (TIChE) Conference, jointly organized by Department of Chemical Engineering, Faculty of Engineering, Khon Kaen University and Thai Institute of Chemical Engineering and Applied Chemistry, at Pullman Khon Kaen Raja Orchid Hotel, Khon Kaen, THAILAND, October 17-18, 2013.

International Transaction Journal of Engineering, Management, & Applied Sciences & Technologies

http://TuEngr.com

An Efficient Formulation of Off-line Model Predictive Control for Nonlinear Systems Using Polyhedral Invariant Sets

Pornchai Bumroongsri [a*], Pornpun Arundechachai [b], and Soorathep Kheawhom [b]

[a] *Department of Chemical Engineering Faculty of Engineering, Mahidol University, THAILAND*
[b] *Department of Chemical Engineering Faculty of Engineering, Chulalongkorn University, THAILAND*

ARTICLEINFO

Article history:
Received 20 August 2013
Accepted 06 December 2013
Available online 09 December 2013

Keywords:
control law;
real-time interpolation;
scheduling parameter;
MPC algorithm

ABSTRACT

In this research, an efficient formulation of off-line model predictive control for nonlinear systems is presented. The nonlinear systems are reformulated as linear parameter varying systems so their complexity is reduced without any loss of generality. The on-line computational burdens are decreased by pre-computing off-line the sequences of explicit control laws corresponding to the sequences of polyhedral invariant sets. At each sampling time, the current state and the scheduling parameter are measured. The real-time control law is then calculated by linear interpolation between the pre-computed control laws. The results indicate that the proposed algorithm can achieve better control performance compared to the previously developed off-line robust model predictive control algorithm because the scheduling parameter is incorporated into the controller design.

1. Introduction

Chemical processes are multivariable processes that change one or more chemical compounds to the desired products. Chemical processes are usually involved with many complex chemical reactions which are nonlinear. In order to efficiently control nonlinear chemical processes, a multivariable nonlinear control algorithm needs to be developed (Qin and Badgwell, 2003; Ramesh, *et al.*, 2009; Manenti, 2011).

*Corresponding author (P.Bumroongsri). Tel: +66-2-8892138 Ext.6101. E-mail address: pornchai.bum@mahidol.ac.th. ©2014. International Transaction Journal of Engineering, Management, & Applied Sciences & Technologies. Volume 5 No.1 ISSN 2228-9860 eISSN 1906-9642. Online available at http://tuengr.com/V05/0025.pdf .

Model predictive control (MPC) is an advanced control algorithm for multivariable processes. MPC is widely used in many chemical processes because input and output constraints are considered in a systematic manner (Morari and Lee, 1999; Mayne, *et al.*, 2000; Lee, 2011). A linear model is typically used in MPC formulation because the on-line optimization problem can be easily solved. However, most of the chemical processes are nonlinear. When the operating conditions undergo changes, the performance of linear MPC can significantly deteriorate (Bumroongsri and Kheawhom, 2012a; Yu, *et al.*, 2012; Suzuki and Sugie, 2007).

In order to deal with nonlinear chemical processes, nonlinear MPC was developed by Magni, *et al.* (2001). A full nonlinear model was used in MPC formulation. The complicated nonlinear control problem had to be solved at each sampling instant so the algorithm was computationally prohibitive in practical situations.

The reformulation of nonlinear systems into linear parameter varying (LPV) systems is a promising technique to reduce the complexity of nonlinear systems. LPV systems are linear systems whose dynamics depend on time-varying parameters that can be measured on-line. Therefore, nonlinear systems can be reformulated as LPV systems without any loss of generality (Park and Jeong, 2004; Toth, 2010; Jungers, *et al.*, 2011). Off-line MPC for LPV systems was previously developed by Bumroongsri and Kheawhom (2012b). Although the on-line computational time was significantly reduced, the stabilizable region of the algorithm was small because the ellipsoidal invariant sets were used in problem formulation.

In order to enlarge the size of stabilizable region, an off-line formulation of robust MPC using polyhedral invariant sets was proposed by Bumroongsri and Kheawhom (2012c). The polyhedral invariant sets were used in the problem formulation so a significantly larger stabilizable region was obtained. Although the stabilizable region was enlarged, the conservativeness was obtained because the scheduling parameter was not incorporated into the controller design.

In this research, an efficient formulation of off-line MPC using polyhedral invariant sets is presented. The sequences of explicit control laws corresponding to the sequences of polyhedral invariant sets are pre-computed off-line. At each sampling instant, the current state and the

scheduling parameter are measured. The real-time control law is then calculated by linear interpolation between the pre-computed control laws. The proposed algorithm can give a relatively large stabilizable region because the polyhedral invariant sets are computed in the off-line problem formulation. Moreover, the scheduling parameter is used in real-time interpolation between the pre-computed control laws so better control performance compared to an off-line robust MPC algorithm of Bumroongsri and Kheawhom (2012c) can be obtained.

This article is organized as follows. In section 2, the problem description is presented. The proposed algorithm is presented in section 3. In section 4, the proposed algorithm is applied to a case study and the results are discussed. Finally, the paper is concluded in section 5.

2. Problem Description

The model considered here is the following linear parameter varying (LPV) systems (The techniques to transform nonlinear systems into LPV systems can be found in Toth (2010).)

$$x(k+1) = A(p(k))x(k) + Bu(k) \quad (1),$$

$$y(k) = Cx(k) \quad (2),$$

where $x(k)$ is a vector of states, $u(k)$ is a vector of control inputs and $y(k)$ is a vector of outputs. In this research, we assume that the scheduling parameters $p(k) = [p_1(k), p_2(k),..., p_L(k)]$ are measurable on-line at each sampling instant. Moreover, we assume that

$$A(p(k)) \in \Omega, \Omega = Co\{A_1, A_2,..., A_L\} \quad (3),$$

where Ω is the polytope, Co is the convex hull, A_j are the vertices of the convex hull and L is the number of vertices of Ω. Any $A(p(k))$ within Ω is a linear combination of the vertices such that

$$A(p(k)) = \sum_{j=1}^{L} p_j(k)A_j, \sum_{j=1}^{L} p_j(k) = 1, 0 \le p_j(k) \le 1 \quad (4),$$

*Corresponding author (P.Bumroongsri). Tel: +66-2-8892138 Ext.6101. E-mail address: pornchai.bum@mahidol.ac.th. International Transaction Journal of Engineering, Management, & Applied Sciences & Technologies. Volume 5 No.1 ISSN 2228-9860 eISSN 1906-9642. Online available at http://tuengr.com/V05/0025.pdf .

The objective is to find a state feedback control law that stabilizes LPV systems (1) and (2) subject to the following input and output constraints

$$u_{h,\min} \le u_h(k+i/k) \le u_{h,\max}, h = 1,2,....,n_u, i = 0,1,2,...,\infty \quad (5),$$

$$y_{r,\min} \le y_r(k+i/k) \le y_{r,\max}, r = 1,2,....,n_y, \ i = 0,1,2,...,\infty \quad (6),$$

where n_u is the number of control inputs, n_y is the number of outputs, $u_{\min}$ and $u_{\max}$ are the vectors of input constraints, $y_{\min}$ and $y_{\max}$ are the vectors of output constraints.

3. The Proposed Off-line MPC Algorithm

In this section, an off-line MPC formulation for nonlinear systems is developed. The nonlinear systems are reformulated as LPV systems so their complexity is significantly reduced. Most of the solutions of the control problem are calculated off-line so the on-line computational time is significantly reduced.

3.1 Off-line Procedures

3.1.1 Off-line Step 1: Compute the Sequences of Off-line State Feedback Gains

Choose a sequence of states $x_i, i \in \{1,2,...,N\}$ and solve the optimization problem presented by Bumroongsri and Kheawhom (2012b) off-line to obtain the sequences of state feedback gains $K_{i,j}, \forall i = 1,2,...., N, \forall j = 1,2,...., L$ where N is the number of the chosen states and L is the number of vertices of Ω.

3.1.2 Off-line Step 2: Compute the Sequences of Polyhedral Invariant Sets

Given the state feedback gains $K_{i,j}$ from 3.1.1. For each $K_{i,j}$, the corresponding polyhedral invariant set $S_{i,j} = \{x / M_{i,j} x \le d_{i,j}\}$ is computed by following these steps

(1) Set $M_{i,j} = [C^T, -C^T, K_{i,j}^T, -K_{i,j}^T]^T$, $d_{i,j} = [y_{\max}^T, y_{\min}^T, u_{\max}^T, u_{\min}^T]^T$ and $m = 1$.

(2) Select row m from $(M_{i,j}, d_{i,j})$ and check $\forall l, \ l = 1,...,L$ whether $M_{i,j,m}(A_l + B_l K_{i,j})x \le d_{i,j,m}$ is redundant with respect to $(M_{i,j}, d_{i,j})$ by solving the following problem

$$\max \; W_{i,j,m,l} \tag{7}$$

$$\text{s.t.} \quad W_{i,j,m,l} = M_{i,j,m}(A_l + B_l K_{i,j})x - d_{i,j,m} \tag{8}$$

$$M_{i,j}x \le d_{i,j} \tag{9}$$

If $W_{i,j,m,l} > 0$, the constraint $M_{i,j,m}(A_l + B_l K_{i,j})x \le d_{i,j,m}$ is non-redundant with respect to $(M_{i,j}, d_{i,j})$. Then, add non-redundant constraints to $(M_{i,j}, d_{i,j})$ by assigning $M_{i,j} = [M_{i,j}^T, (M_{i,j,m}(A_l + B_l K_{i,j}))^T]^T$ and $d_{i,j} = [d_{i,j}^T, d_{i,j,m}^T]^T$.

(3) Let $m = m + 1$ and return to step (2). If m is strictly larger than the number of rows in $(M_{i,j}, d_{i,j})$ then terminate.

3.2 On-line Procedures

At each sampling time, measure the current state $x(k)$ and the scheduling parameter $p(k)$. When $x(k) \in S_{i,j}$, $x(k) \notin S_{i+1,j}$, $\forall j = 1,2,...,L$, $i \ne N$, the real-time state feedback gain $K(\alpha(k)) = \alpha(k)(\sum_{j=1}^{L} p_j(k) K_{i,j}) + (1-\alpha(k))(\sum_{j=1}^{L} p_j(k) K_{i+1,j})$ can be calculated from $\alpha(k)$ obtained by solving the following optimization problem

$$\min \; \alpha(k) \tag{10}$$

$$\text{s.t.} \quad u_{\min} \le K(\alpha(k))x(k) \le u_{\max} \tag{11}$$

$$A(p(k))x(k) + BK(\alpha(k))x(k) \in S_{i,j}, \forall j = 1,2,...,L \tag{12}$$

$$0 < \alpha(k) \le 1 \tag{13}$$

It is seen that the on-line optimization problem is only linear programming so it can be efficiently solved (Boyd and Vandenberghe, 2004). (11) is for guaranteeing input constraint satisfaction and (12) is for guaranteeing that the next predicted state still lies in the polyhedral

*Corresponding author (P.Bumroongsri). Tel: +66-2-8892138 Ext.6101. E-mail address: pornchai.bum@mahidol.ac.th.

International Transaction Journal of Engineering, Management, & Applied Sciences & Technologies. Volume 5 No.1 ISSN 2228-9860 eISSN 1906-9642. Online available at http://tuengr.com/V05/0025.pdf .

invariant sets computed off-line.

4. Results and Discussion

Consider the nonlinear two-tank system (Angeli, *et al.*, 2000) which is described by the following equation

$$\rho S_1 \dot{h}_1 = -\rho A_1 \sqrt{2gh_1} + u \quad (14),$$

$$\rho S_2 \dot{h}_2 = \rho A_1 \sqrt{2gh_1} - \rho A_2 \sqrt{2gh_2} \quad (15),$$

where h_1 is the water level in tank 1, h_2 is the water level in tank 2 and u is the inlet water flow. The schematic diagram of the nonlinear two-tank system is shown in Figure 1.

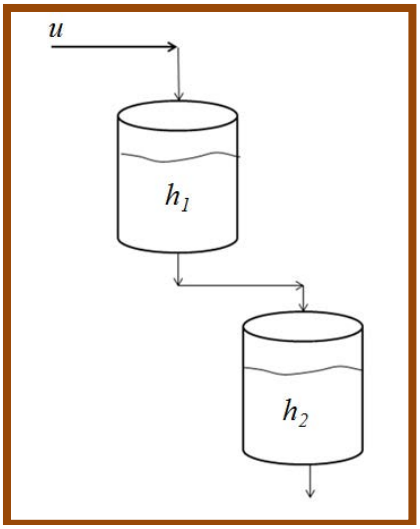

Figure 1: The schematic diagram of the nonlinear two-tank system.

The operating parameters of the nonlinear two-tank system are shown in Table 1.

Table 1: The operating parameters of the nonlinear two-tank system.

Parameter	Value	Unit
S_1	2,500	cm^2
S_2	1,600	cm^2
A_1	9	cm^2
A_2	4	cm^2
g	980	cm/s^2
ρ	0.001	kg/cm^3
$h_{1,eq}$	14	cm
$h_{2,eq}$	70	cm

Let $\overline{h_1} = h_1 - h_{1,eq}$, $\overline{h_2} = h_2 - h_{2,eq}$ and $\overline{u} = u - u_{eq}$ where subscript eq is used to denote the corresponding variable at equilibrium condition, the objective is to regulate $\overline{h_2}$ to the origin by manipulating $\overline{u}$. The input and output constraints are given as follows

$$\left|\overline{u}\right| \le 1.5 \text{ kg/s}, \quad \left|\overline{h_1}\right| \le 13 \text{ cm}, \quad \left|\overline{h_2}\right| \le 50 \text{ cm} \tag{16},$$

By evaluating the Jacobian matrix of (14) and (15) along the vertices of the constraints set (16), we have that all the solutions of (14) and (15) are also the solutions of the following differential inclusion

$$\begin{bmatrix} \rho S_1 \dot{\overline{h}}_1 \\ \rho S_2 \dot{\overline{h}}_2 \end{bmatrix} \in \left(\sum_{j=1}^{4} p_j A_j \right) \begin{bmatrix} \overline{h}_1 \\ \overline{h}_2 \end{bmatrix} + \begin{bmatrix} 1 \\ 0 \end{bmatrix} \overline{u} \tag{17},$$

where $A_j, j = 1,...,4$ are given by

$$A_1 = \begin{bmatrix} -\rho A_1 \sqrt{\frac{2g}{h_{1,\min}}} & 0 \\ \rho A_1 \sqrt{\frac{2g}{h_{1,\min}}} & -\rho A_2 \sqrt{\frac{2g}{h_{2,\min}}} \end{bmatrix}, \quad A_2 = \begin{bmatrix} -\rho A_1 \sqrt{\frac{2g}{h_{1,\max}}} & 0 \\ \rho A_1 \sqrt{\frac{2g}{h_{1,\max}}} & -\rho A_2 \sqrt{\frac{2g}{h_{2,\min}}} \end{bmatrix}$$

$$A_3 = \begin{bmatrix} -\rho A_1 \sqrt{\frac{2g}{h_{1,\min}}} & 0 \\ \rho A_1 \sqrt{\frac{2g}{h_{1,\min}}} & -\rho A_2 \sqrt{\frac{2g}{h_{2,\max}}} \end{bmatrix}, \quad A_4 = \begin{bmatrix} -\rho A_1 \sqrt{\frac{2g}{h_{1,\max}}} & 0 \\ \rho A_1 \sqrt{\frac{2g}{h_{1,\max}}} & -\rho A_2 \sqrt{\frac{2g}{h_{2,\max}}} \end{bmatrix} \tag{18},$$

and $p_j, j = 1,...,4$ are given by

$$p_1 = \left(\frac{(1/\sqrt{h_{1,\max}}) - (1/\sqrt{h_1})}{(1/\sqrt{h_{1,\max}}) - (1/\sqrt{h_{1,\min}})} \right) \left(\frac{(1/\sqrt{h_{2,\max}}) - (1/\sqrt{h_2})}{(1/\sqrt{h_{2,\max}}) - (1/\sqrt{h_{2,\min}})} \right)$$

*Corresponding author (P.Bumroongsri). Tel: +66-2-8892138 Ext.6101. E-mail address: pornchai.bum@mahidol.ac.th.

International Transaction Journal of Engineering, Management, & Applied Sciences & Technologies. Volume 5 No.1 ISSN 2228-9860 eISSN 1906-9642. Online available at http://tuengr.com/V05/0025.pdf .

$$p_2 = \left(\frac{(1/\sqrt{h_1}) - (1/\sqrt{h_{1,\min}})}{(1/\sqrt{h_{1,\max}}) - (1/\sqrt{h_{1,\min}})} \right) \cdot \left(\frac{(1/\sqrt{h_{2,\max}}) - (1/\sqrt{h_2})}{(1/\sqrt{h_{2,\max}}) - (1/\sqrt{h_{2,\min}})} \right)$$

$$p_3 = \left(\frac{(1/\sqrt{h_{1,\max}}) - (1/\sqrt{h_1})}{(1/\sqrt{h_{1,\max}}) - (1/\sqrt{h_{1,\min}})} \right) \cdot \left(\frac{(1/\sqrt{h_2}) - (1/\sqrt{h_{2,\min}})}{(1/\sqrt{h_{2,\max}}) - (1/\sqrt{h_{2,\min}})} \right)$$

$$p_4 = \left(\frac{(1/\sqrt{h_1}) - (1/\sqrt{h_{1,\min}})}{(1/\sqrt{h_{1,\max}}) - (1/\sqrt{h_{1,\min}})} \right) \cdot \left(\frac{(1/\sqrt{h_2}) - (1/\sqrt{h_{2,\min}})}{(1/\sqrt{h_{2,\max}}) - (1/\sqrt{h_{2,\min}})} \right) \quad (19),$$

The discrete-time model is obtained by discretization of (17) using Euler first-order approximation (Seborg, *et al.*, 2004) with a sampling period of 0.5 s and it is omitted here for brevity.

Figure 2 shows the polyhedral invariant sets computed off-line by the proposed algorithm. Figure 3 shows the polyhedral invariant sets computed off-line by an off-line robust MPC algorithm of Bumroongsri and Kheawhom (2012c). For both algorithms, the polyhedral invariant sets are computed by choosing the same sequence of states $x_i, i \in \{1,2,...,5\}$. Note that with the same number of chosen states, the proposed algorithm requires larger number of polyhedral invariant sets than an off-line robust MPC algorithm of Bumroongsri and Kheawhom (2012c). This is due to the fact that for the proposed algorithm, the number of sequences of polyhedral invariant sets computed is equal to the number of the vertices of the polytope Ω. In comparison, only a sequence of polyhedral invariant sets needs to be computed off-line for an off-line robust MPC algorithm of Bumroongsri and Kheawhom (2012c).

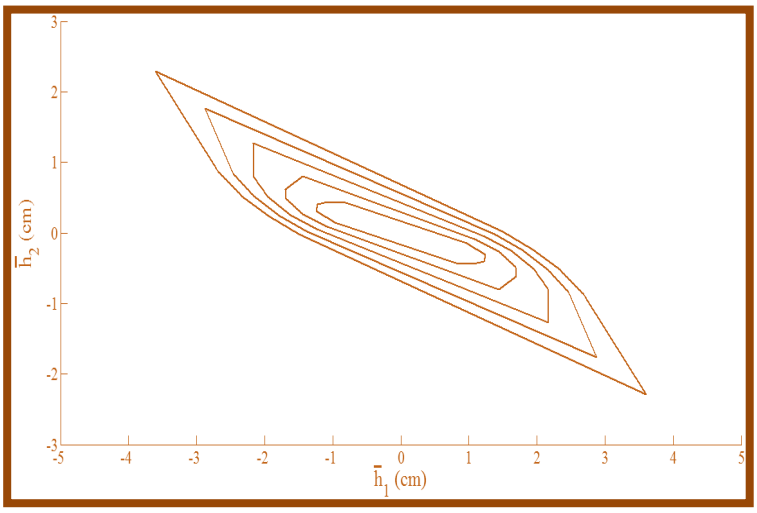

(2.1) $S_{i,1}, i \in \{1,2,...,5\}$

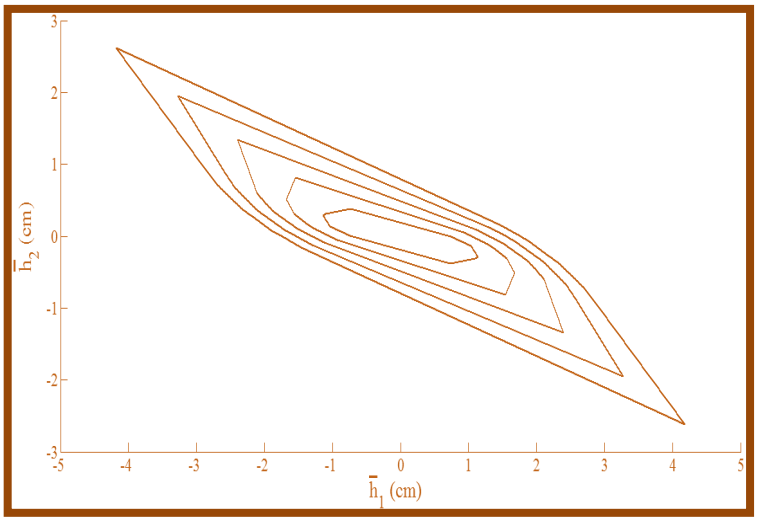

(2.2) $S_{i,2}, i \in \{1,2,...,5\}$

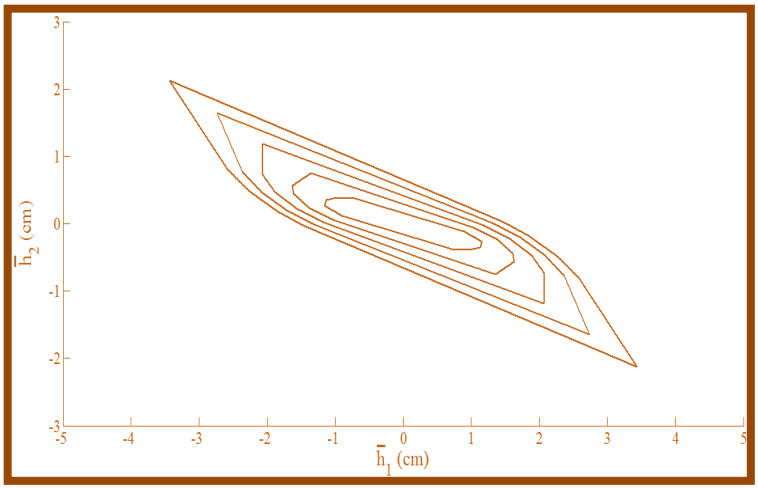

(2.3) $S_{i,3}, i \in \{1,2,...,5\}$

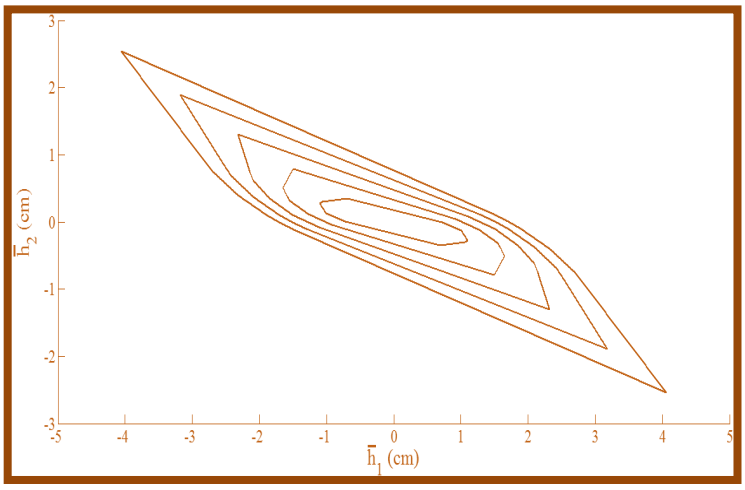

(2.4) $S_{i,4}, i \in \{1,2,...,5\}$

Figure 2: The polyhedral invariant sets computed off-line by the proposed algorithm.

*Corresponding author (P.Bumroongsri). Tel: +66-2-8892138 Ext.6101. E-mail address: pornchai.bum@mahidol.ac.th. International Transaction Journal of Engineering, Management, & Applied Sciences & Technologies. Volume 5 No.1 ISSN 2228-9860 eISSN 1906-9642. Online available at http://tuengr.com/V05/0025.pdf .

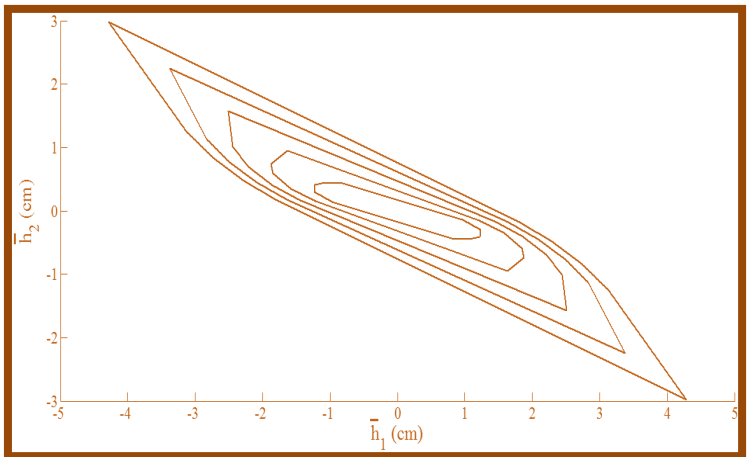

Figure 3: The polyhedral invariant sets computed off-line by an off-line robust MPC algorithm of Bumroongsri and Kheawhom (2012c).

Figure 4 shows the regulated output. For the proposed algorithm, the scheduling parameter is measured on-line at each sampling time so less conservativeness compared to an off-line robust MPC algorithm of Bumroongsri and Kheawhom (2012c) can be obtained. It can be observed that the proposed algorithm requires less time to enter and remain within the settling band ($\pm 0.1\%$ of $h_{2,\text{equilibrium}}$) compared to an off-line robust MPC algorithm of Bumroongsri and Kheawhom (2012c).

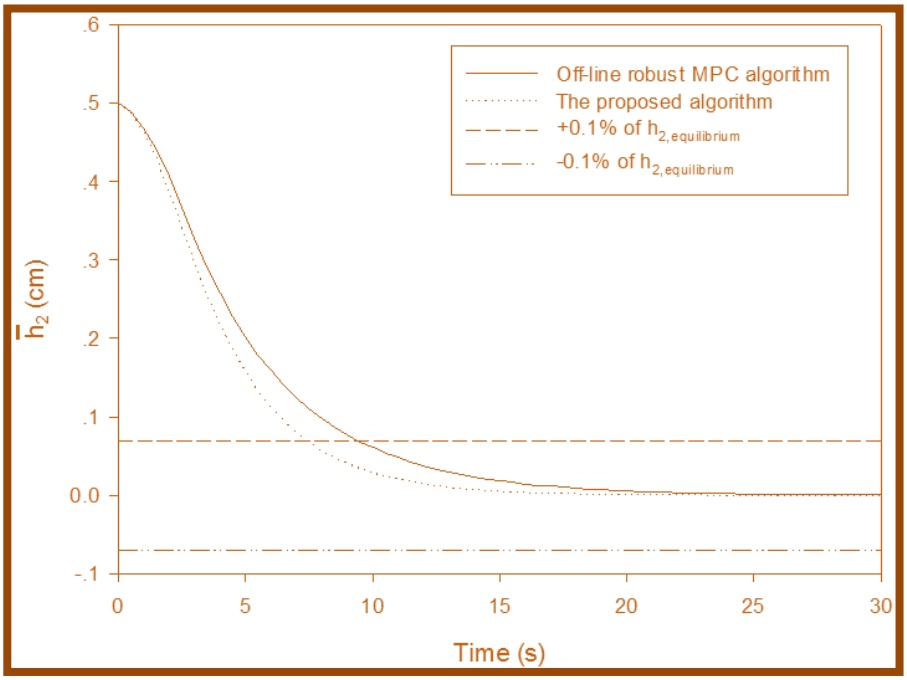

Figure 4: The regulated output.

The control input is shown in Figure 5. For the proposed algorithm, the pre-computed state

feedback gains are interpolated on-line so a smoother input response is obtained.

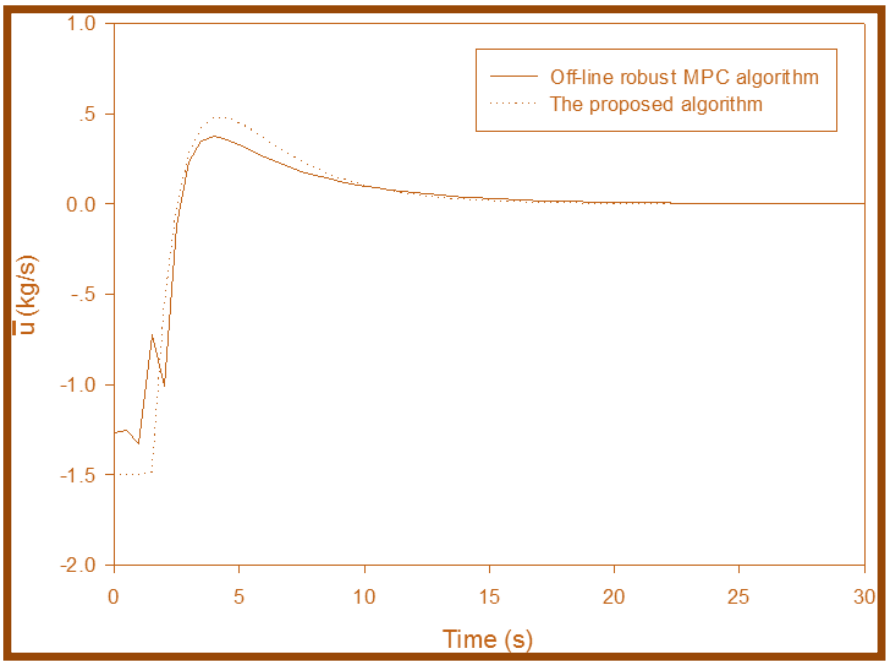

Figure 5: The control input.

The overall computational burdens are shown in Table 2. Although the proposed algorithm requires larger off-line computational time than an off-line robust MPC algorithm of Bumroongsri and Kheawhom (2012c), the on-line computation is tractable because only linear programming needs to be solved on-line. All of the simulations have been performed in Intel Core i-5 (2.4GHz), 2 GB RAM, using SeDuMi (Sturm, 1999) and Yalmip (Löfberg, 2012) within Matlab 2008a environment.

Table 2: The overall computational burdens.

Algorithm	Off-line CPU time (s)	On-line CPU time (s)
An off-line robust MPC algorithm	3.612	-
The proposed algorithm	6.738	0.001

5. Conclusion

In this research, an efficient formulation of off-line MPC for nonlinear systems using polyhedral invariant sets has been developed. The results show that the proposed algorithm can give better control performance than the previously developed off-line robust MPC algorithm. This is due to the fact the scheduling parameter is incorporated into the controller design. The controller design is illustrated with an example of nonlinear two-tank system.

*Corresponding author (P.Bumroongsri). Tel: +66-2-8892138 Ext.6101. E-mail address: pornchai.bum@mahidol.ac.th.

International Transaction Journal of Engineering, Management, & Applied Sciences & Technologies. Volume 5 No.1 ISSN 2228-9860 eISSN 1906-9642. Online available at http://tuengr.com/V05/0025.pdf .

6. Acknowledgements

This research project is supported by Mahidol University.

7. References

Angeli, D., Casavola, A., and Mosca, E. (2000). Constrained predictive control of nonlinear plants via polytopic linear system embedding, *Int. J. Robust Nonlin.*, 10(13), 1091-1103.

Boyd, S., and Vandenberghe, L. (2004). Convex Optimization, Cambridge University Press, Cambridge.

Bumroongsri, P., and Kheawhom, S. (2012a). MPC for LPV systems based on parameter-dependent lyapunov function with perturbation on control input strategy. *Engineering Journal*, 16(2), 61-72.

Bumroongsri, P., and Kheawhom, S. (2012b). An ellipsoidal off-line model predictive control strategy for linear parameter varying systems with applications in chemical processes. *Syst. Control Lett.*, 61(3), 435-442.

Bumroongsri, P., and Kheawhom, S. (2012c). An off-line robust MPC algorithm for uncertain polytopic discrete-time systems using polyhedral invariant sets. *J. Process Contr.*, 22(6), 975-983.

Jungers, M., Oliveira, R.C.L.F., and Peres, P.L.D. (2011). MPC for LPV systems with bounded parameter variations. *Int. J. Control*, 84(1), 24-36.

Lee, J.H. (2011). Model Predictive Control: review of the three decades of development. *Int. J. Control Autom.*, 9(3), 415-424.

Löfberg, J. (2012). Automatic robust convex programming. *Optim. Method Softw.*, 27(1), 115-129.

Magni, L., Nicolao, G.D., Magnani, L., and Scattolini, R. (2001). A stabilizing model-based predictive control algorithm for nonlinear systems. *Automatica*, 37(9), 1351-1362.

Manenti, F. (2011). Considerations on nonlinear model predictive control techniques. *Comput. Chem. Eng.*, 35(11), 2491-2509.

Mayne, D.Q., Rawlings, J.B., Rao, C.V., and Scokaert, P.O.M. (2000). Constrained model predictive control: stability and optimality. *Automatica*, 36(6), 789-814.

Morari, M., and Lee, J.H. (1999). Model predictive control: past, present and future. *Comput. Chem. Eng.*, 23(4), 667-682.

Park, P.G., and Jeong, S.C. (2004). Constrained RHC for LPV systems with bounded rates of parameter variations, *Automatica*, 40(5), 865-872.

Qin, S.J., and Badgwell, T.A. (2003). A survey of industrial model predictive control technology. *Automatica*, 11(7), 733-764.

Ramesh, K., Shukor, S.R.A., and Aziz, N. (2009). Nonlinear model predictive control of a

distillation column using NARX model. *Comp. Aid Ch.*, 27, 1575-1580.

Seborg, D.E., Edgar, T.F., and Mellichamp, D.A. (2004). Process Dynamics and Control, John Wiley & Sons, New York.

Sturm, J.F. (1999). Using SeDuMi 1.02, a Matlab toolbox for optimization over symmetric cones. *Optim. Method Softw.*, 11(1), 625-653.

Suzuki, H., and Sugie, T. (2007). Model predictive control for linear parameter varying constrained systems using ellipsoidal set prediction. *Int. J. Control*, 80(2), 314-321.

Toth, R. (2010). Modeling and Identification of Linear Parameter-Varying Systems, Springer, London.

Yu, S., Böhm, C., Chen, H., and Allgöwer, F. (2012). Model predictive control of constrained LPV systems. *Int. J. Control*, 85(6), 671-683.

Dr. P. Bumroongsri is a lecturer in the Department of Chemical Engineering, Mahidol University. He received his B.Eng. from Chulalongkorn University in 2008. He obtained his M.Eng and D.Eng from Chulalongkorn University in 2009 and 2012, respectively. His current interests involve robust MPC synthesis, modeling and optimization in chemical processes.

P. Arundechachai is a graduate student in the Department of Chemical Engineering, Chulalongkorn University. She received her B.Eng from the Department of Chemical Engineering, Kon Kaen University in 2011. Her research interests are in optimization and printed electronics.

Dr. S. Kheawhom is an Assistant Professor in the Department of Chemical Engineering, Chulalongkorn University. He earned his B. Eng from Chulalongkorn University in 1997. He continued his study at the University of Tokyo where he received his M.Eng and Ph.D. in 2001 and 2004, respectively. He has been working on the use of statistics and optimization, life cycle and printed electronics.

Peer Review: This article has been internationally peer-reviewed and accepted for publication according to the guidelines in the journal's website. Note: Original version of this article was accepted and presented at the Third International-Thai Chemical Engineering and Applied Chemistry (TIChE) Conference, jointly organized by Department of Chemical Engineering, Faculty of Engineering, Khon Kaen University and Thai Institute of Chemical Engineering and Applied Chemistry, at Pullman Khon Kaen Raja Orchid Hotel, Khon Kaen, THAILAND, October 17-18, 2013.

*Corresponding author (P.Bumroongsri). Tel: +66-2-8892138 Ext.6101. E-mail address: pornchai.bum@mahidol.ac.th.

:: International Transaction Journal of Engineering, Management, & Applied Sciences & Technologies

http://TuEngr.com

Call-for-Papers:

ITJEMAST invites you to submit high quality papers for full peer-review and possible publication in areas pertaining to our scope including engineering, science, management and technology, especially interdisciplinary/cross-disciplinary/multidisciplinary subjects.

Next article continue on next page ➔

International Transaction Journal of Engineering, Management, & Applied Sciences & Technologies

http://TuEngr.com

Effect of Modeling Parameters on System Hydrodynamics of Air Reactor in Chemical Looping Combustion Using CFD Simulation

Piriya Laiarpatorn [a], Pornpote Piumsomboon [a,b], Benjapon Chalermsinsuwan [a,b,*]

[a] *Department of Chemical Technology, Faculty of Science, Chulalongkorn University, THAILAND*
[b] *Center of Excellence on Petrochemical and Materials Technology, Chulalongkorn University, THAILAND*

ARTICLEINFO

Article history:
Received 25 October 2013
Received in revised form
25 October 2013
Accepted 25 October 2013
Available online
25 October 2013

Keywords:
Computational fluid dynamics;
Chemical looping combustion;
Modeling parameter;
Multiphase flow

ABSTRACT

The system hydrodynamics or flow behavior of gas and solid particles was simulated using computational fluid dynamic (CFD) model inside air reactor of chemical looping combustion (CLC). The two fluid model or Euler-Euler model was selected to use together with the kinetic theory of granular flow model (KGTF). In this study, the effect of modeling parameters including drag coefficient model, specularity coefficient and restitution coefficient between solid particles were explored. The EMMS drag model gave the highest solid volume fraction inside the system due to the particle cluster assumption in the model development. The specularity coefficient and restitution coefficient between solid particles had slightly effect on the results. In addition, the obtained results were compared with literature experiment by Shuai et al. (2012). The radial profiles of solid concentration from CFD simulation were consistent with the experimental data. The conventional core-annulus flow structure was still observed in the air reactor.

1. Introduction

Nowadays, the amount of released CO_2 into the atmosphere is the main reason for global warming problem. The recent literature shows that the circulating fluidized bed (CFB)

*Corresponding author (B.Chalermsinsuwan). E-mail address: benjapon.c@chula.ac.th
© 2014. International Transaction Journal of Engineering, Management, & Applied Sciences & Technologies. Volume 5 No.1 ISSN 2228-9860 eISSN 1906-9642. Online available at http://tuengr.com/V05/0039.pdf .

technology has been widely applied in many industrial purposes. One of the applications is to use CFB technology for CO_2 capture from power generation using the chemical looping combustion (CLC) (Shuai et al., 2012). In other CO_2 capture processes, the separation of CO_2 from the N_2 requires significant energy and expense. However, CO_2 separation is easily achieved in CLC which provides a self sequestration of CO_2 stream (Mahalatkar et al., 2011a). The typical CLC is consisting of two fluidized bed reactors connecting together (Shuai et al., 2012; Samruamphianskun et al., 2012). Fuel reactor is used for providing oxygen from metal bed material for combustion reaction while air reactor is employed for reducing the metal bed material before sending them back to the fuel reactor. Generally, the metal bed material is an oxygen carrier for oxidizing or transferring oxygen in the air reactor.

For the research study about computational fluid dynamics simulation (CFD), Mahalatkar et al. (2011b) successfully studied the CFD modeling of methane combustion in fuel reactor of CLC system. The result demonstrated that CFD modeling could be an effective approach for the designing of such reactor. Their CFD model precisely predicted the trends of flue gas concentrations. For the CFD simulation of air reactor in CLC, Shuai et al. (2012) simulated CFB with cluster structure-dependent (CSD) drag coefficient model. They observed that the CSD drag coefficient model accurately predicted dynamic formation and dissolution of solid particle clusters. The derivation of this model is based on the particle cluster concept in a heterogeneous gas-solid particles flow system. Then, the model was used to predict system hydrodynamics in CLC. The contour of solid particles was dense near the wall and dilute at the center which generally called the core-annulus flow structure. Lu et al. (2011) revealed that EMMS-based drag coefficient showed good physical predictability flow behavior of both Geldart A and B in the riser. Still, in the previous literature, the suitable or optimum operating condition for simulation of air reactor in CLC reactor system was not clearly studied.

In this study, the flow behavior of gas and solid particles was investigated using CFD model inside air reactor of CLC. The main objective was to explain the obtained system hydrodynamics dynamics inside CLC system. The selected numerical model to simulate flow behavior of gas and solid particles was the two-fluid model or Euler-Euler model. This model treats each phases as fully interpenetrating continua (Cruz et al., 2006; Samruamphianskun et al., 2012). Different modeling parameters were varied to explore the effect of each parameter. The obtained CFD simulation results were validated with the experimental results published in the literature study.

2. Methodology

In this simulation, the ANSYS FLUENT 14.0 was used. The two-dimensional air reactor in CLC had 0.0762 m diameter and 6.10 m height. For two-dimensional system, the solid particles were fed from two system sides into the air reactor and flowed out at the top of the air reactor. The physical properties and simulation settings are listed in Table 1 (Shuai et al., 2011a; 2012). The solid particle was laid in Geldart A classification. Here, six drag coefficient models, four different specularity coefficients and four different solid particle-solid particle restitution coefficients were compared with the experimental results by Shuai et al. (2012).

Table 1: Parameters used in this study CFD simulation.

Description	Value
Diameter of the air reactor (m)	0.0762
Height of the air reactor (m)	6.10
Operating pressure (atm)	1
Operating temperature (K)	293.15
Gas viscosity (kg/m s)	1.85×10^{-5}
Gas density (kg/m^3)	1.20
Solid particle density (kg/m^3)	1,600
Solid particle diameter (μm)	70
Solid particle-solid particle coefficient of restitution (-)	0.97 (vary)
Wall-solid particle coefficient of restitution (-)	0.90
Specularity coefficient (-)	0.00001 (vary)
Maximum solid volume fraction (-)	0.40

The computational domain was drawn using the commercial computer aided design (CAD) program, GAMBIT (Samruamphianskun et al., 2012). The used computational domain of the air reactor in CLC had 3,500, 6,500, 9,500 and 12,500 cells as shown in Figure 1.

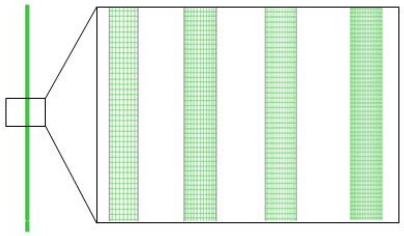

Figure 1: The computational domains of air reactor in CLC with (a) 3,500 cells, (b) 6,500 cells, (c) 9,500 cells and (d) 12,500 cells.

2.1 Mathematical model

In this study, the used numerical model of gas-solid particle two-phase flow was the

*Corresponding author (B.Chalermsinsuwan). E-mail address: benjapon.c@chula.ac.th

2014. International Transaction Journal of Engineering, Management, & Applied Sciences & Technologies. Volume 5 No.1 ISSN 2228-9860 eISSN 1906-9642. Online available at http://tuengr.com/V05/0039.pdf .

Euler-Euler (Eulerian) model. With this model, the conservation equations of mass and momentum for the gas and solid particle phases were separately considered based on their system hydrodynamic properties. For hydrodynamics study, the energy conservation for the gas and solid phases was ignored (Shuai et al., 2011b; Chalermsinsuwan et al., 2012). The temperature of gas phase and solid particle phase then was assumed to be a constant. The conservation equations of mass, momentum and solid particle phase fluctuating energy with their constitutive equations are summarized below. In this study, the constitutive equations based on the kinetic theory of granular flow were needed to close the conservation equations.

2.1.1 Conservation equations

The mass conservation is balanced by the convective mass flux for the gas phase (g) and the solid particle phase (s):

$$\frac{\partial}{\partial t}\left(\varepsilon_g \rho_g\right) + \nabla\left(\varepsilon_g \rho_g V_g\right) = 0 \qquad (1)$$

$$\frac{\partial}{\partial t}\left(\varepsilon_s \rho_s\right) + \nabla\left(\varepsilon_s \rho_s V_s\right) = 0 \qquad (2)$$

where ε is the concentration of each phase, V is the velocity, ρ is the density and t is the time. Here, the mass exchange between the phases due to chemical reaction was not considered.

The momentum conservation equation is balanced by the convective mass fluxes and the other forces such as pressure, gravity, stress tensor and momentum interphase exchange coefficient.

$$\frac{\partial}{\partial t}\left(\varepsilon_g \rho_g V_g\right) + \nabla\left(\varepsilon_g \rho_g V_g V_g\right) = -\varepsilon_g \nabla P + \nabla \tau_g + \varepsilon_g \rho_g g - \beta_{gs}\left(V_g - V_s\right) \qquad (3)$$

$$\frac{\partial}{\partial t}\left(\varepsilon_s \rho_s V_s\right) + \nabla\left(\varepsilon_s \rho_s V_s V_s\right) = -\varepsilon_s \nabla P + \nabla \tau_s + \varepsilon_s \rho_s g + \beta_{gs}\left(V_g - V_s\right) \qquad (4)$$

where g is the gravity acceleration, P is the pressure, β is the interphase momentum transfer coefficient or drag model and τ is the stress tensor.

The fluctuating kinetic energy conservation equation for the solid particles, as derived from the kinetic theory of granular flow (Gidaspow, 1994; Gidaspow and Jiradilok, 2009; Chalermsinsuwan et al., 2012), can be expressed as:

$$\frac{3}{2}\left[\frac{\partial}{\partial t}(\varepsilon_s\rho_s\theta)+\nabla(\varepsilon_s\rho_s\theta)V_s\right]=(-\nabla P_s I+\tau_s):\nabla V_s+\nabla(K_s\nabla\theta)-\gamma_s \quad (5)$$

where θ is the solid fluctuating kinetic energy, K_s is the conductivity of solid fluctuating kinetic energy, I is unit vector and γ_s is the collisional dissipation of solid fluctuating kinetic energy.

2.1.2 Constitutive equations

The constitutive equations based on the kinetic theory of granular flow were needed to close the conservation equations for solving this system of equations.

The stress tensor for gas and solid particle phases are described as:

$$\tau_g=\varepsilon_g\mu_g\left[\nabla V_g+(\nabla V_g)^T\right]-\frac{2}{3}\varepsilon_g\mu_g(\nabla V_g)I \quad (6)$$

$$\tau_s=\varepsilon_s\mu_s[\nabla V_s+(\nabla V_s)^T]-\varepsilon_s\left(\xi_s-\frac{2}{3}\mu_s\right)\nabla V_s I \quad (7)$$

where μ is the viscosity of each phase and ξ_s is the bulk viscosity of solid phase.

The particle pressure can be divided into two portions. The kinetic portion describes the influence of particle translations, whereas the collisional portion accounts for the momentum transfer by direct collisions.

$$P_s=\varepsilon_s\rho_s\theta[1+2g_0\varepsilon_s(1+e)] \quad (8)$$

where g_0 is the radial distribution function and e is the restitution coefficient between solid particles.

The shear viscosity accounts for the tangential forces. The shear viscosity of solid particles was then calculated using the formula below:

$$\mu_s=\frac{4}{5}\varepsilon_s\rho_s d_p g_0(1+e)\sqrt{\frac{\theta}{\pi}}+\frac{10\rho_s d_p}{96(1+e)g_0\varepsilon_s}\left[1+\frac{4}{5}g_0\varepsilon_s(1+e)\right]^2 \quad (9)$$

where d_p is the particle diameter.

*Corresponding author (B.Chalermsinsuwan). E-mail address: benjapon.c@chula.ac.th

2014. International Transaction Journal of Engineering, Management, & Applied Sciences & Technologies. Volume 5 No.1 ISSN 2228-9860 eISSN 1906-9642. Online available at http://tuengr.com/V05/0039.pdf .

The bulk viscosity formulates the resistance of solid particles to comparison and expansion.

$$\xi_s = \frac{4}{3}\varepsilon_s \rho_s d_p g_0 (1+e)\sqrt{\frac{\theta}{\pi}} \tag{10}$$

The radial distribution function is the probability of collisions between solid particles when they become dense:

$$g_0 = \left[1 - \left(\frac{\varepsilon_s}{\varepsilon_{s,max}}\right)^{1/3}\right]^{-1} \tag{11}$$

where $\varepsilon_{s,max}$ is the volume fraction of solid phase at maximum packing condition.

The conductivity of the solid fluctuating kinetic energy specifies the diffusion of granular energy as:

$$K_s = \frac{150\rho_s d_p \sqrt{\theta\pi}}{384(1+e)g_0}\left[1 + \frac{6}{5}\varepsilon_s g_0 (1+e)\right]^2 + 2\rho_s {\varepsilon_s}^2 d_p (1+e) g_0 \sqrt{\frac{\theta}{\pi}} \tag{12}$$

The rate of dissipation of fluctuation kinetic energy due to solid particle collision is expressed as:

$$\gamma_s = 3(1-e^2)\varepsilon_s^2 \rho_s g_0 \theta \left(\frac{4}{d_p}\sqrt{\frac{\theta}{\pi}}\right) \tag{13}$$

2.1.3 Drag coefficient model

In this study, the commercial ANSYS FLUENT 14.0 program with six drag or interphase exchanged coefficient models was explored. The drag coefficient model is the mathematical function which represents the dynamics of solid particles that is described by the product of the interphase momentum exchange coefficient and the slip velocity in the momentum transport equations. The high and low values of drag coefficient model imply more and less anti-translation force of solid particles inside the system, respectively. In this study, the employed drag models were Wen and Yu model, Gidaspow model, Huilin-Gidaspow model, Gibilaro model, Syamlal and O'Brien model and EMMS model (Fluent, Inc., 2011a, 2011b).

The Syamlal-O'Brien model is based on measurements of the terminal velocities of solid particles in fluidized or settling beds, with correlations that are a function of the volume fraction and relative Reynolds number (Fluent, Inc., 2011a, 2011b).

$$\beta_{gs} = \frac{3}{4}\frac{(1-\varepsilon_g)\varepsilon_g}{V_{r,s}^2 d_p}\rho_g \frac{Re_s}{V_{r,s}} C_D |V_g - V_s| \quad (14)$$

With

$$V_{r,s} = 0.5\left(A - 0.06Re_s + \sqrt{(0.06Re_s)^2 + 0.12Re_s(2B - A) + A^2}\right) \quad (15)$$

where $V_{r,s}$ is terminal velocity correlation for the solid particle phase.

$$Re_s = \frac{\varepsilon_g |V_g - V_s| d_p}{\mu_g}; C_D = \left(0.63 + \frac{4.8}{\sqrt{Re_s/V_{r,s}}}\right)^2 \quad (16)$$

$A = \varepsilon_g^{4.14}$; for$\varepsilon_g \leq 0.85$, $B = 0.8\varepsilon_g^{1.28}$ and for $\varepsilon_g > 0.85$, $B = \varepsilon_g^{2.65}$

The Wen and Yu model is appropriate for dilute system simulation (Wen and Yu, 1966).

$$\beta_{gs} = \frac{3}{4}\frac{(1-\varepsilon_g)\varepsilon_g}{d_p}\rho_g |V_g - V_s| C_{D0}\varepsilon_g^{-2.65} \quad (17),$$

where $C_D = \frac{24}{\varepsilon_g Re_s}[1 + 0.15\left((1-\varepsilon_g)Re_s\right)^{0.687}$, $Re_s = \frac{\rho_g d_p |V_s - V_g|}{\mu_g}$

The Gidaspow model is a combination of the Wen and Yu model equation for dilute phase calculation and the Ergun equation for dense phase calculation (Gidaspow et al., 1992; Huilin et al., 2003).

For $\varepsilon_g > 0.8$:

$$\beta_{gs} = \frac{3}{4}\frac{(1-\varepsilon_g)\varepsilon_g}{d_p}\rho_g C_D \varepsilon_g^{-2.65}|V_s - V_g| \quad (18)$$

For $\varepsilon_g \leq 0.8$

$$\beta_{gs} = \frac{150(1-\varepsilon_g)^2\mu_g}{\varepsilon_g d_p^2} + \frac{1.75\rho_g(1-\varepsilon_g)|V_s - V_g|}{d_p} \quad (19)$$

*Corresponding author (B.Chalermsinsuwan). E-mail address: benjapon.c@chula.ac.th

Huilin-Gidaspow model is also a combination of the Wen and Yu model and Ergun equation. However, the smooth switch is provided by the function when the solid volume fraction is less than 0.2. (Du et al., 2006):

$$\beta_{gs} = \Psi\beta_{gs-Ergun}| + (1-\Psi)\beta_{gs-Wen\ and\ Yu} \quad (20)$$

Where $\Psi = \frac{1}{2} + \frac{\arctan(262.5(1-\varepsilon_g)-0.2))}{\pi}$

Gibilaro model provides the continuous single compact equation over the entire range of voidages for a fluidized bed system (Du et al., 2006):

$$\beta_{gs} = \left(\frac{18}{Re} + 0.33\right)\frac{\rho_f|V_s - V_g|}{d_p}(1-\varepsilon_g)\varepsilon_g - 1.8 \quad (21)$$

with $Re = \frac{\varepsilon_g \rho_g d_p |V_s - V_g|}{\mu_g}$

The last drag model is energy minimization multi-scale (EMMS) model that develops based on the particle cluster concept. This drag model includes the effect of heterogeneous structure parameters into the momentum interphase coefficient model (Chalermsinsuwan et al, 2009; 2010).

For $\varepsilon_g \leq 0.74$:

$$\beta_{gs} = 150\frac{(1-\varepsilon_g)^2\mu_g}{\varepsilon_g d_p^2} + 1.75\frac{(1-\varepsilon_g)\rho_g|V_g - V_s|}{d_p} \quad (22)$$

For $\varepsilon_g > 0.74$:

$$\beta_{gs} = \frac{3}{4}\frac{(1-\varepsilon_g)\varepsilon_g}{d_p}\rho_g|V_g - V_s|C_{D0}\omega(\varepsilon_g) \quad (23)$$

With

$0.74 < \varepsilon_g \leq 0.82$;

$$\omega(\varepsilon_g) = -0.5769 + \frac{0.0214}{4(\varepsilon_g - 0.7463)^2 + 0.0044} \quad (24)$$

$0.82 < \varepsilon_g \leq 0.97;$

$$\omega(\varepsilon_g) = -0.0101 + \frac{0.0038}{4(\varepsilon_g - 0.7789)^2 + 0.0040} \quad (25)$$

$\varepsilon_g > 0.97;$

$$\omega(\varepsilon_g) = -31.8295 + 32.8295\varepsilon_g \quad (26)$$

3. Results and discussion

In this CFD simulation, the system hydrodynamics or flow behavior of solid particles inside air reactor of CLC was discussed and compared with experimental data by Shuai et al. (2012). In addition, the effects of various modeling parameters were discussed.

3.1 Time and grid independencies

For time independent study, the computed results showed that the solid particles in air reactor of CLC took around 20 s to fill up and came to stable or quasi-steady state condition after 50 s as shown in Figure 2. The absolute pressure was selected parameter to validate the numerical models. In this study, the results were time-averaged after 50 s and the total simulation time for each case was 70 s.

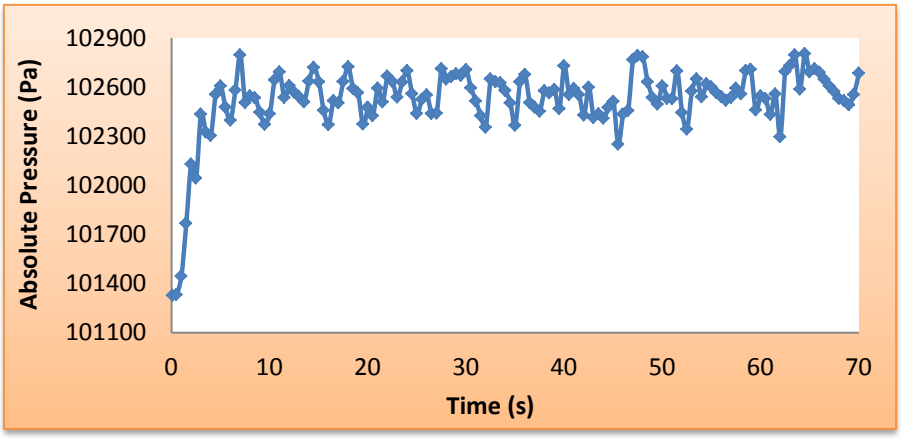

Figure 2: Time independency test by absolute pressure at 2 m height in air reactor of CLC.

For grid independent study, the simulations of air reactor with four different meshes were explored. From the results, the appropriate mesh size was found. As shown in Figure 3, the results of absolute pressure with three different meshes showed the same trend (6,500, 9,500 and 12,500 cells) but the result with 3,500 cells showed somewhat different behavior. Therefore, the 6,500 cells was selected to use in the present simulations because it gave the similar result with the higher computational domains.

*Corresponding author (B.Chalermsinsuwan). E-mail address: benjapon.c@chula.ac.th

2014. International Transaction Journal of Engineering, Management, & Applied Sciences & Technologies. Volume 5 No.1 ISSN 2228-9860 eISSN 1906-9642. Online available at http://tuengr.com/V05/0039.pdf .

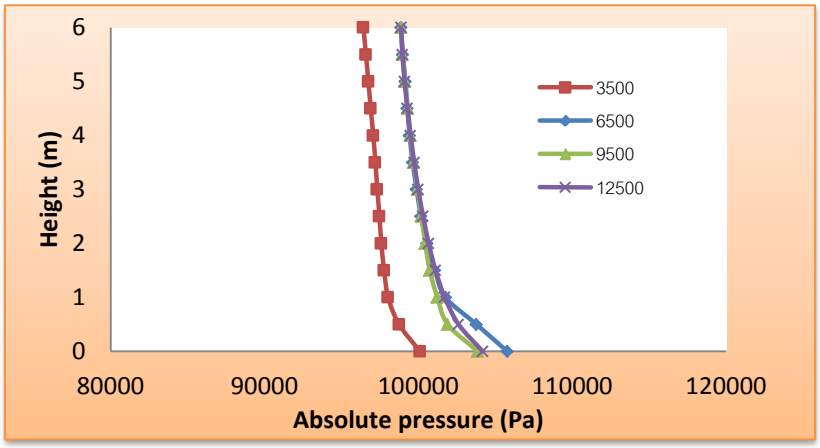

Figure 3: Grid independency test by axial absolute pressure profile in air reactor of CLC.

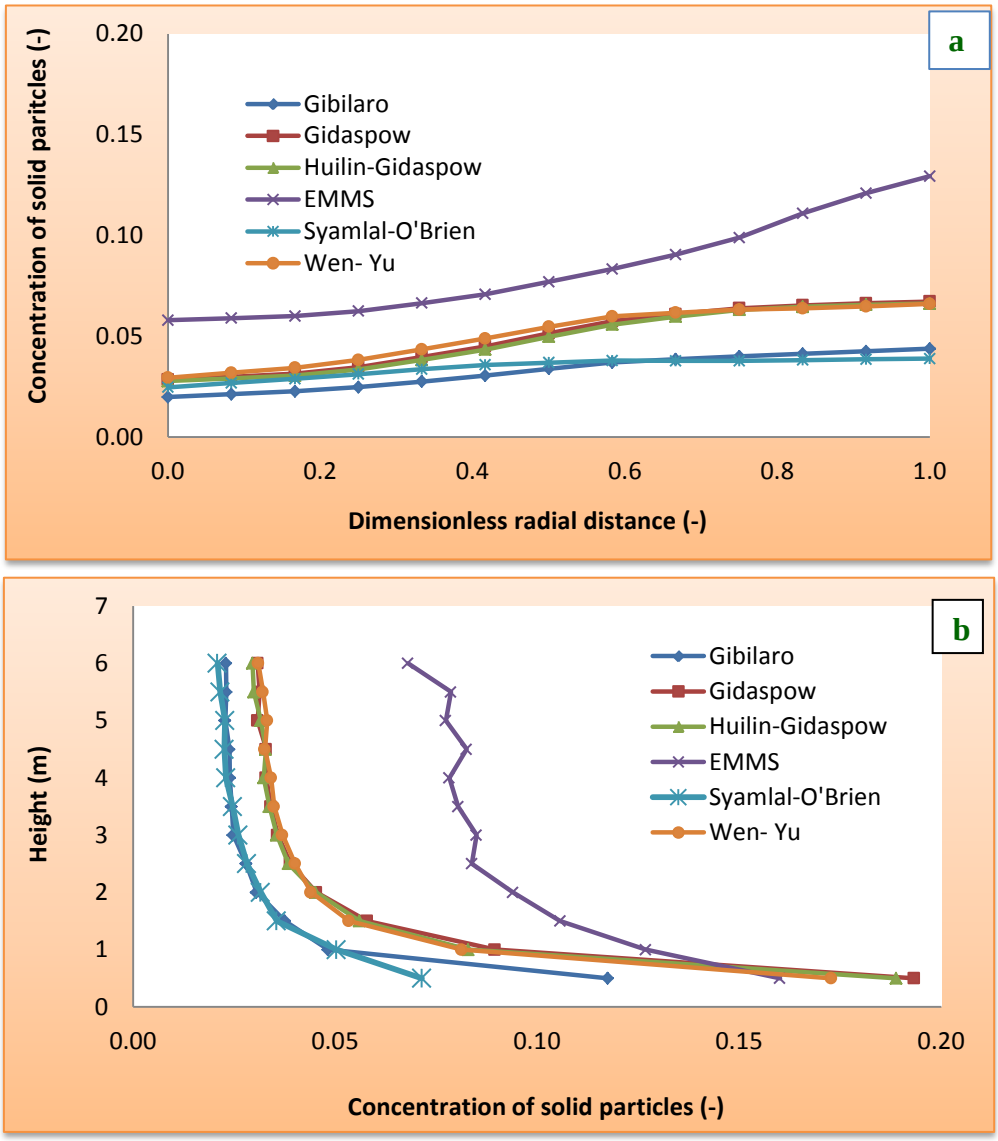

Figure 4: Effect of six drag coefficient models on concentration of solid particles for (a) radial direction at 5 m height and (b) axial direction.

3.2 Effect of drag coefficient model

Figure 4 shows the effect of six drag coefficient models on concentration of solid particles for (a) radial direction at 5 m height and (b) axial direction along the height of air reactor. From Figure 4(a), the obtained results with EMMS drag model showed higher concentration of solid particles comparing with the other drag coefficient models. The reason can be explained by the EMMS drag model is developed based on the solid particle cluster concept. The Geldart A solid particle generally agglomerates together assolid particle cluster (Chalermsinsuwan et al., 2009). The concentration profile of solid particles showed the high value near the wall region than the one at the center region which is commonly called core-annulus flow structure. From Figure 4(b), all the drag model simulations showed the high averaged concentration of solid particles at the bottom region. Then, the concentration of solid particles decreased along the height of air reactor. Again, the EMMS drag model showed higher concentration of solid particles than the other drag models.

3.3 Effect of modeling parameters

In this section, the simulations with EMMS drag model were used to compare different modeling parameters. The effect of specularity coefficient and the solid particle-solid particle restitution coefficient were explored. The other parameters were set according to Table 1. The concentration of solid particle is the factor that can be used to represent the system hydrodynamics.

3.3.1 Specularity coefficient

The specularity coefficient is the modeling parameter that describes the collision fraction of solid particles which transfer momentum to the wall. The value of specularity coefficient varies between zero and one. A value of zero means that a smooth wall is used or a free-slip boundary condition is applied at the wall and a value of one means that a rough wall is used or a partial-slip boundary condition is applied at the wall (Chalermsinsuwan et al., 2012). Chen and Wheeler (2013) reported that air velocities were very sensitive to the specularity coefficient values less than 0.10. Zhou et al. (2013) studied the effect of wall boundary condition in CFB risers. Their specularity coefficient had a pronounced influence on flow behavior when the EMMS-based drag model was used and a small specularity coefficient could result in better agreement with the experimental data.

*Corresponding author (B.Chalermsinsuwan). E-mail address: benjapon.c@chula.ac.th

2014. International Transaction Journal of Engineering, Management, & Applied Sciences & Technologies. Volume 5 No.1 ISSN 2228-9860 eISSN 1906-9642. Online available at http://tuengr.com/V05/0039.pdf .

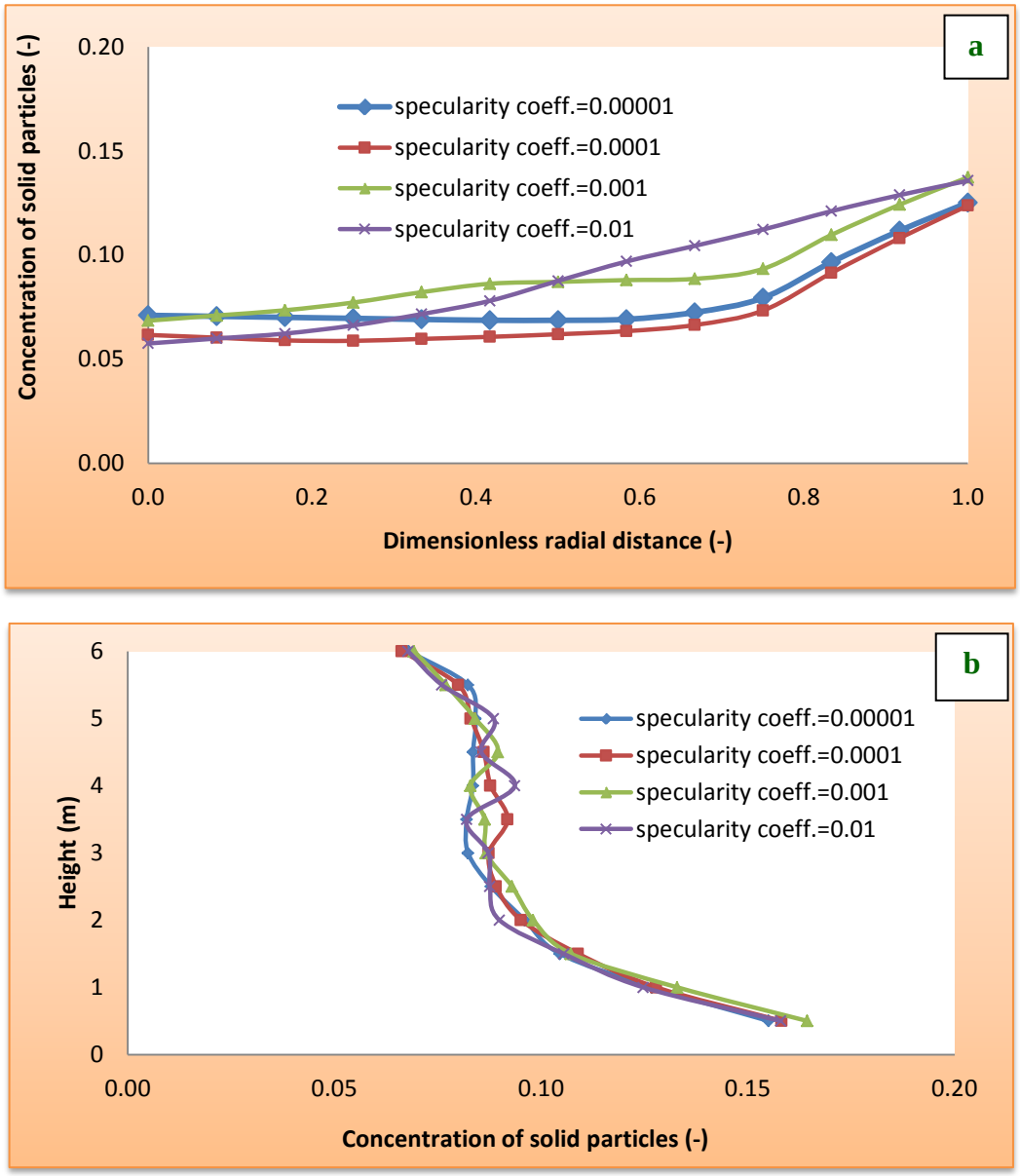

Figure 5: Effect of four specularity coefficients on concentration of solid particles for (a) radial direction at 5 m height and (b) axial direction.

Figure 5 shows the effect of four different specularity coefficients on concentration of solid particles for (a) radial direction at 5 m height and (b) axial direction along the height of air reactor. The selected specularity coefficient values were 0.00001, 0.0001, 0.001 and 0.01. At 5 m height, the system flows were already settled in fully developed condition. The effect of specularity coefficients was seen near the system wall. The high specularity coefficient value ($\varphi = 0.01$) gave higher concentration of solid particles due to the strong friction between solid particles and wall. The low specularity coefficient value ($\varphi = 0.00001$) means that the wall is in free-slip condition. With this condition, there is no friction between solid particles and wall. The solid particles then could freely move along the wall and had a lower concentration of solid

particles. The obtained results were agreed well with Zhou et al. (2013). From Figure 5(b), all the results with different specularity coefficients had the S-shaped profiles. The concentration of solid particles was decrease along the column height. At the bottom and top of the air reactor, the concentration of solid particles was high and low, respectively. There was no significant difference in the concentration of solid particles with different specularity coefficients.

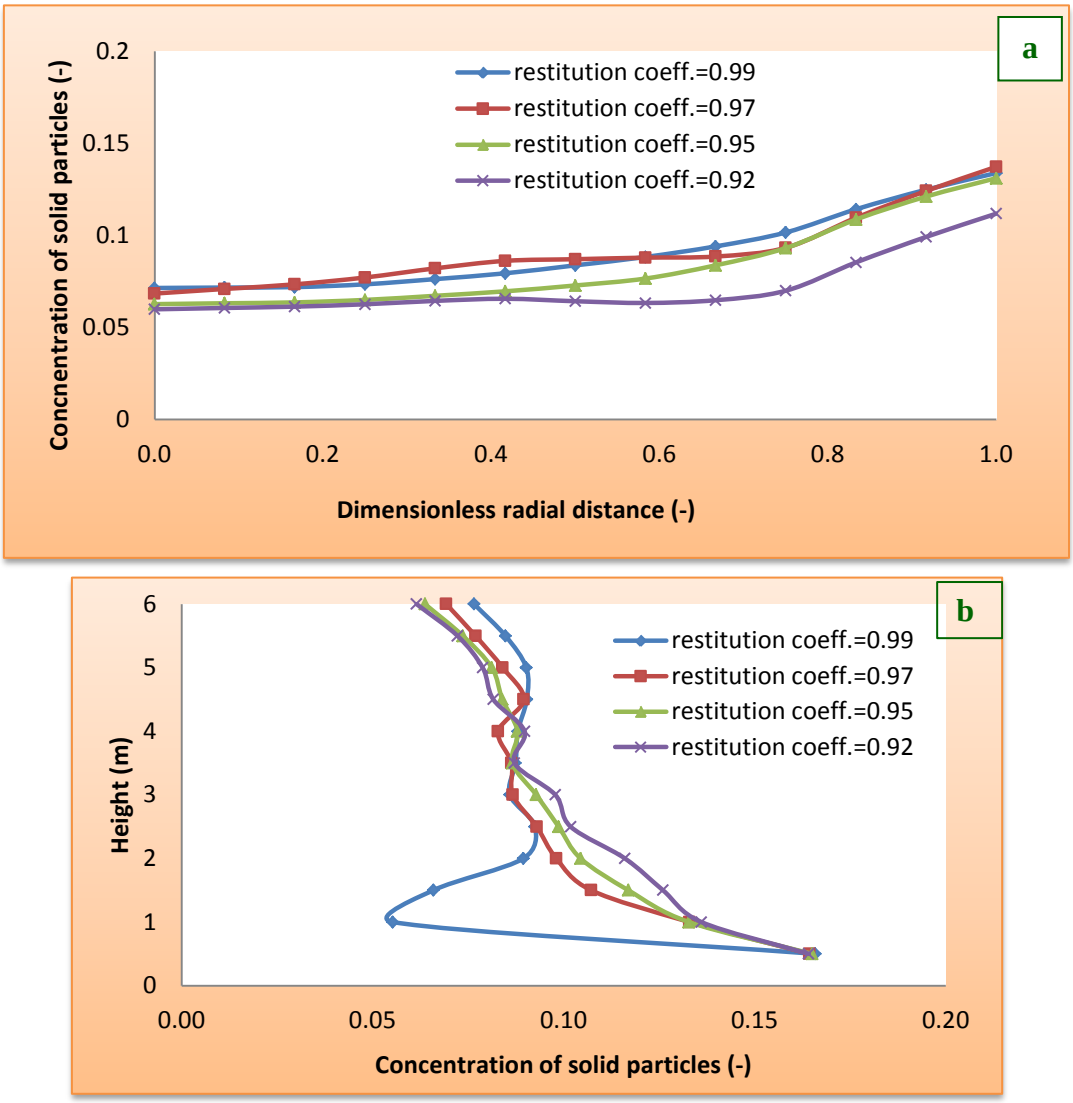

Figure 6: Effect of four solid particle-solid particle restitution coefficients on concentration of solid particles for (a) radial direction at 5 m height and (b) axial direction.

3.3.2 Restitution coefficient between solid particles

The solid particle-solid particle restitution coefficient describes the amount of the energy dissipation due to collisions between solid particles. It has an influence on the momentum conservation and granular temperature conservation of the solid particle phase (Chen and Wheeler, 2013). The restitution coefficient between solid particles also varies from a value of

*Corresponding author (B.Chalermsinsuwan). E-mail address: benjapon.c@chula.ac.th

2014. International Transaction Journal of Engineering, Management, & Applied Sciences & Technologies. Volume 5 No.1 ISSN 2228-9860 eISSN 1906-9642. Online available at http://tuengr.com/V05/0039.pdf .

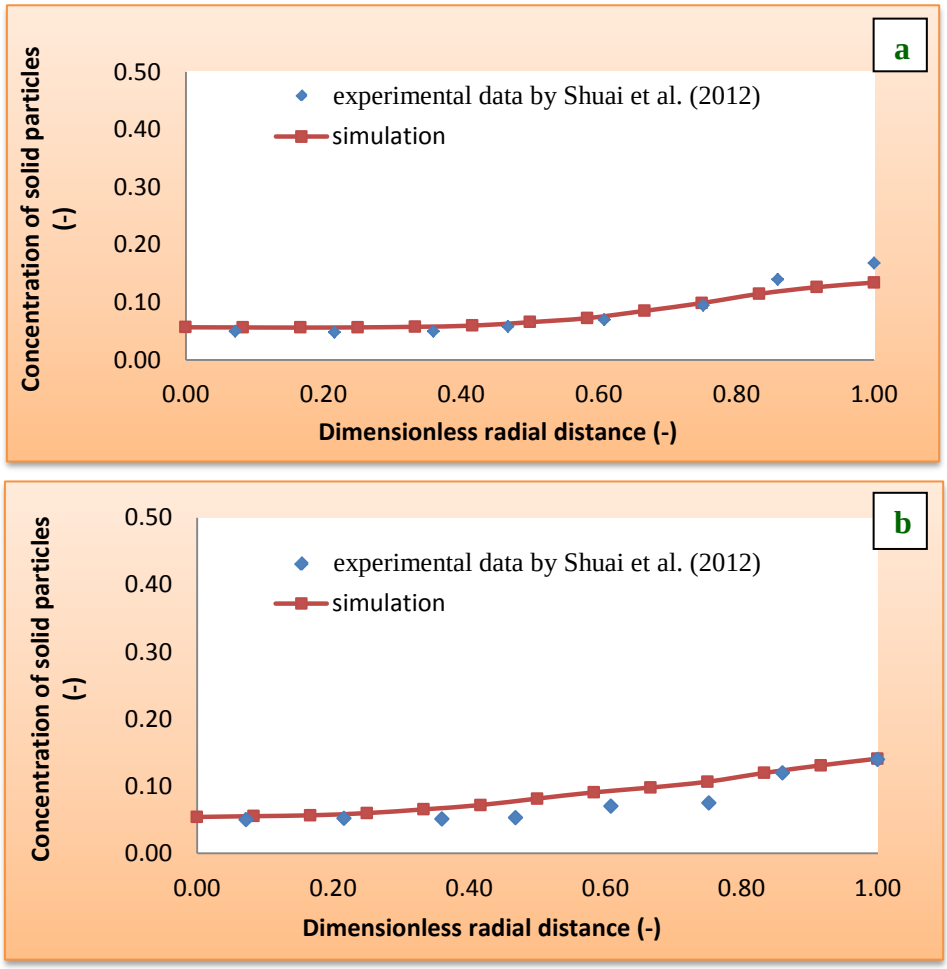

Figure 7: Distribution of solid particle concentration comparing with the experimental data by Shuai et al. (2012) at (a) 3.5 m and (b) 4.5 m heights of air reactor in CLC.

zero to one. A value of zero means that solid fluctuating kinetic energy is laid in inelastic collision while a value of one means that solid particle turbulent kinetic energy is laid in elastic collision. Chen and Wheeler (2013) examined the influence of solid particle-solid particle restitution coefficient. They noted that the free slip condition could not describe the real observed situation.

Figure 6 illustrates the effect of four different solid particle-solid particle restitution coefficients on the concentration of solid particles. The selected restitution coefficient varied among the values of 0.92, 0.95, 0.97 and 0.99. With the EMMS model and specularity coefficient value of 0.001, the overall trends of the concentration of solid particles were almost the same for different solid particle-solid particle restitution coefficient values. From Figure 6(a), the trends of all concentration of solid particles were similar that was high at the wall and low at the center. However, the high (e = 0.99) and low (e = 0.92) values of solid particle-solid particle restitution coefficient gave little higher and lower concentrations of solid particles due

to the amount of elastic solid particle collision and energy loss. This explanation is confirmed in Figure 6(b) which shows high concentration of solid particles at the bottom and low at the top of the air reactor. The result supports to the experimental data by Chen and Wheeler (2013) that high value of solid particle-solid particle restitution coefficient resulted in high concentration of solid particles in the top section.

3.4 Comparison with Shuai et al. (2012) experiments

In order to compare the quantitative result with the results by Shuai et al. (2012), the result with optimum modeling condition was shown in Figure 7. The suitable condition that got closely quantitative result with the experimental data used the EMMS drag model with the specularity coefficient of 0.01 and the solid particle-solid particle restitution coefficient of 0.97. The results gave high and low concentrations of solid particles at the wall and center, respectively. The profile of concentration of solid particles was the conventional core-annulus flow structure.

4. Conclusion

This study used CFD commercial program, ANSYS FLUENT 14.0, to simulate the flow behavior of gas and solid particles in the air reactor of CLC with different modeling parameters. The drag coefficient model, specularity coefficient and solid particle-solid particle restitution coefficient were explored. The solid volume fraction result with EMMS drag model was higher than the other drag models due to the effect of solid particle cluster in model development. The specularity coefficient and restitution coefficient between solid particles had slightly effect on the results. The EMMS drag model, the specularity coefficient of 0.01 and solid particle-solid particle restitution coefficient of 0.97 gave similar result with the experiment by Shuai et al. (2012). It correctly predicted the trends of the observed radial concentration of solid particles. Then, the system hydrodynamics of solid particles was shown. All the results had the similar trend that dense solid particles were formed near the wall and dilute solid particles were occurred at the center. The simulation showed the formation of the core-annular flow structure in the air reactor (Huilin and Gidaspow, 2003).

5. Acknowledgements

This study was financially supported by the Grants from PETRO-MAT and SC-CU, also partially supported by TRF and CHED (MRG5580140), the Grants for Development of New Faculty Staff by CU and the CU Graduate School Thesis Grant.

*Corresponding author (B.Chalermsinsuwan). E-mail address: benjapon.c@chula.ac.th

6. References

Chalermsinsuwan, B., P. Piumsomboon, D. Gidaspow. (2009) Kinetic theory based computation of PSRI riser: Part I–Estimate of mass transfer coefficient. *Chemical Engineering Science*, 64, 1195–1211.

Chalermsinsuwan, B., P. Kuchonthara and P. Piumsomboon. (2010) CFD modeling of tapered circulating fluidized bed reactor risers: Hydrodynamic descriptions and chemical reaction responses. *Chemical Engineering and Processing*, 49, 1144–1160.

Chalermsinsuwan, B., T. Chanchuey, W. Buakhao, D.Gidaspow and P. Piumsomboon. (2012) Computational fluid dynamics of circulating fluidized bed downer: Study of modeling parameters and system hydrodynamic characteristics. *Chemical Engineering Journal*, 189-190, 314–335.

Chen X. and C. Wheeler. (2013) Computational Fluid Dynamics (CFD) modelling of transfer chutes: A study of the influence of model parameters. *Chemical Engineering Science*, 95, 194–202.

Cruz, E., F.R. Steward and T. Pugsley. (2006) New closure models for CFD modeling of high-density circulating fluidized beds. *Powder Technology*, 169, 115–122.

Du, W., X. Bao, J. Xu and W. Wei. (2006) Computational fluid dynamic (CFD) modeling of spouted bed: Assessment of drag coefficient correlations. *Chemical Engineering Science*, 61, 1401–1420.

Fluent Inc. (2011a) *Fluent 14.0 User's Guide*, Fluent Inc., USA.

Fluent Inc. (2011b) *Fluent 14.0 Theory Guide*, Fluent Inc., USA.

Gidaspow, D., R. Bezburuah, and J. Ding. (1992) *Hydrodynamics of Circulating Fluidized Beds, Kinetic Theory Approach*. In Fluidization VII, Proceedings of the 7th Engineering Foundation Conference on Fluidization, 75–82.

Gidaspow, D. (1994) *Multiphase Flow, Fluidization: Continuum, Kinetic Theory Description*. Acedemic Press, Boston.

Gidaspow, D. and V. Jiradilok. (2009) *Computational Techniques the Multiphase CFD Approach to Fluidization and Green Energy Technologies*. Energy Science, New York.

Huilin L. and D. Gidaspow. (2003) Hydrodynamics of binary fluidization in a riser: CFD simulation using two granular temperatures. *Chemical Engineering Science*, 58, 3777–3792.

Huilin, L., D. Gidaspow, J. Bouillard, L.Wentie. (2003) Hydrodynamic simulation of gas-solid flow in a riser using kinetic theory of granular flow. *Chemical Engineering Journal*, 95, 1–13.

Lu, B., W. Wang and J. Li. (2011) Eulerian simulation of gas-solid flows with particles of Geldart group A, B and D using EMMS-based meso-scale model. *Chemical Engineering Science*, 66. 4624–4635.

Mahalatkar, K., J. Kuhlman, E. Huckaby and T. O'Brien. (2011a) Computational fluid dynamic simulations of chemical looping fuel reactors utilizing gaseous fuels. *Chemical Engineering Science*, 66, 469–479.

Mahalatkar, K., J. Kuhlman, E. Huckaby and T. O'Brien. (2011b) CFD simulation of a chemical-looping fuel reactor utilizing solid fuel. *Chemical Engineering Science*, 66, 3617–3627.

Samruamphianskun, T., P. Piumsomboon and B. Chalermsinsuwan. (2012) Effect of ring baffle configurations in a circulating fkuidized bed riser using CFD simulation and experimental design analysis. *Chemical Engineering Journal*, 210, 237–251.

Shuai, W., L. Huilin, L. Guodong, S. Zhiheng, X. Pengfei and D. Gidaspow. (2011a) Modeling of cluster structure-dependent drag with Eulerian approach for circulating fluidized beds. *Powder Technology*, 208, 98–110.

Shuai, W., L. Guodong, L. Huilin, C. Juhui, H. Yurong and W. Jiaxing. (2011b) Fluid dynamic simulation in a chemical looping combustion with two interconnected fluidized beds. *Fuel Processing Technology*, 92, 385–393.

Shuai, W., G. Jianmin, L. Huilin, L. Goudong, X. Pengfei and S. Liyan. (2012) Simulation of flow behavior of particles by cluster structure-dependent drag coefficient model for chemical looping combustion process: Air reactor. *Fuel Processing Technology*, 104, 219–233.

Wen, C.-Y. and Y. H. Yu. (1966) Mechanics of Fluidization. *Chemical Engineering Progress Symposium Series*, 62, 100–111.

Zhou, X., J. Gao, C. Xu and X. Lan. (2013) Effect of wall boundary condition on CFD simulation of CFB risers. *Particuology*, 11, 556–565.

Piriya Laiarpatorn is a master degree student of Department of Chemical Technology at Faculty of Science, Chulalongkorn University. She received her B.Eng. from Chiangmai University in 2012. Her research interest relates to computational fluid dynamics simulation.

Dr. Pornpote Piumsomboon is an Associate Professor of Department of Chemical Technology at Faculty of Science, Chulalongkorn University. He hold a B.Sc. in chemical engineering from Chulalongkorn University, M.E. in chemical engineering and industrial engineering from Lamar University in USA and Ph.D. degree in chemical engineering from the University of New Brunswick in Canada. His research interest relates to proton exchange membrane fuel cell and circulating fluidized bed technology. He has published more than 30 articles in professional journals and published 2 books.

Dr. Benjapon Chalermsinsuwan is an Assistant Professor of Department of Chemical Technology at Faculty of Science, Chulalongkorn University. He hold a B.Sc. in chemical engineering from Chulalongkorn university and Ph.D. degree in chemical technology from Chulalongkorn university. His research interest relates to computational fluid dynamics simulation, experimental design and analysis, carbon dioxide capture and circulating fluidized bed technology.

Peer Review: This article has been internationally peer-reviewed and accepted for publication according to the guidelines in the journal's website. Note: Original version of this article was accepted and presented at the Third International-Thai Chemical Engineering and Applied Chemistry (TIChE) Conference, jointly organized by Department of Chemical Engineering, Faculty of Engineering, Khon Kaen University and Thai Institute of Chemical Engineering and Applied Chemistry, at Pullman Khon Kaen Raja Orchid Hotel, Khon Kaen, THAILAND, October 17-18, 2013.

*Corresponding author (B.Chalermsinsuwan). E-mail address: benjapon.c@chula.ac.th

:: International Transaction Journal of Engineering, Management, & Applied Sciences & Technologies

http://TuEngr.com

Call-for-Papers:

ITJEMAST invites you to submit high quality papers for full peer-review and possible publication in areas pertaining to our scope including engineering, science, management and technology, especially interdisciplinary/cross-disciplinary/multidisciplinary subjects.

Next article continue on next page ➔

International Transaction Journal of Engineering, Management, & Applied Sciences & Technologies

http://TuEngr.com

Flow Behavior of Geldart A and Geldart C Particles in a Co-current Downflow Circulating Fluidized Bed Reactor

Parinya Khongprom [a,b*], Piyanat Soontarose [a,b], Sirilux Manchandrarat [a,b], Sunun Limtrakul [c], and Terdthai Vatanatham [c]

[a] *Department of Industrial Chemistry Faculty of Applied Science, King Mongkut's University of Technology North Bangkok, THAILAND*
[b] *Integrated Nanoscience Research Center, Science and Technology Research Institute, King Mongkut's University of Technology North Bangkok, THAILAND*
[c] *Department of Chemical Engineering, Faculty of Engineer, Kasetsart University, THAILAND*

ARTICLEINFO

Article history:
Received 20 August 2013
Accepted 06 December 2013
Available online 09 December 2013

Keywords:
Geldart particle;
Downer reactor;
Simulation;
CFD;
Two-fluid model.

ABSTRACT

The purpose of this research is to study the effect of Geldart A and C particles on the hydrodynamics behavior in a 9.3 m height, 0.1 m diameter co-current downflow circulating fluidized bed (downer reactor) using CFD simulation. Two-fluid model with kinetic theory of granular flow was adopted to predict flow behavior in the system. The simulation results show that hydrodynamics behavior in the downer strongly depends on the type of the particle. Geldart C particle exhibits a more uniform distribution along the lateral direction as compared with Geldart A particle. In addition, the effects of operating conditions were also studied. The uniformity of lateral direction of solids fraction increases with decreasing of solids circulation rate (Gs) or increasing of inlet superficial gas velocity (Ug). However, the radial distributions of gas and solids velocity are more uniform when Ug decreases especially for Geldart C particle.

*Corresponding author (P. Khongprom). Tel/Fax: +66-2-5552000 Ext.4811. E-mail addresses: parinyak@kmutnb.ac.th ©2014. International Transaction Journal of Engineering, Management, & Applied Sciences & Technologies. Volume 5 No.1 ISSN 2228-9860 eISSN 1906-9642. Online available at http://tuengr.com/V05/0057.pdf .

1. Introduction

A co-current downflow circulating fluidized bed (downer reactor) has been developed to overcome the drawback of a co-current upflow circulating fluidized bed or riser reactor. In the downer, both gas and solids particles are fed to the reactor at the top section. The suspension of gas and particle mixture co-currently downward flows along the gravitational direction. According to this feed setup, flow behavior in the downer is much more uniform as compared with that in the riser (Zhang *et al.,* 2001). Moreover, the particle residence time is lower and the particle residence time distribution (RTD) is narrower due to less back mixing (Khongprom *et al.,* 2012; Wei and Zhu, 1996).

Hydrodynamics behavior in the fluidized bed reactor strongly depends on the physical properties of particle (Khongprom, 2011; Khongprom *et al.,* 2012; Limtrakul *et al.,* 2008; Ye *et al.,* 2005). Small or fine particles are desired to apply in the chemical processes due to low mass and heat transfer resistances. Geldart A particles are normally applied due to its small particle size and can be easily fluidized at ambient conditions (Geldart, 1973). Geldart C particles are defined as an extremely fine particle. However, this particle type is rarely used in the conventional fluidized bed because these particles are very difficult to fluidize. According to feeding system and the assistant of gravitational force in the dower, Geldart C particles might be able to use in the downer reactor. Therefore, the objective of this research is to study the effect of Geldart A and C particles on the hydrodynamics behavior in the downer reactor.

2. Methodology

2.1 Reactor Geometry

The typical circulating fluidized bed (CFB) system is shown in Figure 1(a). This system mainly consists of downer section, gas-solids separator, riser section and gas and solids distributors. This work focuses on the hydrodynamics behavior in the 0.1 m inner diameter and 9.3 m height downer reactor (Figure 1(b)). Gas and solids particle are fed into the reactor at the top section and the exit locates at the bottom. To simplify the system, 2-D simulation was considered (see Figure 1(c). Physical properties of particle used are shown in Table 1. Air at ambient condition was used as a fluidizing gas. The operating conditions used in this work are shown in Table 2.

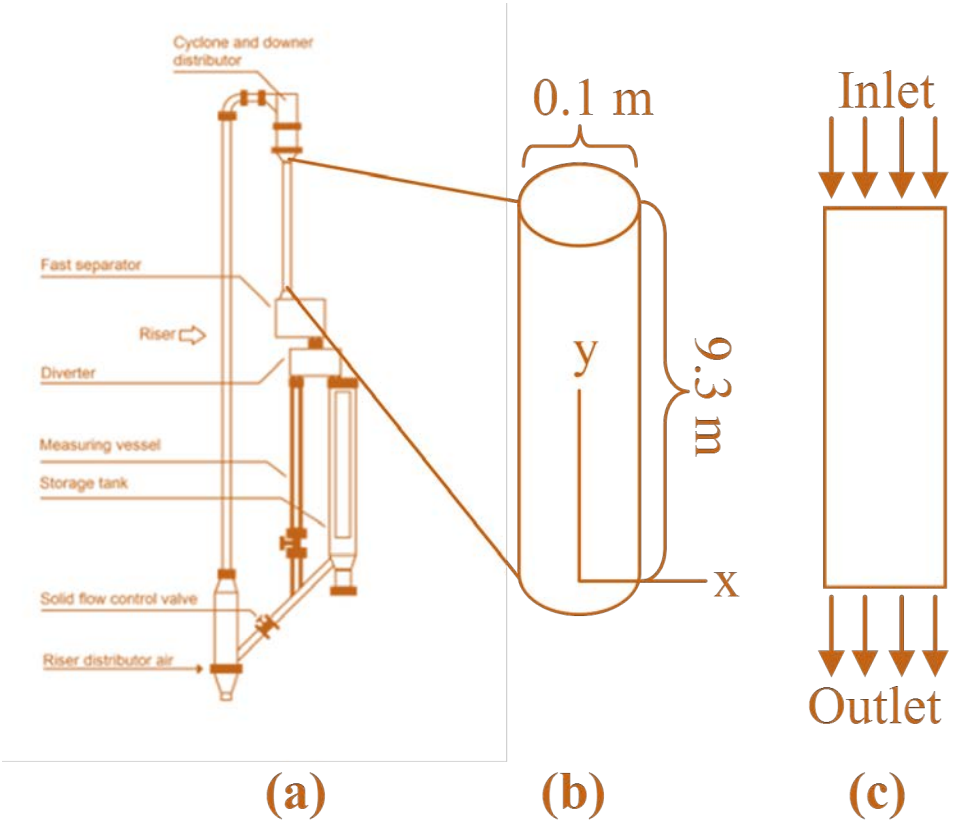

Figure 1: Typical CFB system (a); downer section (b); 2-D downer section (c).

Table 1: Physical properties of particle used in this study.

Particle type	D_p (μm)	ρ_p (kg/m^3)
Geldart A	80	1,500
Geldart C	20	1,500

Table 2: Operating conditions used in this study.

Case	U_g (m/s)	Gs (kg/m^{2}s)
Effect of Gs	3.5	150 200 250
Effect of Ug	2.5 5.0 7.0	101

2.2 Mathematical Modeling

Two-fluid model was adopted to predict flow behavior in the reactor. This model treats each phase as an interpenetrating continuum. Flow behavior of each phase was characterized by its own governing equations. The conservation equations are as follow,

*Corresponding author (P. Khongprom). Tel/Fax: +66-2-5552000 Ext.4811. E-mail addresses: parinyak@kmutnb.ac.th International Transaction Journal of Engineering, Management, & Applied Sciences & Technologies. Volume 5 No.1 ISSN 2228-9860 eISSN 1906-9642. Online available at http://tuengr.com/V05/0057.pdf .

The continuity equation for phase q is expressed as:

$$\frac{\partial}{\partial t}\left(\alpha_q \rho_q\right)+\nabla\cdot\left(\alpha_q \rho_q \vec{u}_q\right)=0 \tag{1}$$

where t stands for time (s), α_q the volume fraction, ρ_q the density (kg/m^3), and $\vec{u}_q$ the velocity vector (m/s).

Momentum conservation equation for gas phase is

$$\frac{\partial}{\partial t}\left(\alpha_g \rho_g \vec{u}_g\right)+\nabla\cdot\left(\alpha_g \rho_g \vec{u}_g \vec{u}_g\right)=-\alpha_g \nabla p+\alpha_g \rho_g \vec{g}+\nabla\cdot\bar{\bar{\tau}}_g+\nabla\cdot\bar{\bar{\tau}}_{tu,g}+\beta_{gp}(\vec{u}_p-\vec{u}_g) \tag{2}$$

where p is gas pressure (Pa), $\vec{g}$ gravitational acceleration (m/s^2), $\bar{\bar{\tau}}_g$ and $\bar{\bar{\tau}}_{tu,g}$ the viscous stress tensor and the Reynolds stress tensor, respectively (Pa), β_{gp} the interphase momentum transfer coefficient (kg/m^{3}s).

Momentum conservation equation for solids phase (p) is

$$\frac{\partial}{\partial t}\left(\alpha_p \rho_p \vec{u}_p\right)+\nabla\cdot\left(\alpha_p \rho_p \vec{u}_p \vec{u}_p\right)=-\alpha_p \nabla p-\nabla p_p+\nabla\cdot\bar{\bar{\tau}}_p+\nabla\cdot\bar{\bar{\tau}}_{tu,p}+\alpha_p \rho_p \vec{g}+\beta_{pg}(\vec{u}_g-\vec{u}_p) \tag{3}$$

Interphase momentum transfer coefficient (Gidaspow's drag model) is defined as

For $\alpha_g \le 0.80$:
$$\beta_{gp}=150\frac{\left(1-\alpha_g\right)^2 \mu_g}{\alpha_g d_p^2}+1.75\frac{(1-\alpha_g)\rho_g\left|\vec{u}_g-\vec{u}_p\right|}{d_p} \tag{4}$$

For $\alpha_g > 0.80$:
$$\beta_{gp}=\frac{3}{4}\frac{\left(1-\alpha_g\right)\alpha_g}{d_p}\rho_g\left|\vec{u}_g-\vec{u}_p\right|C_D\alpha_g^{-2.65} \tag{5}$$

where
$$\mathrm{Re}=\frac{\rho_g \alpha_g\left|\vec{u}_g-\vec{u}_p\right|d_p}{\mu_g} \tag{6}$$

where μ is gas viscosity (kg/m.s), d_p particle diameter (m), C_D drag coefficient (-).

Granular temperature conservation can be expressed in the form

$$\frac{3}{2}\left[\frac{\partial}{\partial t}\left(\rho_p \alpha_p \Theta_p\right)+\nabla\cdot\left(\rho_p \alpha_p \vec{u}_p \Theta_p\right)\right]=\left(-p_p \overline{\overline{I}}+\overline{\overline{\tau}}_p\right):\nabla\vec{u}_p+\nabla\cdot\left(k_{\Theta p}\nabla\Theta_p\right)-\gamma_{\Theta p}+\phi_p \qquad (7)$$

where Θ_p is granular temperature (m^2/s^2), $\overline{\overline{I}}$ unit tensor (-), $k_{\Theta p}$ diffusion coefficient of granular temperature (kg/m.s), γ_Θ collisional dissipation of solid fluctuating energy (kg/ms^3), ϕ_p energy exchange between phases (kg/ms^3).

The detail of this model has been discussed in previous works (Khongprom, 2011; Khongprom *et al.*, 2012).

k-ε turbulent model was used to explain the turbulent in the system. k equation for *q* phase is defined as

$$\frac{\partial}{\partial t}\left(\alpha_q \rho_q k_q\right)+\nabla\cdot\left(\alpha_q \rho_q \vec{u}_q k_q\right)=\nabla\cdot\left(\alpha_q \frac{\mu_{tu,q}}{\sigma_k}\nabla k_q\right)+\left(\alpha_q G_{k,q}-\alpha_q \rho_q \varepsilon_q\right)+K_{pq}(C_{pq}k_p-C_{qp}k_q- K_{pq}(\vec{u}_p-\vec{u}_q).\frac{\mu_{tu,p}}{\alpha_p\sigma_p}\nabla\alpha_p+K_{pq}(\vec{u}_p-\vec{u}_q).\frac{\mu_{tu,q}}{\alpha_q\sigma_q}\nabla\alpha_q \qquad (8)$$

where k_q is the turbulent kinetic energy (m^2/s^2), G_k production of turbulent kinetic energy (kg/ms^3), ε_q turbulent dissipation rate (m^2/s^3), K_{pq} turbulent momentum transfer coefficient (kg/m^3s), σ_p turbulent Prandtl number.

Turbulent dissipation rate (ε) is expressed in the form

$$\frac{\partial}{\partial t}\left(\alpha_q \rho_q \varepsilon_q\right)+\nabla\cdot\left(\alpha_q \rho_q \vec{u}_q \varepsilon_q\right)=\nabla\cdot\left(\alpha_q \frac{\mu_{tu,q}}{\sigma_\varepsilon}\nabla\varepsilon_q\right)+\frac{\varepsilon_q}{k_q}\left[C_{1\varepsilon}\alpha_q G_{k,q}-C_{2\varepsilon}\alpha_q \rho_q \varepsilon_q+ C_{3s}\left[K_{pq}(C_{pq}k_p-C_{qp}k_q)-K_{pq}(\vec{u}_p-\vec{u}_q)\frac{\mu_{tu,p}}{\alpha_q\rho_q}\nabla\alpha_q+K_{pq}(\vec{u}_p-\vec{u}_q).\frac{\mu_{tu,q}}{\alpha_q\sigma_q}\nabla\alpha_q\right]\right. \qquad (9)$$

where ε_q is turbulent dissipation rate (m^2/s^3), $C_{1\varepsilon}$, $C_{2\varepsilon}$, $C_{3\varepsilon}$ turbulent constants.

The kinetic theory of granular flow was used to predict the fluid properties of solids phase such as solids viscosity and solids pressure. The detail of this model was described somewhere else (Gidaspow, 1994).

*Corresponding author (P. Khongprom). Tel/Fax: +66-2-5552000 Ext.4811. E-mail addresses: parinyak@kmutnb.ac.th

International Transaction Journal of Engineering, Management, & Applied Sciences & Technologies. Volume 5 No.1 ISSN 2228-9860 eISSN 1906-9642. Online available at http://tuengr.com/V05/0057.pdf .

2.3 Numerical Method

The governing equations were discritized using finite volume method. The first order upwind was applied for convection term. The SIMPLE scheme was used for solving the pressure and velocity in the system (Patankar, 1980). The 49 grid numbers in the radial direction and 140 grid numbers in the axial direction were employed. This grid system was obtained from grid independency study. A time step of 10^{-5} s was adopted. A convergence criterion of 10^{-4} for each scale was used.

3. Result and Discussion

3.1 Effect of Solids Circulation Rate (Gs)

Figure 2 shows the effect of Gs on the radial distribution of solids fraction at various heights. Both Geldart A and C particles exhibit core-annulus flow structure which uniform solids fraction in the center and high density peak near the wall region. This flow structure has been reported by several researchers (Cheng *et al.*, 1999; Khongprom, 2011; Khongprom *et al.*, 2012; Lehner and Wirth, 1999; Limtrakul *et al.*, 2008). However, Geldart C shows a much more uniform profile with smaller density peak near the wall. In addition, solids fraction increases with Gs.

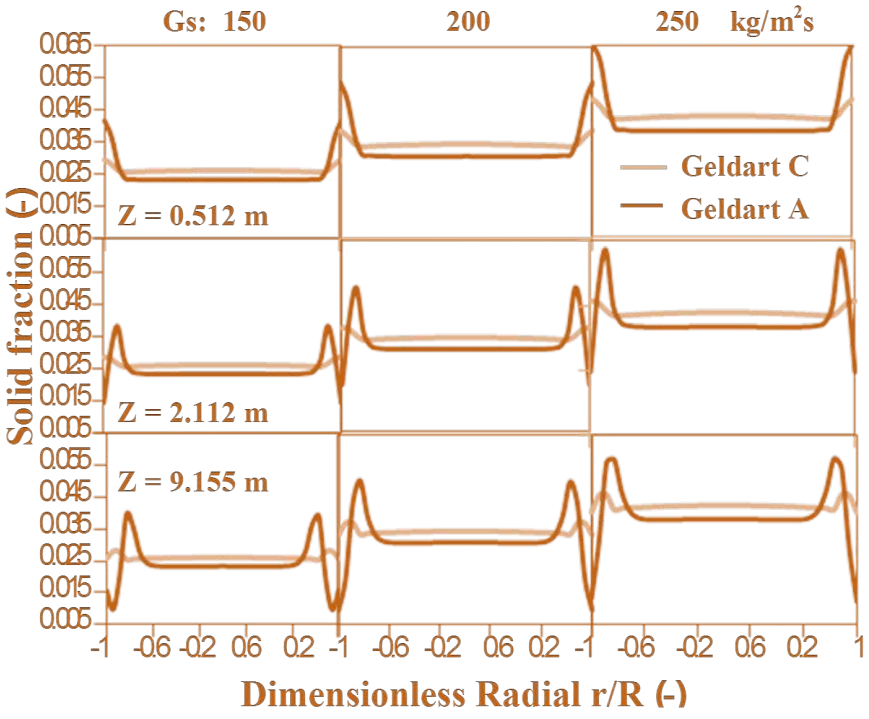

Figure 2: Effect of Gs on the radial distribution of time-averaged solids fraction.

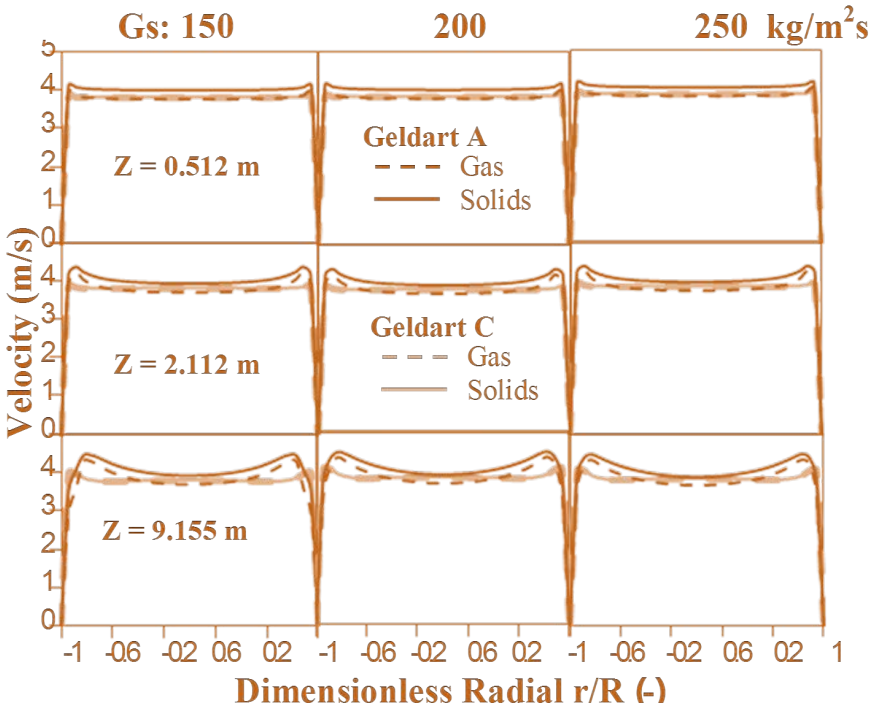

Figure 3: Effect of Gs on the radial distribution of time-averaged gas and solids velocities.

Figure 3 shows the effect of Gs on the radial distribution of gas and solids velocities. Near the inlet section (Z = 0.512 m), both gas and solids velocities are almost constant along the radial direction due to the uniform feed profile. Further down the column, Geldart C particle exhibits an almost uniform gas and solids velocities in the center region with a small velocity peak near the wall. Geldart A particle, both gas and solids velocities slightly increase from the center to the wall and the high velocity peak near the wall was form. This high velocity peak near the wall is the results of the particle cluster formation in this region (see Figure 2). These phenomena can also be observed by several experimental studies (Grassler and Wirth, 1999; Lehner and Wirth, 1999). In addition, the no slip velocity between gas and particles can be observed for Geldart C particle operation. This indicated that gas and Geldart C particle form a homogenous suspension mixture.

3.2 Effect of inlet Superficial Gas Velocity (Ug)

The effect of Ug on the lateral distribution of the solids fraction is shown in Figure 4. It was found that Ug exhibits less effect on the shape of the radial distribution profile of solids fraction. At z = 0.512 m, both Geldart A and C particles show a uniform profile in the center region with high solids fraction at the wall. Further down the column, the radial profiles

*Corresponding author (P. Khongprom). Tel/Fax: +66-2-5552000 Ext.4811. E-mail addresses: parinyak@kmutnb.ac.th International Transaction Journal of Engineering, Management, & Applied Sciences & Technologies. Volume 5 No.1 ISSN 2228-9860 eISSN 1906-9642. Online available at http://tuengr.com/V05/0057.pdf .

developed to form a core-annulus structure. However, solids fraction decreases with increasing of Ug. The density peak near the wall region decreases when Ug increases leading to more uniform in the radial direction especially for Geldart C particle.

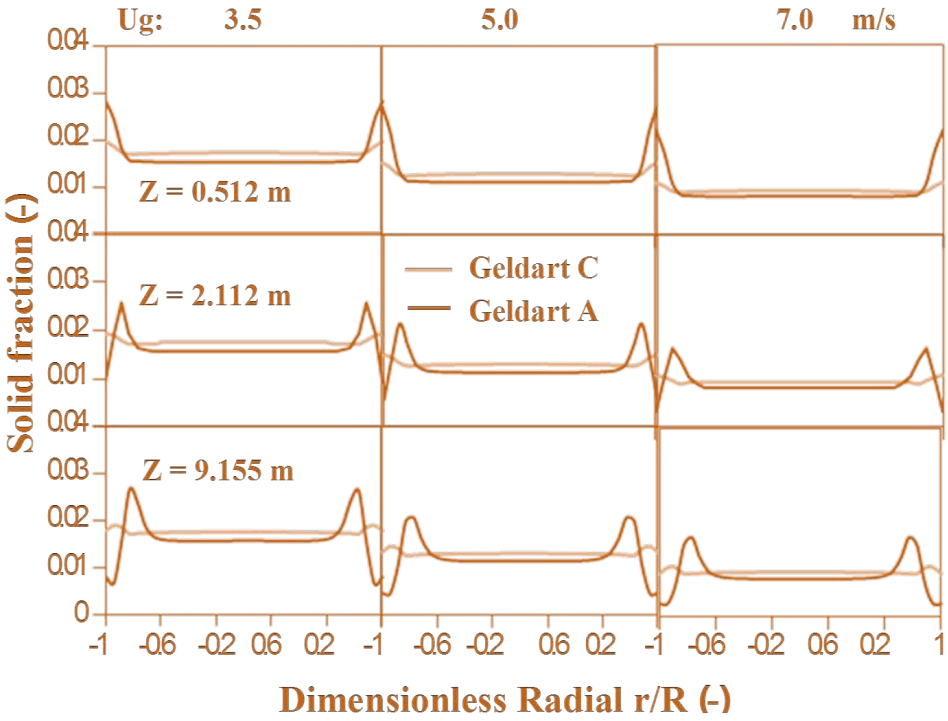

Figure 4: Effect of Ug on the radial distribution of time-averaged solids fraction.

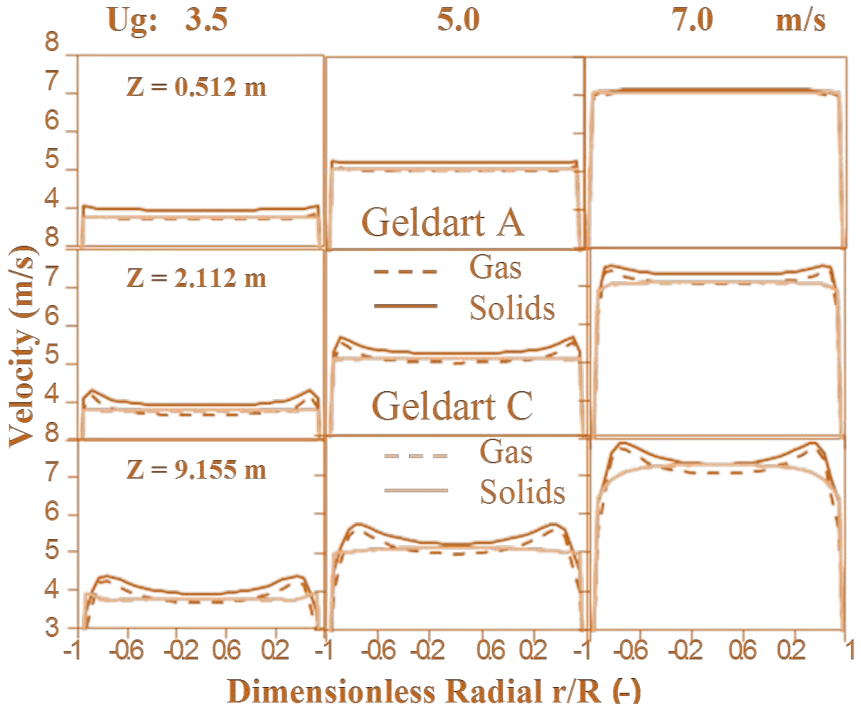

Figure 5: Effect of Ug on the radial distribution of time-averaged gas and solids velocities.

Figure 5 exhibits the effect of Ug on the radial profile of gas and solids velocities. As expected, gas and solids velocities increase with Ug. In case of Geldart C, gas and solids velocity profile in the fully developed region (Z = 9.155 m) can be classified into 2 types. At low Ug (Ug = 3 m/s), gas and solids velocities shows a uniform profile in the center with a small peak near the wall. At high Ug (Ug = 7.0 m/s), gas and solids velocities profiles shows a parabolic shape with consistency with gas velocity profile when operate with no solids particle feeding (did not show here). In this low solids fraction operating regime, gas phase governs the overall flow behavior in the system.

4. Conclusion

Two-fluid model with kinetic theory of granular flow was successfully developed to predict the hydrodynamics behavior in a downer reactor. The simulation results show that Geldart C particle exhibits a more uniform distribution along the lateral direction as compared with Geldart A particle. Geldart C particle exhibits a no-slip velocity between gas and solids particle phases. Moreover, high density peak near the wall region can be observed when operate with Geldart A particle. In addition, the effects of operating conditions were also studied. The uniformity of lateral distribution of solids fraction increases with decreasing of Gs or increasing of Ug. However, the radial distributions of gas and solids velocity are more uniform when Ug decreases especially for Geldart C particle.

5. Acknowledgements

This work was supported by King Mongkut's University of Technology North Bangkok and Faculty of Engineering, Kasetsart University.

6. References

Cheng, Y., Guo, Y., Wei, F., Jin, Y., Lin, W. (1999). Modeling the Hydrodynamics of Downer Reactors Based on Kinetic Theory. *Chemical Engineering Science Journal,* 54, 2019-2027.

Geldart, D. (1973). Type of Gas Fluidization. *Powder Technology*, 7, 285-292.

Gidaspow, D. (1994). Multiphase Flow and Fluidization: Continuum and Kinetic Theory Discription. Academic Press, Boston.

Grassler, T. and K.E. Wirth. (1999). X-ray Computer Tomography—Potential and Limitation for the Measurement of Local Solids Distribution in Circulating Fluidized Bed. In: T. York, T. Dyakowski, T. Peyton, A. Hurt (Eds.), Proceedings of the 1st World Congress on Industrial Process Tomography: Buxton, 402-409.

*Corresponding author (P. Khongprom). Tel/Fax: +66-2-5552000 Ext.4811. E-mail addresses: parinyak@kmutnb.ac.th International Transaction Journal of Engineering, Management, & Applied Sciences & Technologies. Volume 5 No.1 ISSN 2228-9860 eISSN 1906-9642. Online available at http://tuengr.com/V05/0057.pdf .

Lehner, P. and K.E. Wirth. (1999). Characterization of the Flow Pattern in a Downer Reactor. *Chemical Engineering Science Journal*, 54, 5471-5483.

Limtrakul, S., N. Thanomboon, T. Vatanatham, and P. Khongprom. (2008). DEM Modeling and Simulation of a Down-Flow Circulating Fluidized Bed. *Chemical Engineering Communications Journal*, 195, 1328-1344.

Khongprom, P. (2011). Modeling and Simulation of Hydrodynamics, and Heat and Mass Transfer in a Down-Flow Circulating Fluidized Bed Reactor. PhD. Thesis, Kasetsart University, Bangkok, Thailand.

Khongprom, P., A. Aimdilokwong, S. Limtrakul, T. Vatanatham, P.A. Ramachandran. (2012). Axial Gas and Solids Mixing in a Down Flow Circulating Fluidized Bed Reactor Based on CFD Simulation. *Chemical Engineering Science Journal*, 73, 8-19.

Patankar, S.V. (1980). Numerical Heat Transfer and Fluid Flow. Hemisphere, New York.

Wei, F., and J.-X. Zhu. (1996). Effect of Flow Direction on Axial Solids Dispersion in Gas-Solid Concurrent Upflow and Downflow System. *Chemical Engineering Journal and Biochemical Engineering Journal*, 64, 345-352.

Ye, M., M.A. vander Hoef, and J. A.M. Kuipers. (2005). The Effect of Particle and Gas Properties on the Fluidization of Geldart A Particles. *Chemical Engineering Science Journal*, 60, 4567-4580.

Zhang, H., W-X. Huang, and J-X. Zhu. (2001). Gas-Solid Flow Behavior: CFB Riser vs Downer. *AIChE Journal*, 47, 2000-2011.

Dr. P. Khongprom is a lecturer a Department of Industrial Chemistry, Faculty of Applied, King Mongkut's University of Technology Northy Bangkok. He received his B.Eng. of Chemical Engineering from Prince of Songkla University with Honors in 2001. He obtained his PhD also in Chemical Engineering from Kasetsart University in 2011. Dr. Khongprom current interests in modeling and simulation of hydrodynamics heat and mass transfer in a multiphase flow reactor.

Dr.Sunun Limtrakul is an Associate Professor of Department of Chemical Engineering at Kasetsart University. She holds a B.Sc. in Industrial Chemistry from Chiengmai University, MS in Chemical Engineering from Chulalongkorn University and Ph.D. degrees in Chemical Engineering from Washington University. Dr. Sunun is interested in reaction engineering, modeling and simulation, transport phenomena, and polymer electrolyte membrane (PEM) fuel cell.

Dr. Terdthai Vatanatham earned his bachelor degree from Chulalongkorn University Thailand, Master degree in Structural Engineering from Pennsylvania State University and Ph.D. in Chemical Engineering from University of Akron. He is an Associate Professor at Kasetsart University, Thailand. Dr. Terdthai is interested in reaction engineering, equipment design, and PEM fuel cell.

Peer Review: This article has been internationally peer-reviewed and accepted for publication according to the guidelines in the journal's website. Note: Original version of this article was accepted and presented at the Third International-Thai Chemical Engineering and Applied Chemistry (TIChE) Conference, jointly organized by Department of Chemical Engineering, Faculty of Engineering, Khon Kaen University and Thai Institute of Chemical Engineering and Applied Chemistry, at Pullman Khon Kaen Raja Orchid Hotel, Khon Kaen, THAILAND, October 17-18, 2013.

International Transaction Journal of Engineering, Management, & Applied Sciences & Technologies

http://TuEngr.com

Optimization of Enzymatic Clarification from Corncob

Sininart Chongkhong [a*], and Woraluk Kongjindamunee [a]

[a] *Department of Chemical Engineering Faculty of Engineering, Prince of Songkla University, THAILAND*

ARTICLEINFO

Article history:
Received 16 August 2013
Accepted 06 December 2013
Available online 09 December 2013

Keywords:
Alpha-amylase;
Glucose content;
Hydrolysis;
Central composite design;

ABSTRACT

A major content that was 22.76% total carbohydrate of the corncob could be simply hydrolyzed into reducing sugars by using alpha-amylase. The clarification process using alpha-amylase was optimized by response surface methodology (RSM) in this work. Independent variables including: enzyme amount of 0.05-0.2 %w, time of 60-240 min and temperatures of 80-100 °C were investigated. Their effects were found on the reducing sugar (Glucose content) by a second order central composite design (CCD). The optimum condition was 0.2 %w alpha-amylase, 87.6 °C for 150 min. It could provide the highest amount of 6.21 g/L glucose content in the clarified product.

1. Introduction

Ethanol is an alternative energy source as the clean and safe transportation fuels that can be produced domestically in response today's high-energy demand. This renewable energy has been interesting and rapidly developing to be used for substituting on fossil fuels and reducing pollution. Agricultural residues are used economically as raw materials for the ethanol production (Liu *et al*., 2010; Chena *et al*., 2007). The raw materials can be conveniently classified into three types: (i) sugars such as sugar beet, sweet sorghum and sugar cane, (ii) easily degradable carbohydrates such as corn, rice, wheat barley and corncob, (iii) cellulose such as rice bran, rice straw, wood chips, sawdust and waste from industries (Kreuger *et al*.,

*Corresponding author (Sininart Chongkhong). Tel.: +66-7428-7293; fax: +66 7455 8833
E-mail addresses:csininart@yahoo.com. 2014. International Transaction Journal of Engineering, Management, & Applied Sciences & Technologies. Volume 5 No.1 ISSN 2228-9860 eISSN 1906-9642. Online available at http://tuengr.com/V05/0067.pdf

2011; Zhu *et al.*, 2006). The production steps are pretreatment, hydrolysis and fermentation, respectively. The pretreatment are necessary for increasing the porosity of the materials that are active to next steps. Then the hydrolysis, cellulose and/or carbohydrate molecules are converted into reducing sugars or broken down into corresponding monomers. After that the fermentation is carried out to transform the reducing sugars (fermentable sugars) into ethanol (Balata *et al.*,2008). Corncob is a cheap raw that can give a suitable reducing sugar (glucose) content for ethanol production. The components per 100 g of corncob are 22.76 g total carbohydrate, 7.11 g crude fiber, 1.17 g crude protein, 0.15 g fat, 0.44 g ash and 75.48 g moisture (Agro-Industry department center for export, 2011). The alpha-amylases breaks down the long-chain carbohydrates by acting at random locations of the carbohydrate chain. In this process, the pH is adjusted to be about 6.0 - 6.5 and the reaction is performed for about 2 hours at 95°C (Aiyer, 1995; Das *et al.*, 2011; Reed and Nagodawithana, 1995). The optimum condition for the hydrolysis of prebiotic extracted jackfruit seeds using alpha-amylase enzyme was 0.17 %w enzyme amount at 80 °C for 240 min. The highest reducing sugar content in the product was 3.04 g/L (Bancha *et al.*,2011).

Response surface methodology (RSM) is a statistical technique to identify the effect of individual variable for the optimization of multivariable system. It is widely used in optimizing the bioprocesses by the statistical experimental design method. This method can be employed to determine the optimum processes i.e. pretreatment, hydrolysis and fermentation. In addition, it can enhance production yield, reduce process variability, save time and cost (Wang *et al.*, 2008; Bandaru *et al.*, 2006).

Crucial factors (alpha-amylase amount, time and temperature) for clarification process from corncob in this work would be optimized by RSM to obtain the highest glucose content in the product.

2. Materials and Methods

2.1 Materials and chemicals

The corncob of sweet corn, sugar specie, was obtained from a local market in Hat-Yai, Songkhla province, Thailand. The composition of the corncob is shown in Table 1. Alpha-amylase from *Aspergillus oryzae* was purchased from the Sigma-Aldrich company. Dinitrosalicylic solution (DNS) was used for the analysis of the glucose (reducing sugar) in the products (Miller, 1959). DNS was the mixture of 1% dinitrosalicylic acid, 0.2% phenol, 0.05% sodium sulfite, 1% sodium hydroxide and 20% sodium potassium tartrate that were a laboratory

grade.

Table 1: The components of the corncob content.

Test Items	Test Method	Results
Protein	AOAC (Kjeldahl Method)	1.17 %
Crude Fat	AOAC (Soxhlet Extraction Method)	0.15 %
Moisture	AOAC (Loss on Drying at 95-100 °C Method)	75.48 %
Ash	AOAC	0.44 %
Crude Fiber	AOAC (Fritted Glass Crucible Method)	7.11 %
Total Carbohydrate	Calculation	22.76 %
Energy	Calculation	97.07 kcal
Total Sugar	Modified Phenol Sulfuric Method	3.71 %
Reducing sugar	Modified dinitrosalicylic acid method	1.68 g/L

2.2 Pretreatment and pre-hydrolysis (Clarification)

The corncob was firstly cut into small pieces and crushed to be about 2 mm particle size. The 20 g crushed corncob and 100 mL clean water were put into 250 ml screw-capped bottles, and added with 0.05-0.2 %w alpha-amylase. An initial pH was adjusted to be 6.0 by ammonia solution. Then the bottles were immersed in an oil bath at a studied temperature in the range of 80-100 °C for a heating time in the range of 60-240 min with a constant shaking rate of 80 rpm. After that, the clarified products were separated by a fabric filter to get the clear liquid phase product before the analysis of reducing sugar content by a UV-vis spectrophotometer.

2.3 Analytical method

DNS method using a double beam UV-Vis spectrophotometer (Model HP 8453) with UV-Visible Chem-Station software was used to analyze the reducing sugar that was assayed in term of glucose. The reflective light was measured at 520 nm on the spectrophotometer (Chongkhong *et al.*, 2012).

2.4 Experimental design and optimization

Central composite design (CCD) was employed to assign important parameters for investigation. Time (X_1, min), temperature (X_2, °C) and alpha-amylase amount (X_3, %w) were chosen as the independent variables that are shown in Tables 2 and 3. The reducing sugar concentration in the product (Y, g/L) was the dependent output variable. For statistical calculation, the variables were coded according to Equation (1).

*Corresponding author (Sininart Chongkhong). Tel.: +66-7428-7293; fax: +66 7455 8833
E-mail addresses:csininart@yahoo.com. 2014. International Transaction Journal of Engineering, Management, & Applied Sciences & Technologies. Volume 5 No.1 ISSN 2228-9860 eISSN 1906-9642. Online available at http://tuengr.com/V05/0067.pdf

$$x_i = \frac{(X_i - \bar{x}_i)}{\Delta x_j},\ i = 1, 2, 3, \ldots, k \qquad (1),$$

where x_i and X_i are the dimensionless value and the real value of the independent variable, $\bar{x}_i$ is the real value of the independent variable at the center point and Δx_j is the step change.

Table 2: Independent variables for the experimental design.

Variables	Coded levels				
	-1.68	-1	0	1	1.68
Time (min)	60	95	150	205	240
Temperature (°C)	80	85	90	95	100
Alpha-amylase (%w)	0.05	0.08	0.13	0.17	0.2

Table 3: The central composite design matrix employed for the three independent variables (Actual values are given in Table 2)

Run no.	X_1	X_2	X_3
1	1	-1	-1
2	0	0	0
3	-1	1	1
4	-1.68	0	0
5	0	-1.68	0
6	0	0	0
7	-1	-1	-1
8	0	0	1.68
9	1.68	0	0
10	-1	1	-1
11	-1	-1	1
12	0	1.68	0
13	0	0	-1.68
14	1	-1	1
15	1	1	-1
16	1	1	1
17	0	0	0

The 17 experiments (N) were estimated by $N = 2^n+2n+n_0$ that their operating conditions were performed in Table 3. This design consists of the following three portions:

(1) A complete 2^n factorial design, when n is number of test variables.

(2) n_0 center point ($n_0 \geq 1$).

(3) An additional design, the experimental point at a distant ±α from center, while the distance of the axial point was ± 1.68 ($2^{n/4} = 1.682$ for n = 3) calculated by Equation (2).

$$\alpha = (2^n)^{1/4} \qquad (2),$$

where α is the distance of the axial points and *n* is the number of independent variables. The coefficient of the polynomial model was calculated by Equation (3).

$$Y = b_0 + b_1X_1 + b_2X_2 + b_3X_3 + b_{11}X_1^2 + b_{22}X_2^2 + b_{33}X_3^2 + b_{12}X_1X_2 + b_{23}X_2X_3 + b_{13}X_1X_3 \quad (3),$$

where Y is the predicted reducing sugar, X_1, X_2, X_3 are the independent variables, b_0 is the offset term, b_1, b_2, b_3 are the linear effects, b_{11}, b_{22}, b_{33} are the square effects, and b_{12}, b_{23}, b_{13} are the cross effects of the interaction terms (Khuri and Mukhopadhyay, 2010; Bezerra *et al*., 2008).

3. Result and Discussion

3.1 Components of corncob

Components of the fresh corncob are shown in Table 1. The major components are 22.76 % carbohydrate that can be hydrolyzed to fermentable sugars before transforming into ethanol and 75.48 % moisture that can support the good growth of microorganisms and save water material used in the fermentation process. This showed that the corncob was a potential material for the ethanol fermentation.

3.2 Response surface analysis for the optimization of three factors

The important factors for this clarification, hydrolysis process, to produce the reducing sugars are time, temperature and alpha-amylase amount. This method evaluates the effects of the hydrolysis process, design model used to study interaction of the three factors and to find the optimum condition. The experimental conditions are shown in Tables 2 and 3. The results for central composite design (CCD) are shown in Table 4, the second-order polynomial equation giving the reducing sugar as a function of time (X_1,min), temperature (X_2,°C) and alpha-amylase amount (X_3,%w) was shown as Equation (4).

$$Y=-100.01+0.061X_1+2.235X_2+19.90X_3-0.0000176X_1^2-0.01190X_2^2 +85.42X_3^2-0.000540X_1X_2-0.040X_1X_3-0.339X_2X_3 \quad (4),$$

The RSM predicted and experimental values of the reducing sugar are given in Table 4. To test the fit of the CCD model, the regression equation and determination coefficient (R^2) were

*Corresponding author (Sininart Chongkhong). Tel.: +66-7428-7293; fax: +66 7455 8833
E-mail addresses:csininart@yahoo.com. International Transaction Journal of Engineering, Management, & Applied Sciences & Technologies. Volume 5 No.1 ISSN 2228-9860 eISSN 1906-9642. Online available at http://tuengr.com/V05/0067.pdf

estimated. The value of R^2 is 0.906 implied that it was a quite good fit, and that 90.6% of the variation could be explained by the model.

Table 4: Experimental and RSM predicted results

Run no.	X_1	X_2	X_3	Reducing sugar (g/L)	
				Experimental	RSM predicted
1	205	85	0.08	5.64	5.37
2	150	90	0.13	5.26	5.35
3	95	95	0.17	5.25	5.31
4	60	90	0.13	4.82	5.06
5	150	80	0.13	4.37	4.47
6	150	90	0.13	5.36	5.35
7	95	85	0.08	4.76	4.71
8	150	90	0.20	6.17	6.18
9	240	90	0.13	5.30	5.35
10	95	95	0.08	5.18	4.84
11	95	85	0.17	5.71	5.48
12	150	100	0.13	3.75	3.85
13	150	90	0.05	5.20	5.47
14	205	85	0.17	5.61	5.75
15	205	95	0.08	4.90	4.93
16	205	95	0.17	5.15	5.00
17	150	90	0.13	5.39	5.35

From Table 5, the fitting model is predicted by the analysis of variance (ANOVA). The ANOVA of the quadratic regression model indicates that the model is highly significant, because of Fisher's F-test (F-model, mean square regression: mean square residual = 7.53) and a very low probability value (P-model > F = 0.00718). As illustrated in Table 6, some effects of factors and their interactions on reducing sugar concentrations are significant ($p<0.05$) in the ANOVA that indicates a significant effect of the corresponding factors on the response. The p-values from the t-test analysis given in Table 6 are used to determine the significant levels of three process parameters and their interactions on the reducing sugar. The most significant parameter is temperature. The effect of alpha-amylase amount is less significant ($p> 0.05$) so this interaction can be deleted from Equation (4) without significant effect on the accuracy of predicted reducing sugar concentration. (Yu *et al.*, 2009; Wang *et al.*, 2013).

Table 5: ANOVA for the full quadratic model

ANOVA					
Source of variation	%Sum of squares (SS)	Degrees of freedom (DF)	Mean squares (MS)	F-value	Probe > F
Regression	4.397	91	0.489	7.532	0.00718
Residual	0.454	9	0.06487		
Total	4.851	100			

Table 6: Coefficients, t-statistics and significant probability of the model for Equation (4).

Term	Coefficient	Value	Standard Error	t -value	P - value
Constant	b0	-100.01	19.81	-5.048	0.00148
Time (min)	b1	0.06053	0.03149	1.922	0.09605
Temperature (°C)	b2	2.235	0.414	5.397	0.00101
Alpha-amylase (%w)	b3	19.90	38.45	0.518	0.621
Time x Time	b4	-1.76 E-05	2.68 E-05	-0.655	0.533
Temperature x Temperature	b5	-0.01190	0.00226	-5.256	0.00118
Alpha-amylase x Alpha-amylase	b6	85.42	38.89	2.196	0.06408
Time x Temperature	b7	-0.000540	0.000334	-1.617	0.150
Time x Alpha-amylase	b8	-0.04026	0.03705	-1.087	0.313
Temperature x Alpha-amylase	b9	-0.339	0.408	-0.830	0.434

3.3 Interactions among the factors

3.3.1 The effects of alpha-amylase amount and temperature

Figure 1 shows the effects of alpha-amylase amount and temperature on reducing sugar content. The reducing sugar content of clarified product increased with increasing amount of alpha-amylase and temperature in the range of 84.4 to 91.1°C. However, the conversion rate was reduced for a further increase in temperature.

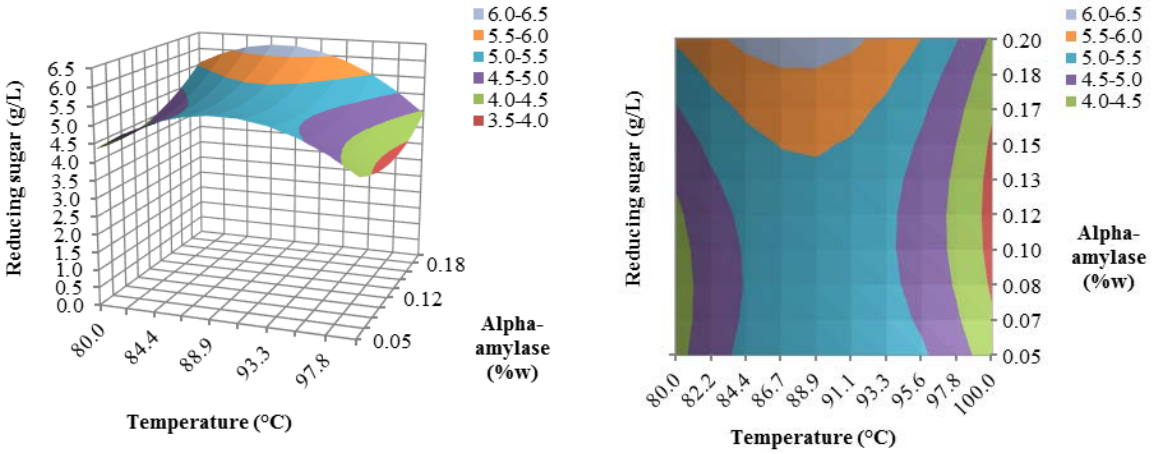

Figure 1: Response surface and contour plot of temperature vs. alpha-amylase on reducing sugar content for 150 min.

3.3.2 The effects of heating time and temperature

The effects of heating time and temperature on reducing sugar content are shown in Figure 2. The reducing sugar increased with an increase in both time and temperature. However a higher temperature from 88.9 to 100 °C caused a reduction in the sugar content. To obtain an

*Corresponding author (Sininart Chongkhong). Tel.: +66-7428-7293; fax: +66 7455 8833
E-mail addresses:csininart@yahoo.com. Volume 5 No.1 ISSN 2228-9860 eISSN 1906-9642. Online available at http://tuengr.com/V05/0067.pdf

optimum reducing sugar content the clarification process should be operated at a temperature in the range of 84.4 to 88.9°C for a time in the range of 150 to 240 min.

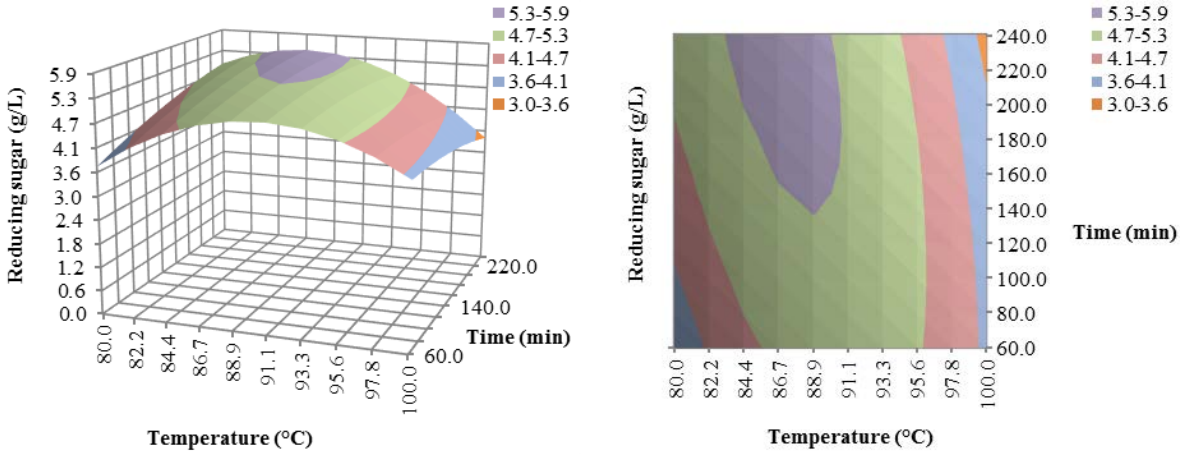

Figure 2: Response surface and contour plot of temperature vs. time on reducing sugar content with 0.13 %w alpha-amylase.

3.3.3 The effects of heating time and alpha-amylase amount

The interaction of time and alpha-amylase amount on reducing sugar content (Figure 3) implies that the clarification process should be carried out for a time in the range of 100 to 180 min with 0.17-0.2 %w alpha-amylase to achieve a maximum content of reducing sugar.

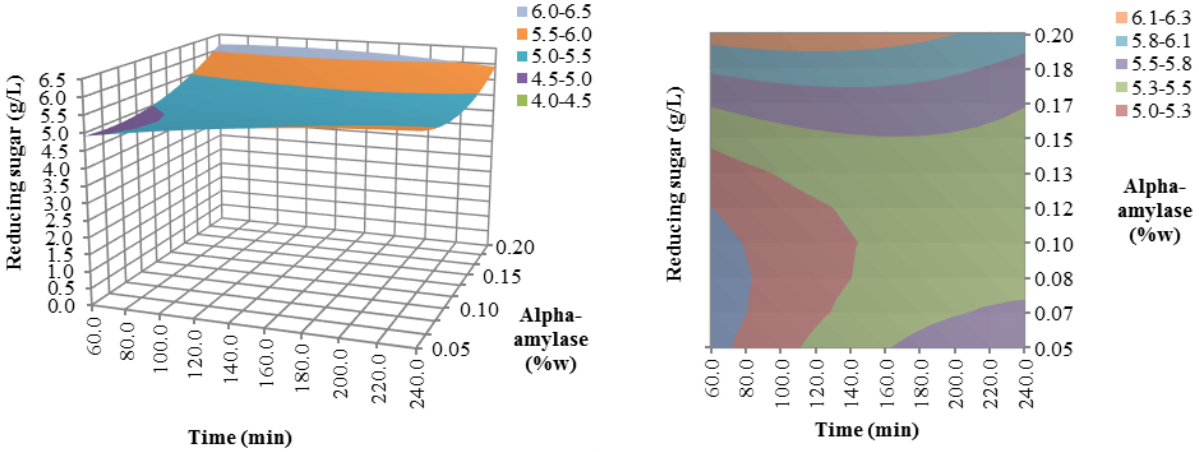

Figure 3: Response surface and contour plot of time vs. alpha-amylase on reducing sugar content at 90 °C.

The results of the influence and interaction of the factors using CCD indicated that the highest yield could be reached near the center point of the operating conditions as on the contour curves. The optimum condition was at 87.6 °C for 150 min with 0.2 %w alpha-amylase which could provide 6.21 g/L for experimental and 6.25 g/L for predicted reducing sugar contents. These showed that the model, Equation (4), could be useful.

4. Conclusion

A clarification step before liquefaction and fermentation steps of the ethanol production from the corncob has been evaluated. The ranges of time, temperature and alpha-amylase amount were established to optimize the operation condition by RSM which could save experimental time and cost. The optimum condition were an alpha-amylase amount of 0.2 %w, a temperature of 87.6 °C and a time of 150 min. that gave the highest amount of 6.21 g/L reducing sugar content.

5. Acknowledgement

The authors gratefully acknowledge the financial support from the Graduate school and Faculty of engineering, Prince of Songkla University.

6. References

Agro-Industry department center for export: ADCET. The faculty of Agro-Industry, Prince of Songkla University HatyaiSongkhla 90112.

Aiyer, P.V. (1995). Amylases and their applications. *African Journal of Biotechnology*, 4(13), 1525-1529.

Balata, M., Balat, H. and Oz, C. (2008) Progress in bioethanol processing. *Progress in Energy and Combustion Science*, 34(5), 551-573.

Bandaru, V.V.R., Somalanka, S.R., Mendu, DR., Madicherla, N.R. and Chityala, A. (2006). Optimization of fermentation conditions for the production of ethanol from sago starch by co-immobilized amyloglucosidase and cells of Zymomonasmobilis using response surface methodology. *Enzyme and Microbial Technology*, 38(1-2), 209-214.

Bezerra, M.A., Santelli, R.E., Oliveira, E.P., Villar, L.S. and Escaleira, L.A. (2008). Response surface methodology (RSM) as a tool for optimization in analytical chemistry. *Talanta*. 76(5), 965-977.

Chena, M., Xia, L. and Xue, P. (2007). Enzymatic hydrolysis of corncob and ethanol production from cellulosic hydrolysate. *International Biodeterioration& Biodegradation*, 59(2), 85–89.

Chongkhong, S., Lolharat, B. and Chetpattananondh, P. (2012). Optimization of Ethanol Production from Fresh Jackfruit Seeds Using Response Surface Methodology. *Journal of Sustainable Energy & Environment*, 3, 97-101.

Das, S., Singh, S., Sharma, V. and Lalsoni, M. (2011). Biotechnological applications of industrially important amylase enzyme. *International Journal of Pharma and Bio Sciences*, 2(1), 486-496.

Khuri, A. and Mukhopadhyay, S. (2010). Response surface methodology. *Wiley*

*Corresponding author (Sininart Chongkhong). Tel.: +66-7428-7293; fax: +66 7455 8833
E-mail addresses:csininart@yahoo.com.

Interdisciplinary Reviews-Computational Statistics, 2, 128-149.

Kreuger, E., Sipos, B., Zacchi, G., Svensson, S. and Björnsson, L. (2011). Bioconversion of industrial hemp to ethanol and methane: The benefits of steam pretreatment and co-production. *Bioresource Technology*, 102(3), 3457-3465.

Liu, K., Lin, X., Yue, J., Li, X., Fang, X., Zhu, M., Lin, J., Qu, Y. and Xiao, L. (2010). High concentration ethanol production from corncob residues by fed-batch strategy. *Bioresource Technology*, 101(13), 4952-4958.

Lolharat, B., Chongkhong, S. and Chetpattananondh, P. (2011). Optimizing conditions for enzymatic clarification of prebiotic extracted jackfruit seeds using response surface methodology. *Proceeding of the 5th International Conference on Engineering and Technology (ICET-2011)*, May 2-3, 2011, Phuket, Thailand.

Miller, G.L. (1959). Use of dinitrosalicyclic acid reagent for determination of reducing sugar. *Analytical Chemistry*, 31(3), 426-428.

Reed, G. and Nagodawithana, T.W.(1995). Enzyme, Biomass, Food and feed. *Biotechnology*, 9(2),676.

Wang, Q., Ma, H., Xu, W., Gong, L., Zhang, W. and Zou, D.(2008).Ethanol production from kitchen garbage using response surface methodology. *Biochemical Engineering Journal*, 39(3), 604-610.

Wang, L., Luo, Z. and Shahbazi,(2013). A. Optimization of simultaneous saccharification and fermentation for the production of ethanol from sweet sorghum (Sorghum bicolor) bagasse using response surface methodology. *Industrial Crops and Products*, 42, 280-291.

Yu, J., Zhang, Xu. and Tan, T. (2009). Optimization of media conditions for the production of ethanol from sweet sorghum juice by immobilized *Saccharomyces cerevisiae*. *Biomass and Bioenergy*, 33(3), 521-526.

Zhu, S., Wu, Y., Yu, Z., Chen, Q., Wu, G., Yu, F., Wang, C. and Jin, S. (2006). Microwave-assisted Alkali Pre-treatment of Wheat Straw and its Enzymatic Hydrolysis. *Biosystems Engineering*, 94(3), 437-442.

Dr.Sininart Chongkhong is an Assistant Professor of Department of Chemical Engineering at Prince of Songkla University. She received her B.Eng. from Prince of Songkla University with Honors in 2002. She continued her Ph.D. study at Prince of Songkla University, where she obtained her Ph.D. in Chemical Engineering. Dr. Sininart Chongkhong currently works on ethanol/biodiesel technologies.

Woraluk Kongjindamunee holds a degree in Chemical Engineering from Prince of Songkla University, Thailand. She is interested in applications of a green chemical technology.

Peer Review: This article has been submitted, peer-reviewed, and awarded best paper from the Third International-Thai Chemical Engineering and Applied Chemistry (TIChE) Conference, jointly organized by Department of Chemical Engineering, Faculty of Engineering, Khon Kaen University and Thai Institute of Chemical Engineering and Applied Chemistry, at Pullman Khon Kaen Raja Orchid Hotel, Khon Kaen, THAILAND, October 17-18, 2013.

International Transaction Journal of Engineering, Management, & Applied Sciences & Technologies

http://TuEngr.com

Synthesis of Alkali Metal/CaO Sorbent for CO_2 Capture at Low Temperature

Nusavadee Pojananukij [a], Nannaphas Runruksa [a], Sutasinee Neramittagapong [a], and Arthit Neramittagapong [a]*

[a] *Department of Chemical Engineering, Faculty of Engineering, Khon Kaen University, Khon Kaen, 40002, Thailand*

ARTICLEINFO

Article history:
Received 23 August 2010
Received in revised form
23 September 2010
Accepted 26 September 2010
Available online
26 September 2010

Keywords:
potassium carbonate;
decarbonation process;
Thermogravimetric Analyser;

ABSTRACT

In order to improve their CO_2 absorption capacity at low temperature, alkali-based sorbents were prepared by impregnation method. It was found that supported CaO modified with a K/Ca molar ratio of 3 kept the most favorable stability and CO_2 uptake capacity among the proposed K_2CO_3-stabilized samples. The result showed that the total CO_2 capture capacity of 3K/CaO was 3.84 mg CO_2/g sorbent at 50°C. The X-ray diffraction (XRD) result revealed the new structure was formed during CO_2 adsorption such as $CaCO_3$ and $K_2Ca(CO_3)_2$.

1. Introduction

Carbon dioxide (CO_2) in the atmosphere is approximately 300 ppm while humans can live in an atmosphere of CO_2 up to 5,000 ppm. After the air is taken into the lung, oxygen will be absorbed and CO_2 will be desorbed. It can cause toxicity to the body when one gets it in large quantity. The accumulation of CO_2 occurs in confined and poorly ventilated spaces, such as in the vault or in diving activities. As a result, the body gets the excess CO_2. This will cause rapid breathing, rapid heartbeat, dizziness, and can be fatal. CO_2 can be removed by various methods such as membrane separation, absorption with a solvent, and adsorption using molecular sieves (Lee, *et al.*, 2009). However, these methods are costly and consume high energy.

*Corresponding author (A. Neramittagapong). Tel/Fax: +66-43-362240 E-mail address: artner@kku.ac.th ©2014. International Transaction Journal of Engineering, Management, & Applied Sciences & Technologies. Volume 5 No.1 ISSN 2228-9860 eISSN 1906-9642. Online available at http://tuengr.com/V05/0077.pdf

One of the improved techniques for CO_2 removal is the chemical absorption of CO_2 with solid sorbents. The use of solid sorbents containing alkali and alkali-earth metals for CO_2 absorption has been reported in many literatures (Gupta and Fan, 2002; Lee, *et al.*, 2008). Among the materials studied, calcium oxide (CaO) has attracted most attention because of its low cost, high capture capacity, and suitable reaction kinetics. However, the lack of long-term stability, mainly due to the unstable structures upon high-temperature decarbonation is still an important drawback in industrial applications. Currently, many researches focus on the performance improvement of CaO-based sorbents by increasing the porosity and improving the stability. In the past, several studies regarding the efficient chemical absorption over K_2CO_3 supported on carbon (Lee, *et al.*, 2006) employed alkali metal carbonate in CO_2 absorption at low temperatures (50-60°C) with thermal regeneration easily occurring at a low temperature.

One objective of this work was to develop a new solid sorbent for being used to absorb CO_2 at low temperatures below 60°C. The CO_2 capture capacities of several potassium-based sorbents were studied in TGA reactor using multiple tests. The role of support in CO_2 absorption at low temperatures was also investigated. In addition, the changes in the physical properties of the sorbents before/after CO_2 absorption and its mechanism were investigated with the aid of power X-ray diffraction (XRD) and Temperature Program Desorption (TPD).

2. Methodology

2.1 Catalyst preparation

The alkali metal-based sorbent used in this study was prepared by the impregnation method. A typical preparation procedure for the sorbent supported on the calcium oxide (99% CaO, Aldrich) is as follows: 5.0 g of supports were added to an aqueous solution containing 2.5 g of potassium carbonate (K_2CO_3, Aldrich) in 25 ml of deionized water and the percentage weight ratio of K:CaO was studied at 3, 5, 10, 20, and 30, respectively. Then, the content was mixed by using a magnetic stirrer for 24 h at room temperature. The dried samples were calcined in a furnace with N_2 flow for 2 h at 450°C and 750°C. The ramping rate of the temperature was maintained at 3°C/min.

2.2 Characterization of the catalyst

The specific surface area and total pore volume were determined by nitrogen adsorption method at 77 K on the ASAP 2010 analyzer (Micromerition, USA) using a Burnauer-Emmrtt-Teller (BET) theory. X-ray diffraction (XRD, Bruker D8 advance, USA) was used to find the

chemical composition and the crystallographic structure with Cu α K radiation in an angular range (2θ) and the scanning range from 5° to 80° with 40 mA and 40 kV. The functional groups of components in a mixture and interfacial bonding mechanism of Ca and C were characterized by using Fourier transform infrared spectroscopy (FTIR, Bruker Tensor 27), with the sample mixed in KBr pellet at room temperature, Spectra were got over the range of 400-4,000 cm^{-1}

2.3 Reaction study

Carbon dioxide adsorption on the prepared powders was studied using a TGA. The weight losses of the substance were calcined to analyze in a furnace under a N_2 flow (100 mL/min) at 450°C and 750°C. The ramping rate of the temperature was maintained at 3°C/min. Decarbonation/carbonation experiments were conducted with thermogravimetric analyzer (TGA). All the steps of carbonation and decarbonation experiments, sample heating, sample cooling, and gases shifting between CO_2 and nitrogen were programmable. A small amount of sorbent was placed in an alumina crucible and heated to the decarbonation temperatures (50, 70 and 100°C) at a ramp rate of 20°C/min under nitrogen with 2-hour temperature maintaining. During the entire process, the sorbent weight and the temperature were continuously recorded.

3. Results and discussion

The calcium oxide sorbents in the present study were subjected to thermogravimetric (TGA) analysis. The thermograms obtained between 30 and 750°C are shown in Figure 1. In general, the TG profiles of calcium oxide exhibit a three-step weight-loss system. Firstly, the weight loss with the temperature range of 30-340°C occurred on account of dehydration. Secondly, the weight loss of adsorbent was changed to about 21% within the temperature range of 380-440°C, at which $Ca(OH)_2$ was complete changed to CaO (Lu, *et al.*, 2006; Karami and Mahinpey, 2012) as expressed in Equation (1).

$$Ca(OH)_2 \rightarrow CaO + H_2O \quad (1)$$

A little weight of adsorbent was changed within the temperature range of 450-750°C due to the stable structure. This is because the reaction (1) is completed at low temperature.

*Corresponding author (A. Neramittagapong). Tel/Fax: +66-43-362240 E-mail address: artner@kku.ac.th

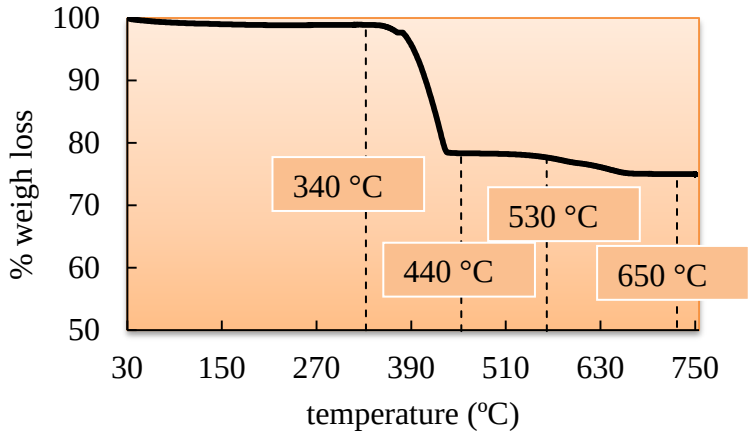

Figure 1: The relationship between weight changes with temperature by TGA.

Therefore, the temperatures were select at 450°C and 750°C to study the adsorbent calcinations before CO_2 adsorption because these temperatures stimulated the structure of the adsorbent. Figure 2 shows that the calcination temperature of 450°C presents the higher ability to absorb CO_2 than that of 750°C about 1 mg/g, because the calcination temperature at 750°C caused the adsorbent breakdown and the structure decimation. This negatively impacts the ability to decrease the absorption. To compare the adsorption capacity of CaO and 30K/CaO, they were calcined at the both calcination temperature mentioned above. Similarly, at the temperature of 450°C, CaO and 30K/CaO have the higher ability to absorb CO_2 than that of 750°C. In addition, at the calcination temperatures of 450°C, 30K/CaO had higher adsorption capacity than CaO by 30% as depicted in Figure 2.

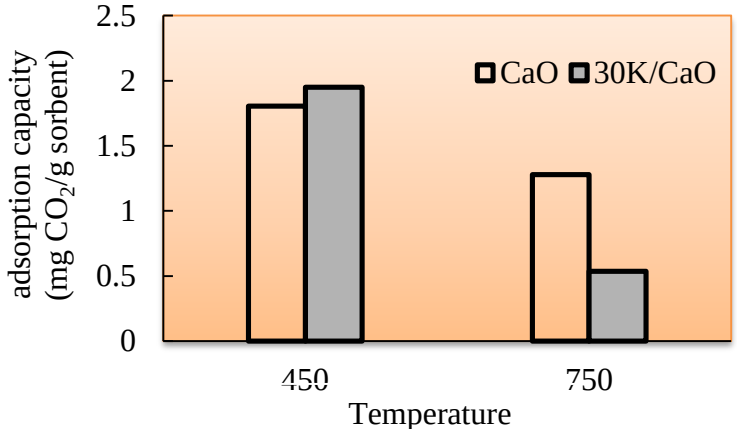

Figure 2: The CO_2 absorption capacity of the sorbents burned at different temperatures

FTIR technique provides information about vibrational state of adsorbed molecules and hence the nature of surface complexes. The FTIR spectra of CaO impregnated with potassium carbonate can be seen from Figure 3, where the bands due to hydroxyl and carbonate are

distinctly displayed in the spectrum. The strong band at 3,643 cm^{-1} corresponds to the O-H bonds from the remaining hydroxide. The bands at 1,417 cm^{-1} and 866 cm^{-1} correspond to the C-O bond. The wide and strong bands at around 418 cm^{-1} and 578 cm^{-1} correspond to the Ca-O bonds (Roy and Bhattacharya, 2011), while the peak found of potassium carbonate at 1,776 cm^{-1} (Hilliard, 2008) were indicative of the increment of functional groups by K_2CO_3 impregnation on CaO.

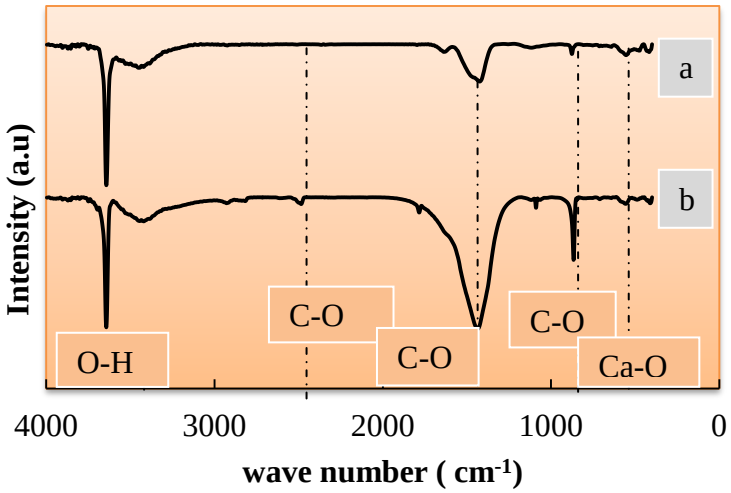

Figure 3: IR spectra of samples: (a) CaO (b) 30K/CaO.

The surface areas of various alkali metal/CaO sorbent were depicted in Table 1. The BET surface area of commercial calcium oxide (4.96 m^2/g) is lower than that of K/CaO because potassium carbonate entering the structure of CaO increases the surface area. The highest surface area was 3K/CaO which showed a maximum of 24.88 m^2/g. Meanwhile, the increasing amount of potassium carbonate enhanced the surface area. However, an excessive amount of potassium carbonate could damage the mesoporous structure since it aggregated with K_2CO_3 and blocked the pore structure of CaO.

Figure 4 shows the carbonic dioxide adsorption ratio of 3K/CaO, 30K/CaO and CaO at 50°C, 0-120 minutes. It is found that, in this temperature range at the initial 0-3 minutes, there is no CO_2 absorption because CO_2 disseminates into the absorbed surface area. As time increases to 4-10 minutes, the adsorption rapidly occurs and is constant at 10 minutes onwards. The period of 7 minutes gives the highest absorption. In this research, the

*Corresponding author (A. Neramittagapong). Tel/Fax: +66-43-362240 E-mail address: artner@kku.ac.th

absorbents are able to absorb CO_2 quickly within 10 minutes, while the research of Lee, *et al*., 2009 took the time to absorb more than 100 minutes to reach equilibrium. The 3K/CaO has the absorption ability of 3.84 mg/g, whereas 30K/CaO and CaO have the absorption ability of 1.95 and 1.8 mg/g, respectively, as presented in Figure 4.

Table 1: The surface area of CaO and potassium carbonate supported on CaO

Type sorbent	% wt potassium	BET (m^2/g)
CaO	-	4.96
3K/CaO	3	24.88
5K/CaO	5	22.41
10K/CaO	10	18.97
30K/CaO	30	5.90

It has been found from the experiments that the 3K/CaO sorbent is the best and the burning temperature before the absorption of the catalyst is at the temperature of 450°C. Therefore, 3K/CaO was used to study the effects of temperature for adsorbing carbon dioxide at various temperatures of 50, 70 and 100°C with the time spent in absorbing of 120 minutes.

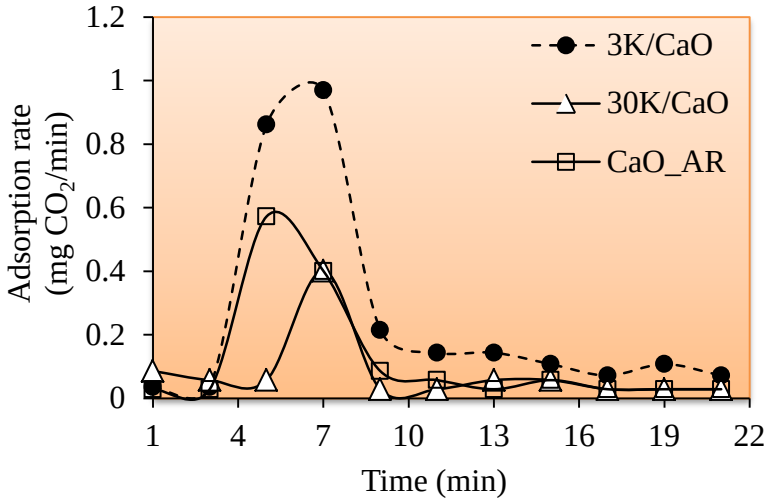

Figure 4: The adsorption rates at time adsorption, calcined in a furnace under a N_2 flow of 100 mL/min at 450°C

The potassium increased ability to absorb carbon dioxide decreased, while 3K/CaO had higher CO_2-absorbing ability than that of 30K/CaO by 50%. Since the addition of potassium in excessive amounts to the catalyst support could cause clogging of the pores of CaO and porosity, the surface area of the adsorbent decreased. Similarly, the surface area decreased with the increasing amount of potassium as shown in Figure 4. For the first four minutes of running, the CO_2-absorbing ability was low; but during 6-20 minutes, the ability increased.

Then, it took 80 minutes to be constant and steady continuously until 120 minutes. As in Figure 5, when comparing the absorption temperature, the best absorption was at 50°C, followed by 70 and 100°C, with the absorbing ability of 3.84, 3.68, 3.66 mg/g, respectively. It has been found that the adsorption temperature of 70°C and 100°C had the decreasing CO_2-absorbing ability to 4.16 and 4.68%, respectively.

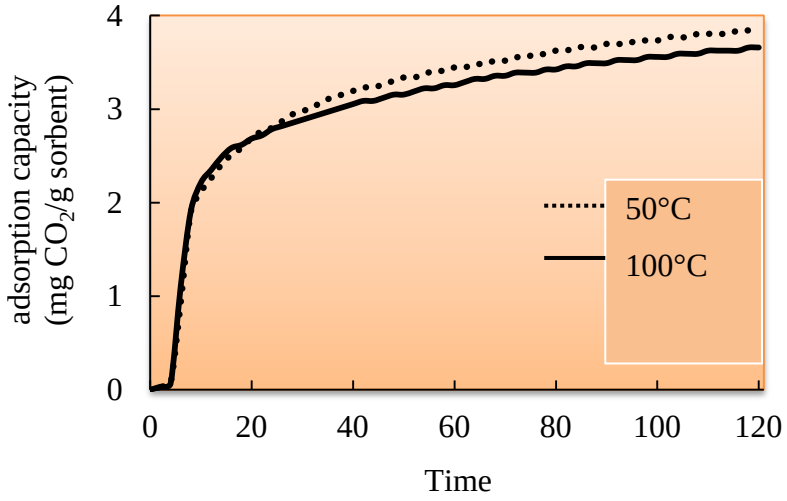

Figure 5: The adsorption capacity at 50°C and 100°C, calcined in a furnace under a N_2 flow of 100 mL/min at 450°C

Due to the breakdown of the bond between the burning structures, the study of Lee, *et al.*, 2009 found that the burning of adsorbent at higher temperatures would decrease potassium calcium carbonate coating on the surface. The results showed that the adsorbents calcined at 450°C would have higher CO_2-absorbing ability than that of the burning temperature of 750°C.

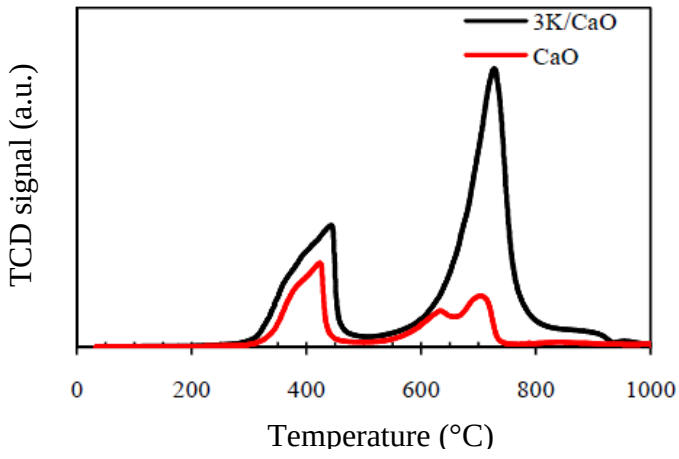

Figure 6: CO_2 Temperature-Programmed Desorption (CO_2-TPD).

*Corresponding author (A. Neramittagapong). Tel/Fax: +66-43-362240 E-mail address: artner@kku.ac.th

International Transaction Journal of Engineering, Management, & Applied Sciences & Technologies. Volume 5 No.1 ISSN 2228-9860 eISSN 1906-9642. Online available at http://tuengr.com/V05/0077.pdf

From the study of the base sorbent with Chemisorptions Analyzer by TPD, it has been found that the highest temperature causing CO_2 desorption of CaO and 3K/CaO was 450°C, the absorption is due to bonding weak. While at 725°C, the adsorbents were strongly base resulting in the difficulty exothermic adsorption of CO_2 due to the chemical bonding.

The CO_2-TPR graph indicated that the base value of adsorbent of 3K/CaO was higher than that of CaO, showing that carbonic dioxide adsorption was a chemical bond. It could be concluded from TPD curves that CaO and 30K/CaO had 2 period bases. The temperature range of 250-450°C for weak bases and the range of 600-800°C during the period of strong bases were presented in Figure 6. It was found that the strong bases had higher CO_2-absorbing ability than the weak bases up to 2-3 times.

For 3K/CaO, the area under the graph was more than that of CaO by 43%. It could be concluded that the addition of potassium carbonate on supports resulted in increasing base of sorbent. Meanwhile, the absorbing ability increased. The results confirmed that of 3K/CaO has higher carbon-dioxide-adsorbing ability than that of CaO by 52%. The optimum temperature of the sorbent regeneration was at 450°C because at 750°C the structure of the adsorbent was destroyed.

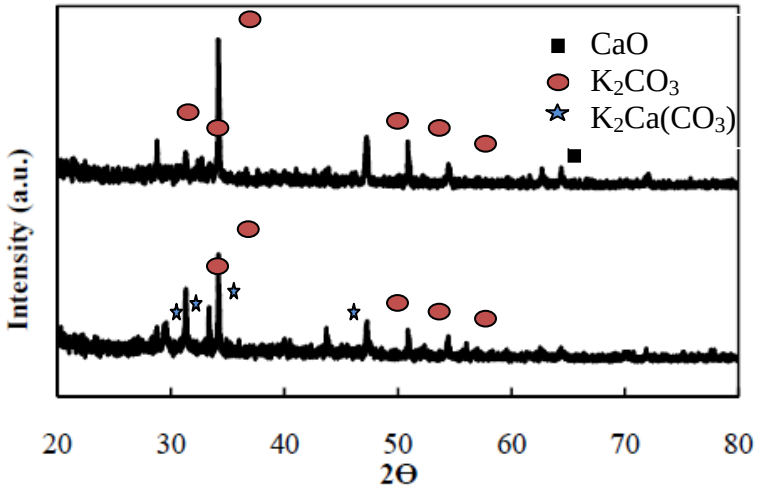

Figure 7: XRD patterns of 30K/CaO sorbents
(a) before and (b) after CO_2 adsorption

Analysis of structural changes in the adsorbent after adsorption showed that the adsorption of CaO formed the new compounds, $CaCO_3$, following the reaction (2). And after adsorption, 30K/CaO adsorbent also incarnated the new compounds, $K_2Ca(CO_3)_2$, (present in Figure 7) due to the addition of potassium carbonate which reacted with CaO to support and

absorb carbon dioxide during the process of equation (3).

$$CaO + CO_2 \rightarrow CaCO_3 \quad (2)$$

$$K_2CO_3 + CaO + CO_2 \rightarrow K_2Ca(CO_3)_2 \quad (3)$$

4. Conclusion

It has been found that K_2CO_3 supported on CaO results in the most promising sorbents for CO_2. Total carbon dioxide capture capacity of 3K/CaO was 3.84 $mgCO_2/g$ sorbent mostly abundant in all conditions. The enhanced performance could be attributed to the high surface area and large pore volume of the sorbent with the appropriate amounts of K_2CO_3. For higher K_2CO_3 loadings, the performance did not improve further due to the formation of paracrystalline K_2CO_3 on the CaO support surface. The CO_2-TPD indicated that there was a chemical reaction between the sorbent and the adsorbate. Considering the regeneration capacity as an important factor in addition to the CO_2-capture capacity, 3K/CaO could be used as a sorbent that had the potential for CO_2 absorption.

5. Acknowledgements

The authors express their thanks to Department of Chemical Engineering, Faculty of Engineering, and Graduate School of Khon Kaen University for the financial supports.

6. References

Gupta, Himanshu, and Liang-S. Fan. (2002). Carbonation−Calcination Cycle Using High Reactivity Calcium Oxide for Carbon Dioxide Separation from Flue Gas. *Industrial & Engineering Chemistry Research*, 41 (16), 4035–4042.

Hilliard, Marcus Douglas. (2008). A Predictive Thermodynamic Model for an Aqueous Blend of Potassium Carbonate, Piperazine, and Monoethanolamine for Carbon Dioxide Capture from Flue Gas. http://repositories2.lib.utexas.edu/handle/2152/3900.

Karami, Davood, and Nader Mahinpey. (2012). Highly Active CaO-Based Sorbents for CO2 Capture Using the Precipitation Method: Preparation and Characterization of the Sorbent Powder. *Industrial & Engineering Chemistry Research*, 51(12), 4567–4572.

Lee, Soo Chool, Ho Jin Chae, Soo Jae Lee, Bo Yun Choi, Chang Keun Yi, Joong Beom Lee, Chong Kul Ryu, and Jae Chang Kim. (2008). Development of Regenerable MgO-Based Sorbent Promoted with K_2CO_3 for CO_2 Capture at Low Temperatures." *Environmental Science & Technology* ,42 (8), 2736–2741.

*Corresponding author (A. Neramittagapong). Tel/Fax: +66-43-362240 E-mail address: artner@kku.ac.th

Lee, Soo Chool, Ho Jin Chae, Soo Jae Lee, Yong Hee Park, Chong Kul Ryu, Chang Keun Yi, and Jae Chang Kim. (2009). Novel Regenerable Potassium-based Dry Sorbents for CO2 Capture at Low Temperatures. *Journal of Molecular Catalysis B: Enzymatic* , 56 (2–3), 179–184.

Lee, Soo Chool, Bo Yun Choi, Chong Kul Ryu, Young Soo Ahn, Tae Jin Lee, and Jae Chang Kim. (2006). The Effect of Water on the Activation and the CO_2 Capture Capacities of Alkali Metal-based Sorbents." *Korean Journal of Chemical Engineering*, 23 (3), 374–379.

Lu, Hong, Ettireddy P. Reddy, and Panagiotis G. Smirniotis. (2006). Calcium Oxide Based Sorbents for Capture of Carbon Dioxide at High Temperatures. *Industrial & Engineering Chemistry Research*, 45 (11)

Roy, Arup, and Jayanta Bhattacharya. (2011). Microwave-Assisted Synthesis and Characterization of Cao Nanoparticles. *International Journal of Nanoscience*, 10 (03), 413–418.

Nusavadee Pojanaukij is a Ph.D. student in Chemical Engineering program of Khon Kaen University. She received M.Eng in Chemical Engineering from Faculty of Engineering, Khon Kaen University and B.Sc. in Environmental Science from Faculty of Science, Khon Kaen University. She interests in the adsorption and application of catalysis or adsorbent.

Nannaphas Runruksa earned her B.Eng and M.Eng in Chemical Engineering from Khon Kaen University. She is interested in the application of catalysis. She is a licensed engineer in Chemical Engineering.

Dr.Arthit Neramittagapong is an Assistant Professor in the Chemical Engineering Department at Khon Kaen University. He holds a B.Eng. in Chemical Engineering from Khon Kean University, M. Eng. in Chemical Engineering from Chulalongkorn University and D.Eng. in Environmental Chemistry and Engineering from Tokyo Institute of Technology. He has been working on the environmental catalysis, design of industrial catalysts, chemical reaction engineering, and hazardous waste treatment and pollution control.

Dr.Sutasinee Neramittagapong is an Assistant Professor in the Chemical Engineering Department at Khon Kaen University. She holds a B.Eng. in Chemical Engineering from Khon Kean University, M. Eng. in Chemical Engineering from Chulalongkorn University and D.Eng. in Environmental Chemistry and Engineering from Tokyo Institute of Technology. Her research works have been focused on the environmental catalysis, renewable energy, green productivity, synthesis of high value-added compounds from industrial or agriculture wastes, and hazardous waste treatment and pollution control.

Peer Review: This article has been internationally peer-reviewed and accepted for publication according to the guidelines in the journal's website. Note: Original version of this article was accepted and presented at the Third International-Thai Chemical Engineering and Applied Chemistry (TIChE) Conference, jointly organized by Department of Chemical Engineering, Faculty of Engineering, Khon Kaen University and Thai Institute of Chemical Engineering and Applied Chemistry, at Pullman Khon Kaen Raja Orchid Hotel, Khon Kaen, THAILAND, October 17-18, 2013.

:: International Transaction Journal of Engineering, Management, & Applied Sciences & Technologies

http://TuEngr.com

Call-for-Papers:

ITJEMAST invites you to submit high quality papers for full peer-review and possible publication in areas pertaining to our scope including engineering, science, management and technology, especially interdisciplinary/cross-disciplinary/multidisciplinary subjects.

Next article continue on next page ➔

ISSN 2228-9860

eISSN 1906-9642